Magnetic Properties of Low-Dimensional Molecule-based Magnets Consisting of Transition Metals and Organic Radicals

Youhei Numata

Doctor of Philosophy

Department of Structural Molecular Science,
School of Physical Science,
The Graduate University for Advanced Studies

2006

Index

Chapter 1. General Introduction

Chapter 2. Preparation, Structure and Magnetic Properties of Cyclic Dimer Complex, $[\{Co(hfac)_2\}\bullet BNO^{t\text{-}Bu}]_2$

Chapter 3. Field-induced Ferrimagnetic State in a New Molecule-based Magnet Consisting of Co^{II} ion and Chiral π-conjugated Triplet Radical

Chapter 1. General Introduction

Chapter 1.

General Introduction

1.1. Molecule-based Magnets

Molecule-based magnets are investigated in several decades. In first 18th century, Prussian blue was already synthesized as a pigment, and later, it was revealed that Prussian blue shows ferromagnetic transition at 5.5 K. First structurally identified molecule-based magnet, $[Fe(C_5Me_5)_2]$•TCNE•$n$$CH_3CN$ (TCNE = tetracyanoethylene), was reported by J. S. Miller *et al.* in 1987.[1] This compuond shows ferromagnetic transition at 4.8 K, and $[Fe(C_5Me_5)_2]^+$ and $TCNE^{\bullet-}$ ions form alternate sandwich structure (Chart 1–1).

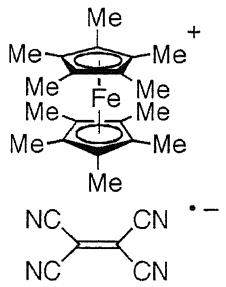

Chart 1–1. $[Fe(C_5Me_5)_2]$•TCNE•$n$$CH_3CN$

Consequently, C. Benelli *et al.* reported $[Mn(hfac)_2]$•NN-*R* (hfac = 1,1,1,5,5,5-hexafluoroacetylacetonato and NN-*R* = 2-*R*-4,4,5,5-tetramethylimidazolyl-1-oxy-3-oxide, *R* = Et, *n*-Pr, *i*-Pr) in 1989, which construct 1–D alternate chain structure and show ferrimagnetic phase transitions (Chart 1–2, Table 1).[2]

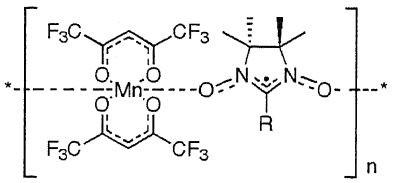

Chart 1–2. $[Mn(hfac)_2]$•NN-*R*

Table 1–1. $[Mn(hfac)_2]$•NN-*R* complexes.

R	Type	T_C	Ref.
Et	Ferri	8.4 K	2b
n-Pr	Ferri	8.6 K	2c
i-Pr	Ferri	7.6 K	2a

And after a while, as the first pure organic magnet, NN-*p*-$PhNO_2$ (T_C = 0.65 K) (NN-*p*-$PhNO_2$ = 2-(*p*-nitrophenyl)-4,4,5,5-tetramethylimidazolyl-1-oxy-3-oxide) (Chart 1–3) was synthesized by Awaga *et al.* in 1989[3] and ferromagnetic phase transition was observed at 0.65 K by Kinoshita *et al.* in 1991.[4]

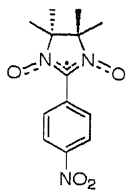

Chart 1–3. NN-*p*-$PhNO_2$.

After these discoveries, persistent and hard efforts of many scientists were devoted to prerare them and many novel and interesting molecule-based magnets were synthesized. Molecule-based magnets are roughly categolized by constructing style as pure organic radicals, metal–radical complexes and the coordination polymers consisting of metal ions and bridging ligands. At first, pure organic radical magnets are mentioned. For example, nitronylnitroxide (NN-*R*), nitroxide (NO), TEMPOL, verdazyl, thiazolyl, dithiazolyl and their substituent radical based bulk magnets are reported (Figure 1–1).[3,4,5]

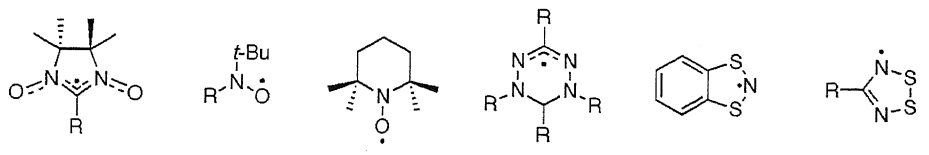

Figure 1–1. Stable organic radicals.

Organic radical metal complexes consisting of magnetic metal ions and organic polydentate radicals[1,2,6] are often used to construct molecule-based magnets, too, because they can form coordination polymer, which have strong magnetic interactions between magnetic metal ions and organic radicals. For example, M-(NN-*R*), which showed above, M-polynitroxide complexes (M = magnetic transition metals and lanthanoids) are listed in Table 1–2.

Table 1–2. Metal organic radical molecule-based magnetic compounds.

Complex	Type	T_C (T_N)	Ref.
$[Ni(hfac)_2]$•NN-Me	1-D Ferri	5.3 K	6e
$[Mn(pfbz)_2]$•NN-*R*, *R* = Me, Et	1-D Ferri	24, 20.4 K	6b
$[L^{III}(hfac)_3]$•NNPhOMe, L^{III} = lanthanoid ions (+3)	1-D SCM	—	19f
$[Mn(hfac)_2]$•BNO^H	1-D Meta	5.5 K	6f
$[Mn(hfac)_2]_3$•$TNOB_2$	2-D Ferri	3.4 K	6c
$[Mn(hfac)_2]_3$•$TNOP_2$	3-D Ferri	46 K	6d
$[Co(hfac)_2]$•NNPhOMe	1-D SCM	—	19a
$[Co(hfac)_2]$•NN-H, *trans*-, *cis*-	1-D SCM	—	19e

(pfbz = pentafluorobenzoate, BNO^H = 1,3-Bis(*N*-*t*-butyl-*N*-oxylamino)benzene, TNOB = 1,3,5-Tris-[*p*-(*N*-*t*-butyl-*N*-oxylamino)phenyl]-benzene, TNOP = Bis[3-*t*-butyl-5-(*N*-*t*-butyl-*N*-oxylamino)phenyl]nitroxide and SCM = single chain magnet).

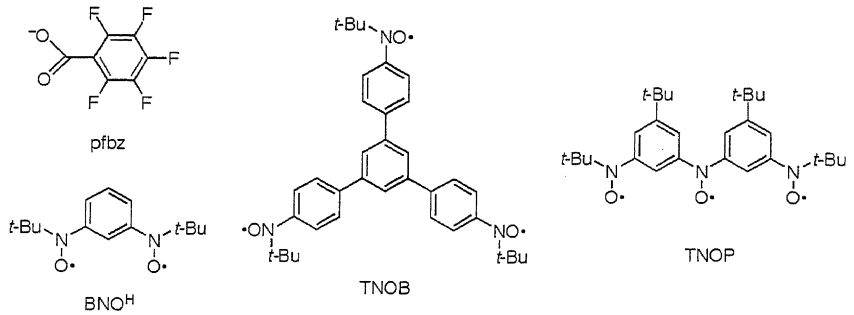

And the compound consisting of the magnetic metal ions bridged by the bridging ligands such as oxalate,[7] azide,[8] poly carboxylic acid,[9] cyanide,[10] and etc.,[11] (Figure 1–2) are most typical examples of molecule-based magnets and many compounds are reported. These ligands can connect metal ions and form magnetic coordination polymers. Some coordination styles of these ligands are shown in Figure 1–3, and resulting compounds are listed in Table 1–3.

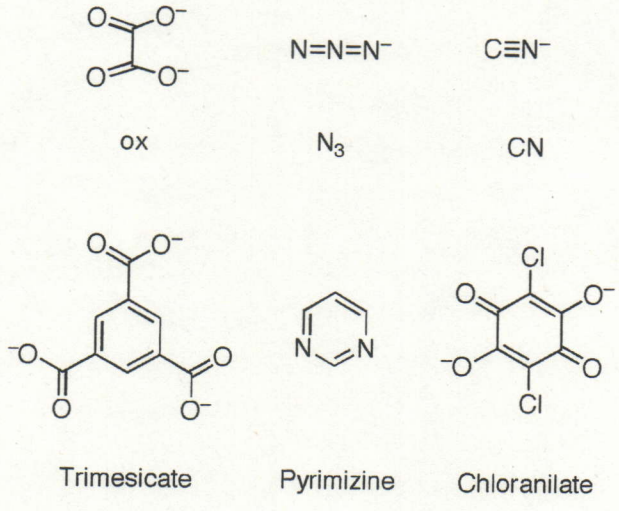

Figure 1–2. Polydentate Ligands.

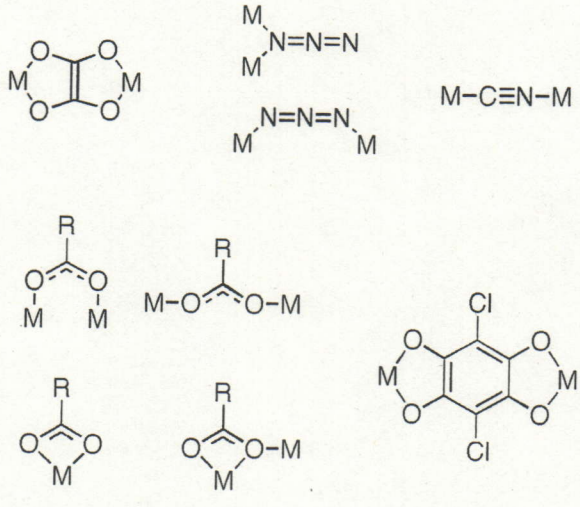

Figure 1–3. Coordination styles of above ligands.

Table 1–3. The examples of magnetic coordination polymers.

Complex	Type	T_C (T_N)	Ref.
$A^+[M^{II}_A M^{III}_B (ox)_3]$, M^{II}_A = Cr, Mn, Fe, etc., M^{III}_B = Cr, Fe	2-D layer, Ferri or Ferro	43 K (Fe, Fe), 30 K (Ni, Fe)	7e, f
$A^+[M_A M_B (ox)_3]$,	3-D network	various	7e
$[Co_3(OH)_2(ox)_2]\bullet 3H_2O$	3-D network	8 K	7g
$[Ni(Et_2Meen)(N_3)_2]$	1-D meta	~ 25 K	8e
$[Mn(R\text{-py})_2(N_3)_2]$	1-D cant	~ 20 K	8e
$[Co_2Na(4\text{-cpa})_2(\mu_3\text{-OH})(H_2O)]$	1-D frustrate	4 K	9f
$[Co_3(\mu_3\text{-OH})_2(1,2\text{-chdc})_2]$	2-D frustrate	12 K	9d
$[Co_2(OH)_2BDC]$	2-D Antiferro	48 K	9e
$A^+M[M(CN)_6]\bullet nH_2O$	3-D network	various	10
$[M\{N(CN)_2\}(pm)(guest)]$, M = Fe, Co	3-D weakferro	various, varied by guest	11d

(Et_2Meen = *N*,*N*-diethyl-*N*'-methylethylenediamine, *R*-py = *R*-piridine (R = 3-acetyl, Et, CN), 4-cpa = 4-carboxylphenoxyacetone, 1,2-chdc = 1,2-cyclohexanedicarboxylato, BDC = telephtalato, pm = pyrimidine).

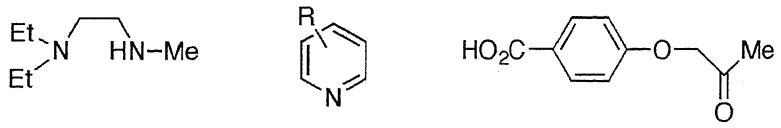

Et_2Meen

R-Py

4-cpa

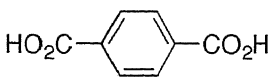

BDC

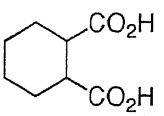

1,2-chdc

Molecule-based magnets, which are introduced above, show novel and characteristic magnetic properties. The first example that comes to our mind is the room temperature molecule-based magnets, which T_C is higher than room temperature, $A^+_nV_x[Cr(CN)_6]_y \cdot zH_2O$ (A^+ is counter cation, n, x, y, z are various numbers, please see references) (T_C = 315 ~ 376 K (42 ~ 103 °C))[12] and $V(TCNE)_x \cdot yCH_2Cl_2$ (TCNE = tetracyanoethylene, $x \sim 2$, $y \sim 1/2$) (T_C = extrapolated ~ 400 K (~ 123 °C))[13]. Room temperature molecule-based magnets are listed in Table 1-4.

Table 1–4. Room temperature molecule-based magnets.

Compound	Type	T_C	Ref.
$V(TCNE)_x \cdot yCH_2Cl_2$	Ferri	~ 400 K (123 °C)	13
$KV^{II}[Cr^{III}(CN)_6]$	Ferri	376 K (103 °C)	12b,d
$V^{II}[Cr^{III}(CN)_6]_{0.86} \cdot 2.8H_2O$	Ferri	372 K (99 °C)	12c,d
$K_{0.5}V[Cr(CN)_6]_{0.95} \cdot 1.7H_2O$	Ferri	350 K (77 °C)	12c,d
$Cs_{0.8}V[Cr^{III}(CN)_6]_{0.94} \cdot 1.7H_2O$	Ferri	337 K (64 °C)	12b,d
$V^{II}[Cr^{III}(CN)_6]_{2/3} \cdot 3.5H_2O$	Ferri	330 K (57 °C)	12b,d
$V[Cr^{III}(CN)_6]_{0.86} \cdot 2.8H_2O$	Ferri	315 K (42 °C)	12a,d

As other examples, photo-response magnets,[14] which is changed its magnetic state (from non magnetic state to magtetic state or between high spin and low spin state) by photo irradiation, magnetic sponge,[15] whose magnetic properties changes accompanying hydration water desorption and absorption, the magnet, which has two compensation points,[16] and the paramagnetic compounds, which show spin crossover phenomena (multistep crossover,[17b] light-induced excited-spin-state trapping (LIESST)[17d] and the compound whose crossover temperature changes by solvent desorption and absorption[17e]) are cited (Figure 1–4). These physical properties are characteristic in molecule-based magnets.

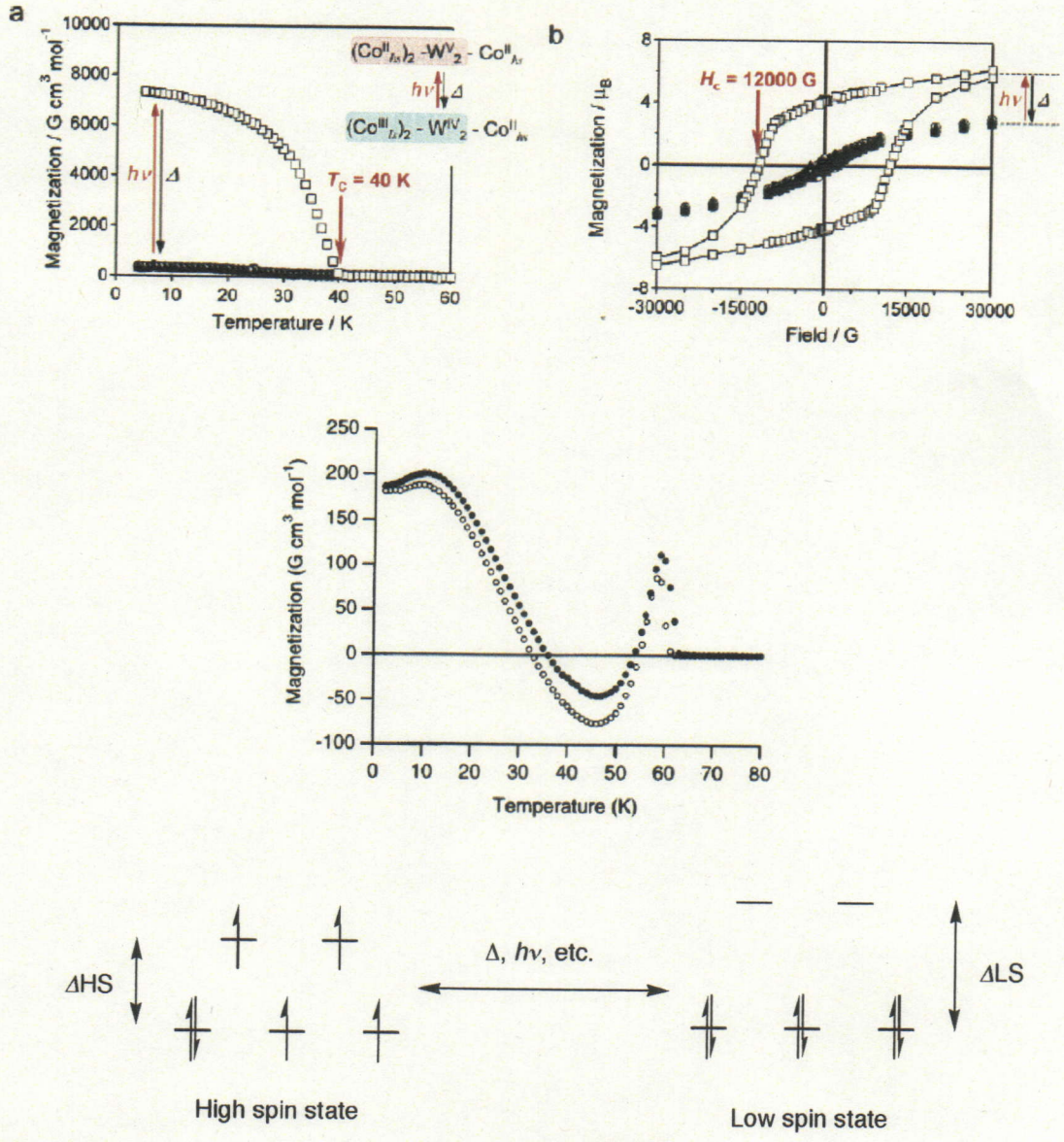

Figure 1–4. *M-T* (top, a) and *M-H* (top, b) plots of Photo-response magnet, $Co^{II}_3[W^V(CN)_8]_2$(pyrimidine)•$6H_2O$. Markers correspond to before irradiation (black triangle), after irradiation (square), and after heating uo to 150 K (circle), respectively.[14e] ZFC-FC magnetizations of $(Ni^{II}_{0.22}Mn^{II}_{0.60}Fe^{II}_{0.18})_{1.5}[Cr^{III}(CN)_6]$•$7.6H_2O$, which shows two compensation points at around 35 and 53 K (middle). Spin crossover of Fe^{II} ion, d^6 (bottom).

On the other hand, as molecule-based magnets, which have novel magnetic properties that come from their molecular structures, discret magnetic cluster; Single Molecule Magnets (SMMs)[18] and one-dimensional magnetic chain; Single Chain Magnets (SCMs)[19] are considered. These magnets show unique magnetic hysteresis and relaxation properties based on their molecular structure and magnetic anisotropy. And as the one of their remarkable magnetic properties, magnetic quantum tunneling is mentioned and it is the focus of interest, because this is the good example that quantum phenomenon can be observed in macroscale. SMMs and SCMs are shown in Figure 1–5.

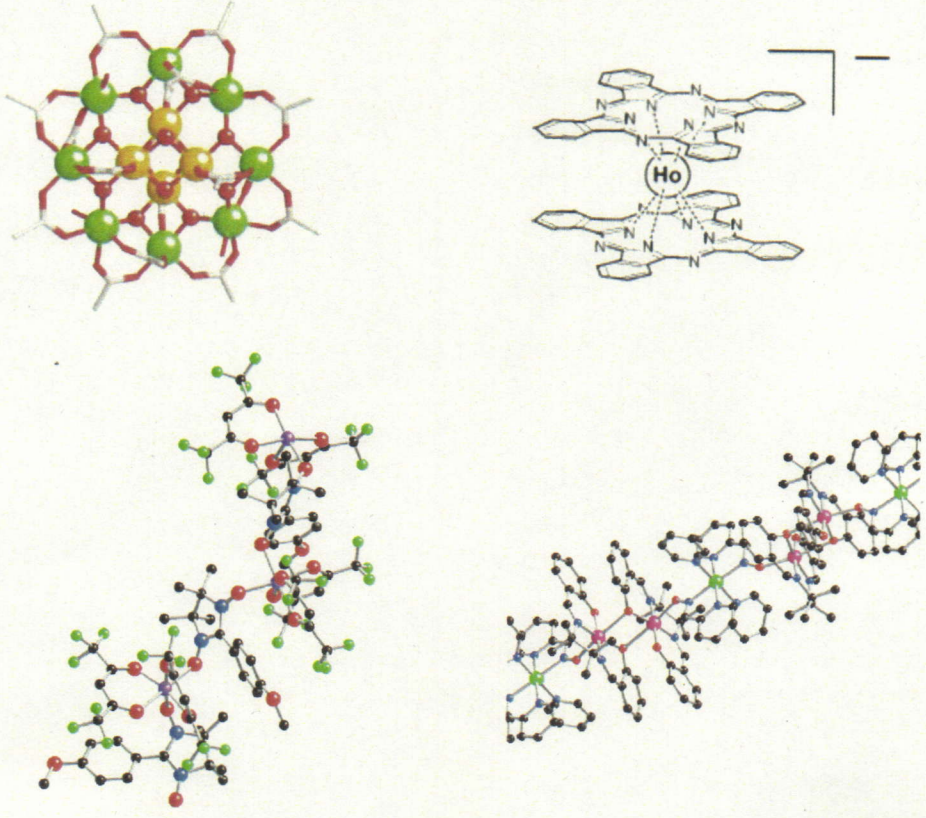

Figure 1–5. The examples of SMMs, $[Mn_{12}O_{12}(acetate)_{16}(H_2O)_4]$ (green Mn^{III}, yellow Mn^{IV}, red O, white C)[18a] (top left) and $[Ho(Pc)_2]^-$ (top right),[18c] and SCMs, $[Co(hfac)_2]$•NNPhOMe (purple Co, green F, red O, blue N, black C)[19a] (bottom left) and 1-D chain unit of $[Mn_2(saltman)_2Ni(pao)_2(py)_2]^{2+}$ (pink Mn, green Ni, red O, blue N, black C)[19b] (bottom right).

It is mentioned that the new multi-functional materials can be constructed by the combination of two (or more) components, which have different physical properties, as remarkable feature of molecular compounds. For example, the combinations between magnetism and conductivity,[20] superconductivity,[21] photo reactivity[22] and electricity[23] are reported. The examples of these compounds are shown in Figure 1–6.

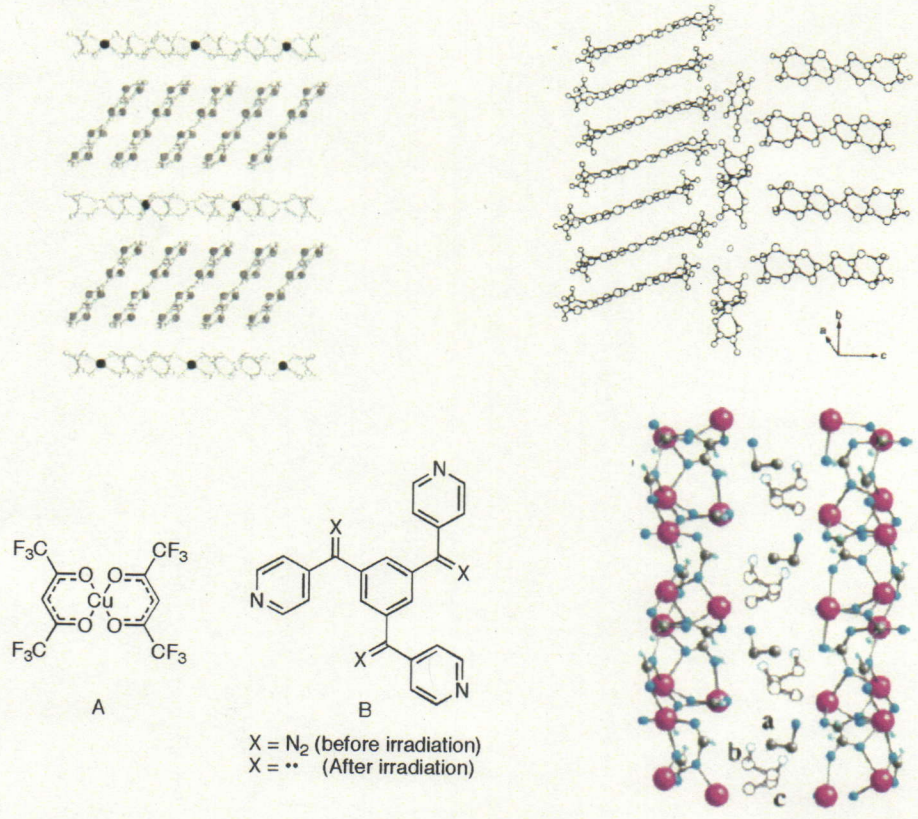

Figure 1–6. Ferromagnetic metallic conductor, $[BEDT\text{-}TTF]_3[Mn^{II}Cr^{III}(ox)_3]$ (T_C = 5.5 K, σ = 250 S cm^{-1} at r.t.)[20a] (top, left), paramagnetic superconductor, (T_C = 8.5 K)[21a] (top, right), Photo-reactive magnet, frozen solution of A_3B_2 mixture[22] (bottom, left). Ferroelectric ferrimagnet, $[Mn_3(HCOO)_6]$•EtOH (magnetic T_C = 8.5 K, electric T_C = 177 K),[23] a, b and c mean disorder of EtOH molecules (bottom, right).

1.2. Chiral and Non-centrosymmetric Magnets

Chiral magnets show novel and interesting magnetic properties based on breaking of its structural and/or magnetic symmetries. Metal Lanthanides, MnSi, MnP are known as helimagnets and in some metal compounds spin frustlation and spin chirality are investigated.[24,25] Non-centrosymmetric structural compounds show interesting physical properties, which are based on the relationship between their crystal structures and magnetism. α-Fe_2O_3 shows weakferromagnetism and Cr_2O_3 shows Magneto-Electro (M-E) effect. The weakferromagnetism of α-Fe_2O_3 is resulting from Dzyaloshinsky-Moriya (DM) interaction. At first, DM interaction was led by Dzyaloshinsky and consequently modified by Moriya.[26] DM exchange interaction and its Hamiltonian, which interact between two spins (S_1, S_2) are given by the equation 1. 1 and 1. 2.

$$\varepsilon = D \bullet \left[S_1 \times S_2 \right] \quad (1.\ 1)$$

$$D = -2i\lambda \left[\sum_{n_1} \frac{\langle g_1 | L_1 | n_1 \rangle}{E_{n_1} - E_{g_1}} J(n_1 g_2, g_1 g_2) - \sum_{n_2} \frac{\langle g_2 | L_2 | n_2 \rangle}{E_{n_2} - E_{g_2}} J(g_1 n_2, g_1 g_2) \right] \quad (1.\ 2)$$

Here, g_n is ground state of S_n, n_n is excited state of S_n, L_n is excitation process between g_n and n_n and E_n is energy levels of every g_n and n_n states, respectively. And the magnitude of $\boldsymbol{D}$ value is given by equation 1. 3.

$$|D| \cong \frac{\lambda J}{\Delta E} \sim \frac{\Delta g}{g} J \quad (1.\ 3)$$

Therefore, magnitude of DM interaction is proportional to $\Delta g/g$ value of spins. As seen in equation 1.1, this interaction interacts between spins as vector product and cants them. Altough M-E effect is also related with crystal structure and magnetism, it's not important in this thesis, so explaination is omitted.

In Figure 1–7, the relationships between magnetic interaction, J, DM interaction, D and spin arrangements. J makes spins parallel or antiparallel arrangement. D makes spins perpendicular arrangement. And the combination of J and D makes canted spin arrangement ($J < 0$).

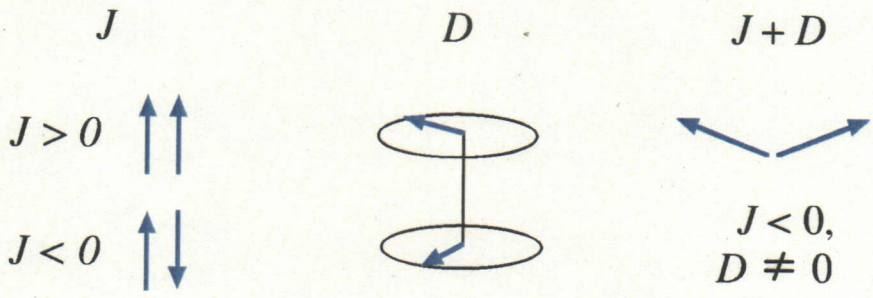

Figure 1–7. Magnetic interaction J, DM interaction D and combination of J and D ($J < 0$).

Additionally, not only magnetism, but also (magneto-) optical properties are interesting. From the correlation between magnetism and structural chirality, magnetization-induced second harmonic generation (MSHG) is expected,[27] For example, giant nonliner magneto-optical Kerr effects from interface of Fe thin film are reported. Now such MSHG is only observed at surface and interface, because of broken symmetry. But in chiral (structural) magnets, MSHG is expected based on space (from chiral structure) and time (from magnetism) symmetry violations. And the combination between neutral circular dichroism (NCD), which comes from optical activity and magnetic circular dichroism (MCD), which comes from Faraday effect, generate Magneto Chiral Dichroism (MChD) effect in absorption or emission and Magneto Chiral Birefringence (MChB) in reflection (Figure 1–8).

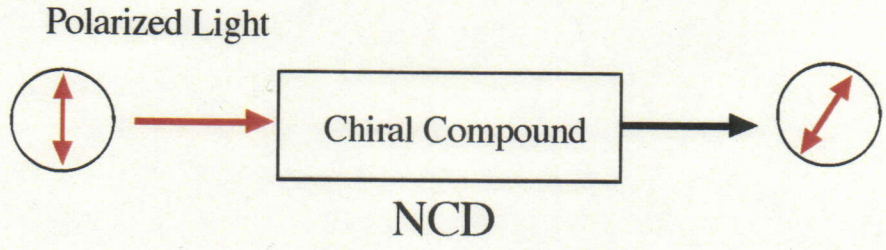

Figure 1–8a. Model of NCD effect (optical activity) to linear polarized light.

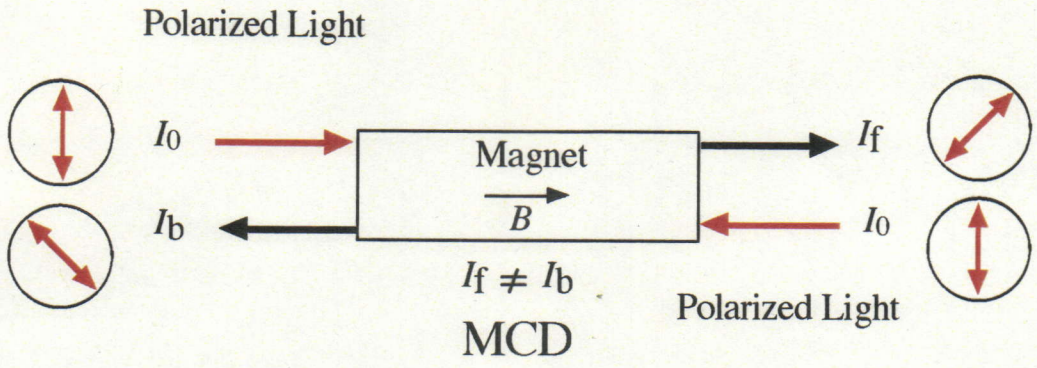

Figure 1–8b. Model of MCD effect (Faraday effect) to linear polarized light. B corresponds to magnetic field and its direction. I_f and I_b correspond to induced light direction parallel to B and antiparallel to B, respectively.

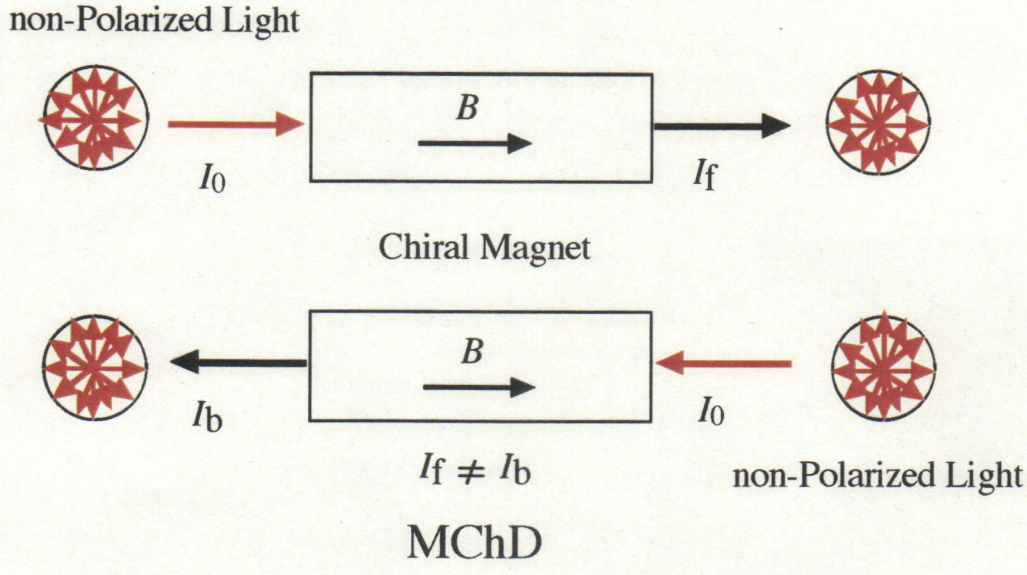

Figure 1–8c. Model of MChD effect to non-polarized light. B, I_f and I_b are similar with caption of Figure 1–7b.

MChD effect can be observed in discrete molecules. This effect was theoretically expected[28a] in 1982 by G. Wagniéra and for the first time, MChD was experimentally observed in the deutrated dimethyl sulphoxide solution of chiral structural molecule, [Eu((+ or –)-tfc)$_3$] in 1997 ((+ or –)-tfc = trifluoro-(+ or –)-camphorato) (Chart 1–4) by G. L. J. A. Rikken *et al.*[29a] NCD and MCD are observed only using polarized light, MChD can be observed using non-polarized light. Because MChD amplitude is proportional to magnetic field intensity (Figure 1–9 inset), strong MChD effect is expected in bulk chiral ferro- (or ferri-) magnet.

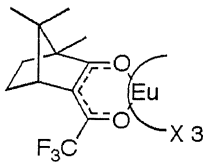

Chart 1-4. [Eu(tfc)$_3$]

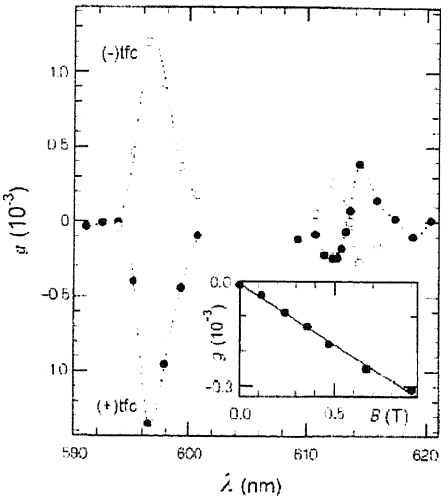

Figure 1–9. Magneto-Chiral anisotropy of [Eu(tfc)$_3$].[29a] Inset: Magneto-Chiral ansotropy intensity vs B plot.

In Figure 1-9, First observed magneto-chiral anisotropy, g plot is shown. g is given by equation 1. 4.

$$g = \frac{\frac{\partial}{\partial B}\left(I_{\hat{B}\uparrow\uparrow\hat{k}} - I_{\hat{B}\uparrow\downarrow\hat{k}}\right)B}{I_{\hat{B}\uparrow\uparrow\hat{k}} + I_{\hat{B}\uparrow\downarrow\hat{k}}} \quad (1.4)$$

Here, I_n means intensity of luminescent, $\hat{B}\uparrow\uparrow\hat{k}$ means B (Magnetic field) parallel to k (wavevector) and $\hat{B}\uparrow\downarrow\hat{k}$ means B antiparallel to k.

1.3. Design of Chiral Structural Molecule-based Magnets

In Chapter 1.2, the author introduced interesting and novel properties of chiral magnets. But only few examples were exsist, because to construct inorganic chiral magnets depend on the chance. First molecule-based chiral structural magnet was $[Mn(hfac)_2]$•NNPhOMe (NNPhOMe = 2-(*p*-methoxyphenyl)-4,4,5,5-tetramethylimidazolyl-1-oxy-3-oxide) (ferrimagnet T_C = 4.8 K) (Chart 1–5), and it was reported by A. Caneschi *et al.* in 1991.[30a] This complex has one-dimensional chain structure and crystallized in the hexagonal chiral crystal system, $P3_1$ from achiral molecules ($[Mn(hfac)_2]$ and NNPhOMe).

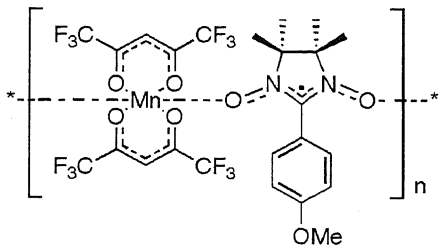

Chart 1–5. $[Mn(hfac)_2]$•NNPhOMe

M. Hernández-Molina *et al.* reported chiral structural magnet $[Co(bpy)_3]$ $[Co_2(ox)_3]ClO_4$ (bpy = 2,2'-bipyridine) in 1998.[31a] It had been known that transition metal oxalato comlexes make 2-D or 3-D structural molecule-based magnets and in this network, each building unit $M(ox)_3$, which is coordinated by tris-bidentate ligands, has Δ- or Λ-chirality, but finally they construct enantiostructures. Their idea was to lead single chirality into oxalato 2-D or 3-D network using tris-chelated transition metal diimine complex as the templating counter ion. The projections of 3-D network of $[Co_2(ox)_3]^{2-}$ and template molecule, $[Co(bpy)_3]^{3+}$ locations are shown in Figure 1–10.

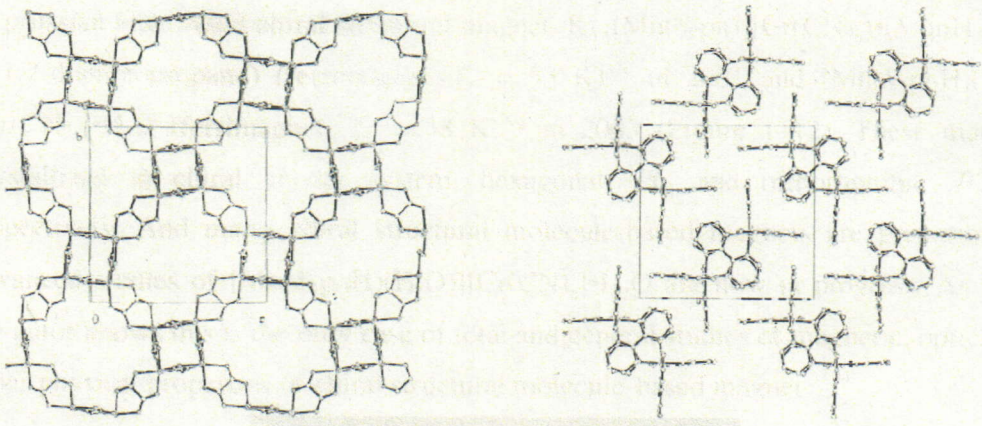

Figure 1–10. 3-D network of $[Co_2(ox)_3]^{2-}$ down in *bc* plane (right) and $[Co(bpy)_3]^{3+}$ down in *bc* plane for $[Co(bpy)_3][Co_2(ox)_3]ClO_4$.

H. Kumagai *et al.* worked out the strategy of chiral inducing to molecule-based magnets from chiral substituents and designed chiral radical as the bridging ligand. In 1999, $[Mn(hfac)_2]$•BNO* (BNO* = 1,3-bis(*N-tert*-butyl-*N*-oxylamino)-5-(1'-methyl-1'-{2"-(*S*)-methylbutoxy}ethyl)benzene) (Chart 1–6) was synthesized.[32a] This molecule has chiral crystal group *P*1 (No. 1) and 1-D alternate chain structure (Figure 1–11) and shows metamagnetic phase transition at 5.4 K. This compound shows remarkable magnetic properties and the author shows the magnetic properties of single crystal of this compound in Chapter 4 of this thesis.

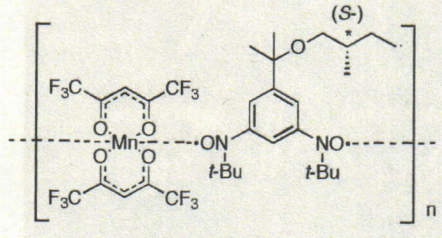

Chart 1–6. $[Mn(hfac)_2]$•BNO*

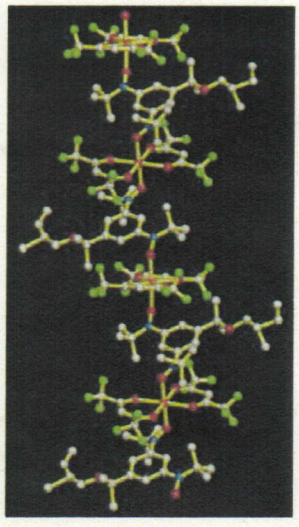

Figure1–11. 1-D chain structure of $[Mn(hfac)_2]$•BNO*

Consequently, K. Inoue *et al.* prepared and showed magnetic and optical properties of prussian blue based chiral structural magnet, $K_{0.4}[Mn(S\text{-pn})][Cr(CN)_6]\bullet(S\text{-pnH})_{0.4}$ (pn = 1,2-diaminopropane) (ferrimagnet, T_C = 53 K)[32c] in 2001 and $[Mn(S\text{-pnH})(H_2O)][Cr(CN)_6]\bullet H_2O$ (ferrimagnet, T_C = 38 K)[32g] in 2003 (Figure 1–12). These materials crystallized in chiral crystal system, hexagonal, $P6_1$ and orthorhombic, $P2_12_12_1$, respectively. And many chiral structural molecule-based magnets are preparing and advanced studies of $[Mn(S\text{-pnH})(H_2O)][Cr(CN)_6]\bullet H_2O$ are now in progress. As far as the autor knows this is the only case of total and general studies of magnetic, optical and other physical properties of chiral structural molecule-based magnet.[33,34]

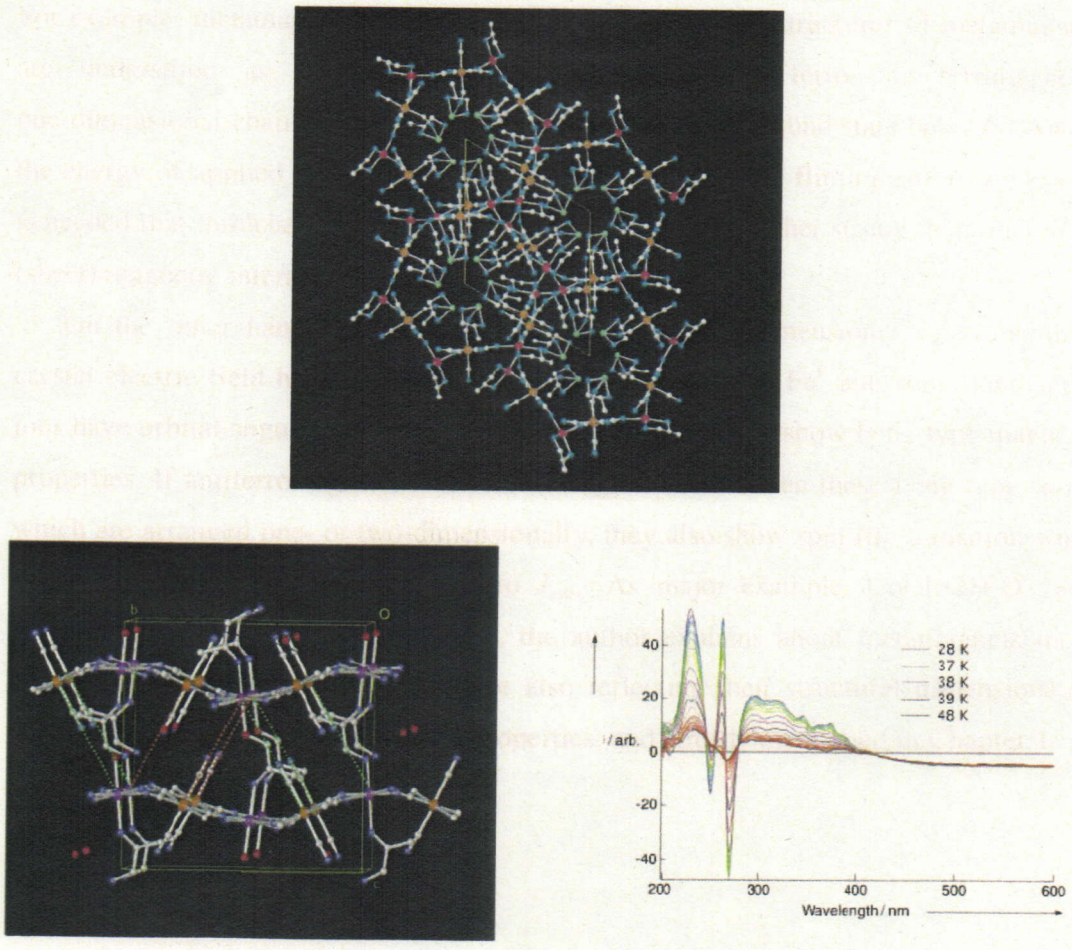

Figure 1–12. $K_{0.4}[Mn(S\text{-pn})][Cr(CN)_6]\bullet(S\text{-pnH})_{0.4}$ (down to 6_1 axis, in *ab* plane) (top), $[Mn(S\text{-pnH})(H_2O)][Cr(CN)_6]\bullet H_2O$ (side view of 2-D layer, in *bc* plane) (bottom left) and its MCD spectra (bottom right).

1.4. Low dimensional magnets

The low-dimensional structural magnets show characteristic magnetic properties reflecting their structural low dimensionality. In particular, because of low densities of magnetic ions in molecule-based magnets, they tend to have such styles. Therefore, in some molecule-based magnets, magnetic ions are one- or two-dimensionally interacted. In such systems, because magnetic interactions between interchain (sheet) and intrachain (sheet) are very different, they show highly anisotropic magnetic properties. For example, metamagnets reflect such characters. The spin structures of metamagnets are understood as the antiferromagnetic orderings of ferro- or ferrimagnetic one-dimensional chains or two-dimensional sheets in their ground state belw T_N. And if the energy of applied magnetic field corresponds to J_{inter}, spin flip transition occurrs (It is needed that intrachain (sheet) magnetic interactions are further strong than interchain (sheet) magnetic interactions, and $J_{inter} < 0$).

On the other hand, in the crystals, which have low dimensional structure, their crystal electric field has axial properties. In such cases, Co^{II}, Fe^{II} and some lanthanoid ions have orbital angular momentum in their ground state and show Ising type magnetic properties. If antiferromagnetic interactions, J_{inter} affect between these Ising type spins, which are arranged one- or two-dimensionally, they also show spin flip transition when applying magnetic field corresponds to J_{inter}. As major example, $CoCl_2 \cdot 2H_2O$[35] and $FeCl_2$[36] are well known. In Chapter 4, the author explains about metamagnets more accuratelly. And SMMs and SCMs are also reflecting their structural dimensionality and magnetic anisotropy to magnetic properties, and already mentioned in Chapter 1. 1.

1.5. Scope of This Thesis

In this thesis, the main purpose of the author is to construct chiral structural molecule-based magnets, and to investigate their chiral structural based novel magnetic properties.

In Chapter 2, the author shows synthesis, crystal structure and magnetic properties of cyclic dimer complex $[\{Co(hfac)_2\}\bullet BNO^{t\text{-}Bu}]_2$ ($BNO^{t\text{-}Bu}$ = 1,3-bis(*N-tert*-butyl-*N*-oxylamino)-5-*tert*-butylbenzene). The author estimated curie constant and averaged *g* value from magnetic susceptibility data.

In Chapter 3, preparation, crystal structure, magnetic properties and magnetic phase diagram of new one-dimensional chiral structural molecule-based magnet, $[Co(hfac)_2]\bullet BNO^*$ are described. This compound shows novel and interesting magnetic properties. The author tried to reval the origin of the magnetic behaviors.

In Chapter 4, Magnetic properties of single crystal of chiral structural molecule-based magnet, $[Mn(hfac)_2]\bullet BNO^*$ is shown. The author explains about the direction dependent magnetic behaviors of single crystal of simple metamagnet and characteristic magnetic behavior of $[Mn(hfac)_2]\bullet BNO^*$. And possible magnetic structure of this compound is calculated from magnetic data of single crystal.

Chapter 5 is the total conclusion of this thesis.

Appendex shows submitted papers, abstract of conferences and another contents.

1.6. Reference

1 J. S. Miller, J. C. Calabrase, H. Rommelmann, S. R. Chittipeddi, J. H. Zhang, W. M. Reiff, A. J. Epstein, *J. Am. Chem. Soc.* **1987**, *109*, 769.

2 (a) A. Caneschi, D. Gatteschi, J. P. Renard, P. Ray, R. Sessoli, *Inorg. Chem.* **1989**, *28*, 1976. (b) A. Caneschi, D. Gatteschi, J. P. Renard, P. Ray, R. Sessoli, *Inorg. Chem.* **1989**, *28*, 2940. (c) A. Caneschi, D. Gatteschi, J. P. Renard, P. Ray, R. Sessoli, *Inorg. Chem.* **1989**, *28*, 3314.

3 (a) K. Awaga, Y. Maruyama, *J. Chem. Phys.* **1989**, *91*, 2743. (b) K. Awaga, T. Inabe, U. Nagashima, Y. Maruyama, *J. Chem. Soc. Chem. Commun.* **1989**, 1617. (c) *ibid.* **1990**, 520.

4 (a) M. Tamura, Y. Nakazawa, D. Shiomi, K. Nozawa, Y. Hosokoshi, M. Ishikawa, M. Takahashi, M. Kinoshita, *Chem. Phys. Lett.* **1991**, *186*, 401, (b) Y. Nakazawa, M. Tamura, N. Shirakawa, D. Shiomi, M. Takahashi, M. Kinoshita, M. Ishikawa, *Phys. Rev. B* **1992**, *46*, 8906.

5 (a) D. B. Amabilino, J. Veciana, *Magnetism: Molecules to Materials II*, Eds. J. S. Miller, M. Drillon, Wiley-VCH, Weinheim, **2001**. Chap. 1, p. 1. (b) *Molecular Magnetism, New Magnetic Materials*, Eds. K. Itoh, M. Kinoshita, Kodansha, **2000**. (c) B. D. Koivisto, R. G. Hicks, *Coord. Chem. Rev.* **2005**, *249*, 2612. (d) J. M. Rawson, J. Luzon, F. Palacio, *Coord. Chem. Rev.* **2005**, *249*, 2631.

6 (a) H. Iwamura, K. Inoue, *Magnetism: Molecules to Materials II*, Eds. J. S. Miller, M. Drillon, Wiley-VCH, Weinheim, **2001**, Chap. 2, p. 61. (b) A. Caneschi, D. Gatteschi, J. P. Renard, P. Ray, R. Sessoli, *J. Am. Chem. Soc.* **1989**, *111*, 785. (c) K. Inoue, H. Iwamura, *J. Am. Chem. Soc.* **1994**, *116*, 3173. (d) K. Inoue, T. Hayamizu, H. Iwamura, D. Hashizume, Y. Ohashi, *J. Am. Chem. Soc.* **1996**, *118*, 1803. (e) A. Caneschi, D. Gatteschi, J. P. Renard, P. Ray, R. Sessoli, *Inorg. Chem.* **1989**, *28*, 2940. (f) K. Inoue, H. Iwamura, *J. Chem. Soc. Chem. Commun.* **1994**, 2273.

7 (a) J. J. Girerd, O. Kahn, M. Verdaguer, *Inorg. Chem.* **1980**, *19*, 274. (b) H. Oshio, U. Nagashima, *Inorg. Chem.* **1992**, *31*, 3295. (c) S. Decurtins, H. W. Schmalle, H. R. Oswald, A. Linden, J. Ensling, P. Gütlich, A. Hauser, *Inorg Chim. Acta.* **1994**, *216*, 65. (d) S. Decurtins, H. W. Schmalle, P. Schneuwly, H. R. Oswald, *Inorg. Chem.* **1993**, *32*, 1888. (e) M. Pilkington, S. Decurtins, *Magnetism: Molecules to*

Materials II. Eds. Miller J. S.; Drillon M. Wiley-VCH, Weinheim, **2001**, Chp. 10, p339. (f) H. Ōkawa, N. Matsumoto, H. Tamaki, M. Ohba, *Mol. Cryst. Liq. Cryst.* **1993**, *233*, 257. (g) M. Kurmoo, H. Kumagai, K. W. Chapman, C. J. Kepert, *Chem. Commun.* **2005**, 3012.

8 (a) C. D. Coryell, F. Stitt, *J. Am. Chem. Soc.* **1940**, *62*, 2942. (b) T. Mallah, O. Kahn, J. Gouteron, S. Jeannin, Y. Jeannin, C. J. O'Connor, *Inorg. Chem.* **1987**, *26*, 1375. (c) A. Escuer, J. Cano, M. A. Goher, Y. Journaux, F. Lloret, F. A. Mautner, R. Vicente, *Inorg. Chem.* **2000**, *39*, 4688. (d) L. Li, D. Liao, Z. Jiang, J. M. Mouesca P. Rey, *Inorg. Chem.* **2006**, *45*, 7665. (e) J. Ribas, A. Escuer, M. Monfort, R. Vicente, R. Cortés, L. Lezama, T. Rojo, M. A. S. Goher, *Magnetism: Molecules to Materials II.* Eds. J. S. Miller, M. Drillon, Wiley-VCH, Weinheim, **2001**, Chap. 9, p. 339.

9 (a) E. D. Estes, W. E. Estes, R. P. Scaringe, W. E. Hatfield, D. J. Hodgson, *Inorg. Chem.* **1975**, *14*, 2564. (b) P. Ayyappan, O. R. Evans, W. Lin, *Inorg Chem.* **2001**, *40*, 4627. (c) M. Kurmoo, H. Kumagai, S. M. Hughes, C. J. Kepert, *Inorg. Chem.* **2003**, *42*, 6709. (d) Y. Zheng, M. Tong, W. Zhang, X. Chen, *Angew. Chem. Int. Ed.* **2006**, *45*, 6310. (e) M. Kurmoo, H. Kumagai, M. A. Green, B. W. Lovett, S. J. Blundell, A. Ardavan, J. Singleton, *J. Sol. State Chem.* **2001**, *159*, 343. (f) X. Cheng, W. Zhang, Y. Zheng, X. Chen, *Chem. Commun*, **2006**, 3603.

10 (a) A. S. Cushman, *Science* **1908**, *27*, 666. (b) W. R. Entley, G. S. Girolami, *Science* **1995**, *268*, 397. (c) M. Verdaguer, A. Bleuzen, V. Marvaud, J. Vaissermann, M. Seuleiman, C. Desplanches, A. Scuiller, C. Train, R. Garde, G. Gelly, C. Lomenech, I. Rosenman, P. Veillet, C. Cartier, F. Villain, *Coord. Chem. Rev.* **1999**, *190–192*, 1023. (d) G. Rogez, A. Marvilliers, E. Riviere, J. Audiere, F. Lloret, F. Varret, A. Goujon, N. Mendenez, J. Girerd, T. Mallah, *Angew. Chem. Int. Ed.* **2000**, *39*, 2885. (e) S. Ohkoshi, K. Arai, Y. Sato, K. Hashimoto, *Nature Mat.* **2004**, *3*, 857. (f) B. Sieklucka, R. Podgajny, P. Przychodzen, T. Korzeniak, *Coord. Chem. Rev.* **2005**, *249*, 2203.

11 (a) O. Kahn, *Moleculer Magnetism*, Wiley-VCH, New York, **1993**. (b) Magnetism: Molecules to Materials *I* – *V*, Eds. J. S. Miller, M. Drillon, Wiley-VCH, Weinheim, **2001 – 2005**. (c) C. Benelli, D. Gatteschi, *Chem. Rev.* **2002**, *102*, 2369. (d) N. Takagami, T. Ishida, T. Nogami, Bull, Chem. Soc. Jpn. 2004, 77, 1125.

12 (a) S. Farley, T. Mallah, R. Ouhaes, P. Veillet, M. Verdaguer, *Nature* **1995**, *378*, 701. (b) S. M. Holmes, G. S. Girolami, *J. Am. Chem. Soc.* **1999**, *121*, 5593. (c) Ø.

Hatlevik, W. E. Buschmann, J. Zhang, J. L. Manson, J. S. Miller, *Adv. Mater.* **1999**, *11*, 914. (d) M. Verdaguer, G. S. Girolami, *Magnetism: Molecules to Materials V*, Eds. J. S. Miller, M. Drillon, Wiley-VCH, Weinheim, **2005**, Chap. 9, p. 281.

13 J. M. Manriquez, G. T. Yee, R. S. Mclean, A. J. Epstein, J. S. Miller, *Science* **1991**, *252*, 1415.

14 (a) O. Sato, T. Iyoda, A. Fujishima, K. Hashimoto, *Science* **1996**, *272*, 704. (b) G. Rombaut, S. Golhen, L. Ouhab, C. Mathonière, O. Kahn, *J. Chem. Soc., DaltonTrans.* **2000**, 3609. (c) G. Rombaut, C. Mathonière, P. Guionneau, S. Golhen, L. Ouhab, M. Verelst, P. Lecante, *Inorg. Chim. Acta* **2001**, *326*, 27. (d) S. Ohkoshi, H. Tokoro, T. Hozumi, Y. Zhang, K. Hashimoto, C. Mathonière, I. Bord, G. Rombaut, M. Verelst, C. C. dit Moulin, F. Villain, *J. Am. Chem. Soc.* **2006**, *128*, 270. (e) S. Ohkoshi, S. Ikeda, T. Hozumi, T. Kashiwagi, K. Hashimoto, *J. Am. Chem. Soc.* **2006**, *128*, 5320.

15 (a) O. Kahn, J. Larionova, J. V. Yakhmi, *Chem. Euro. J.* **1999**, *5*, 3443. (b) G. Ferey, *Nature Mater.* **2003**, *2*, 136.

16 (a) S. Ohkoshi, Y. Abe, A. Fujishima, K. Hashimoto, *Phys. Rev. Lett.* **1999**, *82*, 1285. (b) A. K. Zvezdin, V. V. Kostyuchenko, *Phys. Soli. State* **2001**, *43*, 1715.

17 (a) L. Cambi, A. Cagnasso, *Atti Accad. Naz. Lincei Cl. Sci. Fis. Mat. Nat. Re* **1931**, *53*, 809. (b) V. Ksenofontov, A. B. Gaspar, V. Niel, S. Reiman, J. A. Real, P. Gütlich, *Chem. Euro. J.* **2004**, *10*, 1291. (c) S. Hayami, Y. Shigeyoshi, M. Akita, K. Inoue, K. Kato, K. Osaka, M. Takata, R. Kawajiri, T. Mitani, Y. Maeda, Angew. Chem. Int. Ed. 2005, 44, 4899. (d) S. Decurtins, P. Guetlich, C. P. Koehler, H. Spiering, A. Hauser, *Chem. Phys. Lett.* **1984**, *105*, 1. (e) G. J. Halder, C. J. Kepert, B. Moubaraki, K. S. Murray, J. D. Cashion, *Science* **2002**, *298*, 1762.

18 (a) A. Caneschi, D. Gatteschi, R. Sessoli, A. L. Barra, L. C. Brunel, M. Guillot, *J. Am. Chem. Soc.* **1991**, *113*, 5873. (b) D. Gatteschi, R. Sessoli, *Angew. Chem. Int. Ed.* **2003**, *42*, 268. (c) N. Ishikawa, M. Sugita, W. Wernsdorfer, *J. Am. Chem. Soc.* **2005**, *127*. 3650. (d) D. Gatteschi, R. Sessoli, J. Villain, *Molecular Nanomagnets*, OXFORD UNIVERSITY PRESS, New York, **2006**.

19 (a) A. Caneschi, D. Gatteschi, N. Lalioti, R. Sessoli, G. Venturi, A. Vindigni, A. Rettori, M. G. Pini, M. A. Novak, *Angew. Chem. Int. Ed.* **2001**, *40,* 1760. (b) H. Miyasaka, R. Clérac, K. Mizushima, K. Sugiura, M. Yamashita, W. Wernsdofer, C. Coulon, *Inorg. Chem.* **2003**, *42*, 8203. (c) H. Miyasaka, R. Clérac, *Bull. Chem. Soc.*

Jpn. **2005**, *78*, 1725. (d) T. Kajiwara, M. Nakano, Y. Kaneko, S. Takaishi, T. Ito, M. Yamashita, A. Igashira-Kamiyama, H. Nojiri, Y. Ono, N. Kojima, *J. Am. Chem. Soc.* **2005**, *127*, 10150. (e) N. Ishii, T. Ishida, T. Nogami, *Inorg Chem.* **2006**, *45*, 3837. (f) K. Bernot, L. Bogani, A. Caneschi, D. Gatteschi, R. Sessoli, *J. Am. Chem. Soc.* **2006**, *128*, 7947.

20 (a) E. Coronado, J. R. Galan-Mascaros, C. J. Gomez-Garcia, V. Laukhin, *Nature* **2000**, *408*, 447. (b) K. Yamaguchi, T. Kawakami, T. Taniguchi, S. Nakano, Y. Kitagawa, H. Nagao, T. Ohsaku, R. Takeda, *Polyhedron* **2003**, *22*, 2077. (c) H. Akutsu, J. Yamada, S. Nakatsuji, S. S. Turner, *Solid State Commun.* **2006**, *140*, 256.

21 (a) A. W. Graham, M. Kurmoo, P. Day, *J. Chem. Soc., Chem. Commun.* **1995**, 2061. (b) S. Uji, H. Shinagawa, T. Terashima, T. Yakabe, Y. Terai, M. Tokumoto, A. Kobayashi, H. Tanaka, H. Kobayashi, *Nature* **2001**, *410*, 908. (c) H. Fujiwara, H. Kobayashi, *Bull. Chem. Soc. Jpn.* **2005**, *78*, 1181.

22 S. Karasawa, H. Kumada, N. Koga, H. Iwamura, *J. Am. Chem. Soc.* **2001**, *123*, 9685.

23 H. Cui, Z. Wang, K. Takahashi, Y. Okano, H. Kobayashi, A. Kobayashi, *J. Am. Chem. Soc.* **2006**, *128*, 15074.

24 (a) S. W. Loveseyand, G. I. Watson, *J. Phys.: Condense. Matter* **1998**, *10*, 6761. (b) V. P. Plakhty, W. Schweika, Th. Brückel, J. Kulda, S. V. Gavrilov, L-P. Regnault, D. Visser, *Phys. Rev. B* **2001**, *64*, 100402.

25 (a) K. Ohgushi, S. Murakami, N. Nagaosa, *Phys. Rev. B* **2000**, *62*, R6065. (b) S. A. Antonenko, A. I. Sokolov, K. B. Varnashev, *Phys. Rev. Lett.* **1995**, *A208*, 161.

26 (a) I. Dzyaloshinsky, *J. Phys. Chem. Soc.* **1958**, *4*, 241. (b) T. Moriya, *Phys. Rev.* **1960**, *120*, 91.

27 (a) T. Rasing, M. G. Koerkamp, B. Koopmans, *J. Appl. Phys.* **1996**, *79*, 6181. (b) *Magneto-Optics*, Eds. S. Sugano, N. Kojima, Springer, **2000**. (c) *Atarasii Jikito Hikarino Kagaku-sinzairyouto denbakouka,* Eds. S. Sugano, N. Kojima, K. Sato, K. Tsushima, Kodansha, **2001**; 新しい磁気と光の科学　新材料と電場効果，菅野暁，小島憲道，佐藤勝昭，対馬国郎　編，講談社 **2001**.

28 (a) G. Wagniere, A. Mejer, *Chem. Phys. Lett*, **1982**, *93*, 78. (b) L. D. Barron, J. Vrbancich, *Mol. Phys.* **1984**, *110*, 546.

29 (a) G. L. J. A. Rikken, E. Raupach, *Nature* **1997**, *390*, 493. (b) G. L. J. A. Rikken,

E. Raupach, *Nature* **2000**, *405*, 932. (c) H. Tachibana, H. Kishida, Y. Tokura, *Appl. Phys. Lett.* **2000**, *77*, 2443.

30 The examples of chiral structural magnet crystalized from achiral molecules, (a) A. Caneschi, D. Gateschi, P. Ray, R. Sessoli, *Inorg. Chem.* **1991**, *30*, 3936. (b) E. Gao, Y. Yue, S. Bai, Z. He, C. Yan, *J. Am. Chem. Soc.* **2004**, *126*, 1419. (c) W. Liu, Y. Song, Y. Li, Y. Zou, D. Dang, C. Ni, Q. Meng, *Chem. Commun.* **2004**, 2348. (d) L. Bogani, C. Sangregorio, R. Sessoli, D. Gateschi, *Angew. Chem. Int. Ed.* **2005**, *44*, 5817.

31 The examples of chiral structural magnet using with chiral template molecules. (a) M. Hernáckz-Molina, F. Lloret, C. Ruiz-Pérez, M. Julve, *Inorg. Chem.* **1998**, *37*, 4131. (b) E. Coronado, J. R. Galan-Mascaros, C. J. Gomez-Garcia, J. M. Martínez-Agudo, *Inorg. Chem.* **2001**, *40*, 113. (c) E. Coronado, J. R. Galán-Mascarós, C. J. Go´mez-García, J. M. Martínez-Agudo, *Inorg. Chem.* **2001**, *40*, 113.

32 (a) H. Kumagai, K. Inoue, *Angew. Chem. Int. Ed.* **1999**, *38*, 1601. (b) K. Inoue, H. Kumagai, A. S. Markosyan, *Synth. Met.* **2001**, *121*, 1772. (c) K. Inoue, H. Imai, P. S. Ghalasasi, K. Kikuchi, M. Ohba, H. Ōkawa, J. V. Yakhmi, *Angew. Chem. Int. Ed.* **2001**, *40*, 4242. (d) R. Andres, M. Brissard, M. Gruselle, C. Train, *Inorg. Chem.* **2001**, *40*, 4633. (e) P. S. Ghalasasi, K. Inoue, S. D. Samant, J. V. Yakhmi, *Polyhdron*, **2001**, *20*, 1495. (f) E. Coronado, C. J. Gómez-García, J. M. Martínez-Agudo, *Inorg. Chem.* **2002**, *41*, 4615. (g) K. Inoue, K. Kikuchi, M. Ohba, H. Ōkawa, *Angew. Chem. Int. Ed.* **2003**, *42*, 4810. (h) E. Coronado, C. Giménez-Saiz, J. M. Martínez-Agudo, A. Neuz, F. M. Romero, H. Stoeckli-Evans, *Polyhedron*, **2003**, *22*, 2435. (i) H. Imai, K. Inoue, K. Kikuchi, Y. Yoshida, M. Itoh, T. Sunahara, S. Onaka, *Angew. Chem. Int. Ed.* **2004**, *43*, 5618. (j) E. Coronado, J. R. Galán-Mascaróf, C. J. Gómez-García, A. Murcia-Martínez, E. Canadell, *Inorg. Chem.* **2004**, *43*, 8072. (k) K. Inoue, S. Ohkoshi, H. Imai, *Magnetism: Molecules to Materials V*, Eds. J. S. Miller, M. Drillon, Wiley-VCH, Weinheim, **2005**, Chap. 2, p. 41. (l) F. Cinti, M. Affronte, A. Lascialfari, M. Barucci, E. Olivieri, E. Pasca, A. Rettori, L. Risegari, G. Ventura, M. G. Pini, A. Cuccoli, T. Roscilde, A. Caneschi, D. Gatteschi, D. Rovai, *Polyhedron* **2005**, *24*, 2568. (m) H. Imai, K. Inoue, K. Kikuchi, *Polyhedron* **2005**, *24*, 2808. (n) E. Coronado, J. R. Galán-Mascaróf, C. J. Gómez-García, A. Murcia-Martínez, *Chem. Eur. J.* **2006**, *12*, 3484. (o) M.

Clemente-León, E. Coronado, C. J. Gómez-García, A. Soriano-Portillo, *Inorg. Chem.* **2006**, *45*, 5653. (p) E. Coronado, C. J. Gómez-García, A. Nuez, F. M. Romer, J. C. Waerenborgh, *Chem. Mater.* **2006**, *18*, 2670. (q) W. Kaneko, S. Kitagawa, M. Ohba, *J. Am. Chem. Soc.* **2007**, A.S.A.P. (r) Y. Numata, K. Inoue, N. Baranov, K. Kikuchi, *J. Am. Chem. Soc.* in revising.

33 (a) A. Hoshikawa, T. Kamiyama, A. Purwanto, K. Ohishi, W. Higemoto, T. Ishigaki, H. Imai, K. Inoue, *J. Phys. Soc. Jpn.* **2004**, *73*, 2597. (b) J. Kishine, K. Inoue, Y. Yoshida, *Prog. Theor. Phys. Suppi.* **2005**, *159*, 82.

34 Solid state NMR, ESR, XMCD, X-ray magnetic diffraction, neutron diffraction and other physical measurements of [Mn(*R* or *S*-pnH)(H_2O)][$Cr(CN)_6$]•H_2O (ref 32g) are in progress.

35 H. Kobayashi, T. Haseda, *J. Phys. Soc. Jpn.* **1964**, *19*, 765.

36 I. S. Jacob, P. E. Lawrence, *Phys. Rev.* **1967**, *164*, 866.

Chapter 2. Preparation, Structure and Magnetic Properties of Cyclic Dimer Complex, $[\{Co(hfac)_2\}\bullet BNO^{t\text{-}Bu}]_2$

(*J. Mag. Mag. Mat.* **2007**, *310*, 1847)

Chapter 2.

Preparation, Structure and Magnetic Properties of Cyclic Dimer Complex $[\{Co(hfac)_2\}\cdot BNO^{t\text{-}Bu}]_2$

2.1. Introduction

Mn^{III}, Fe^{II} and Co^{II} ions of high spin state have a large magnetic single ion anisotropy and the molecule-based magnets, which are containing these metal ions, show characteristic magnetic properties based on its anisotropy. For example, low dimensional Ising type magnets,[1] Single Molecule Magnets (SMMs)[2] and Single Chain Magnets (SCMs)[3] are cited as the candidates (please see Chapter 1). In particular, Co^{II} complexes such as $[Co(hfac)_2]$ and $[Co(Racetate)_2]$ are useful as the building units to construct molecule-based magnets,[4] because they are stable, and can be coordinated to unsaturated site (Figure 2–1). Additionally, because these complexes are neutral molecules, they are soluble to organic solvents, and reacted with neutral radicals auch as nitronylnitroxide, polynitroxide, verdazyl and thiazolyl radicals.

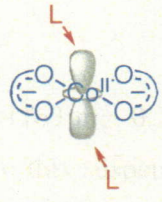

O = bidentate monoanionic ligand

L = bridging ligand

Figure 2–1.

To construct chiral molecule-based magnets, the author used $[Co(hfac)_2]$ and substituted BNO (BNO = 1,3-bis(*N*-*t*-butyl-*N*-oxylamino)benzene) radical. At first, the author tried to synthesis 1-D structural molecule-based magnet using non-chiral $BNO^{t\text{-}Bu}$ radical ($BNO^{t\text{-}Bu}$ = 1,3-bis(*N*-*t*-butyl-*N*-oxylamino)-5-*t*-butylbenzene), but this reaction gave discrete paramagnetic cyclic dimer complex, $[\{Co(hfac)_2\}\cdot BNO^{t\text{-}Bu}]_2$ (**1**). Although complex **1** was a paramagnet, it is a good example to estimate its magnetic parameters.

The author measured its magnetic properties and estimated its Curie constant C and average g_{eff} value, and in this chater, discribed and discussed about these results in this Chapter.

2.2. Preparation

$[Co(hfac)_2(H_2O)_2]$ and $BNO^{t\text{-}Bu}$ was synthesized according to literature methods.[5,6,7] All reactions are carried out under N_2 atmosphere with distilled solvents.

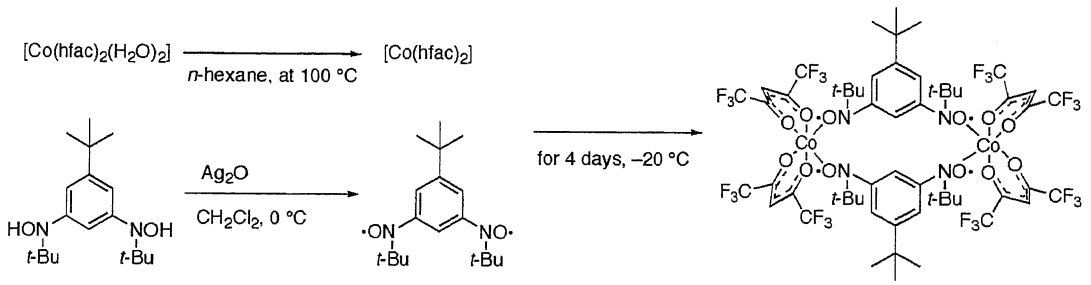

Scheme 2–1.

Synthetic details

A suspension of $[Co(hfac)_2(H_2O)_2]$ (163 mg, 0.32 mmol) in *n*-hexane was refluxed for 5 hours and cooled down to r. t. To this suspension, a few amount of diethylether was added to solve $[Co(hfac)_2]$. A suspension of 1,3-bis(*N*-*t*-butyl-*N*-hydroxyamino)-5-*t*-butylbenzene (100 mg, 0.32 mmol) in 20 mL of dichloromethane was cooled down to 0 °C with ice bath. To this suspension, silver(I)oxide (360 mg, 1.60 mmol) was added and stirred for 3 hours. This mixture was purified by silica gel column chromatography with dichloromethane as eluent to give deep orange solution of $BNO^{t\text{-}Bu}$. To the solution of $[Co(hfac)_2]$, a solution of $BNO^{t\text{-}Bu}$ was added and concentrated to ca. 20 mL in reduced pressure and cooled at –20 °C for 4 days, to give black prisms of **1** (121 mg, 42 %). $C_{58}H_{64}Co_2F_{24}N_4O_{12}$, fw = 1558.97, IR (KBr pellet) ν = 584, 669, 793, 1097, 1145, 1207, 1254, 1482, 1525, 1555, 1643, 2982, 3442 cm^{-1}.

2.3. Experimental Section

Physical measurement

Magnetic susceptibilities were measured by Quantum Design MPMS-5S SQUID magnetometer. Temperature dependences of magnetic susceptibilities were corrected by Pascal's constants. IR spectrum was measured on KBr disk with a JASCO FT/IR-660 plus spectrometer.

Crystallography

Single crystal of **1** using for X-ray crystallography was prepared by the described method in the preparation section. The single crystal was mounted on a glass fiber and its size was $0.25 \times 0.25 \times 0.20$ mm^3. The X-ray data were collected at r. t. with a Bruker SMART-APEX diffractometer, equipped with CCD area detector (graphite monochromated $Mo_{K\alpha}$ radiation, λ = 0.71073 Å, ω-scan mode (0.3 ° step), semi-empirical absorption correction on Laue equivalents). The structure was solved by direct method and refined by full-matrix least squares against F^2 of all data, using SIR-97 and SHELXTL softwares.[8,9] All non-hydrogen atoms were refined anisotropically. All hydrogen atoms were placed in calculated positions, and not refined. The refinement converges with R1 = 5.66 % for 3538 data ($I > 4\sigma(I)$), wR2 = 12.85 % for 14270 unique data ($1.31 \geq \theta \geq 28.45$), max/min residual electron density 0.37 / –0.27 eÅ^3.

2.4. Crystal Structure

Molecular and crystal structures of **1** are shown in Figure 2–2 and 2–3. and crystallographic data is presented in Table 2–1. Space group of **1** is monoclinic $P2_1/c$ (No. 14). This molecule has cyclic dimer structure which is consisting of two $[Co(hfac)_2]$ molecules are bridged by two $BNO^{t\text{-}Bu}$ molecules. Both of two Co ions have a distorted octahedral coordination environment and two $BNO^{t\text{-}Bu}$ radical molecules and two hfac molecules coordinate to Co ions by *cis*- conformations. Because two Co ions in the cyclic dimer, have Δ- and Λ- configurations, respectively, there is an inversion center at the central position of the dimer. Intramolecular Co–Co distance is 7.476 Å. The nearest intermolecular Co–Co distance is 9.492 Å. This value is judged as intermolecular magnetic interactions can be neglected in the high temperature region.

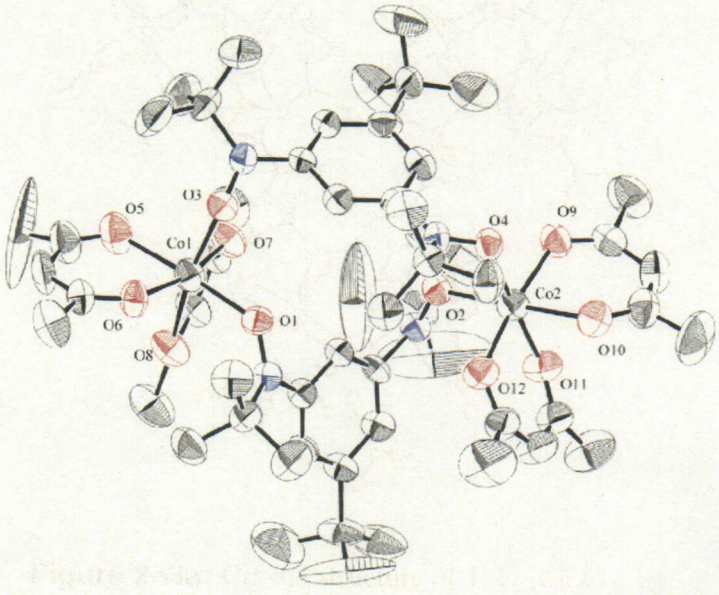

Figure 2–2. ORTEP drawing of molecular structure of **1**. Thermal ellipsoids are at the 50 % level. Hydrogen and fluorine atoms are omitted for clarify. Black labeled: Co, red: oxygen, blue: nitrogen and black non-labeled: carbon atoms.

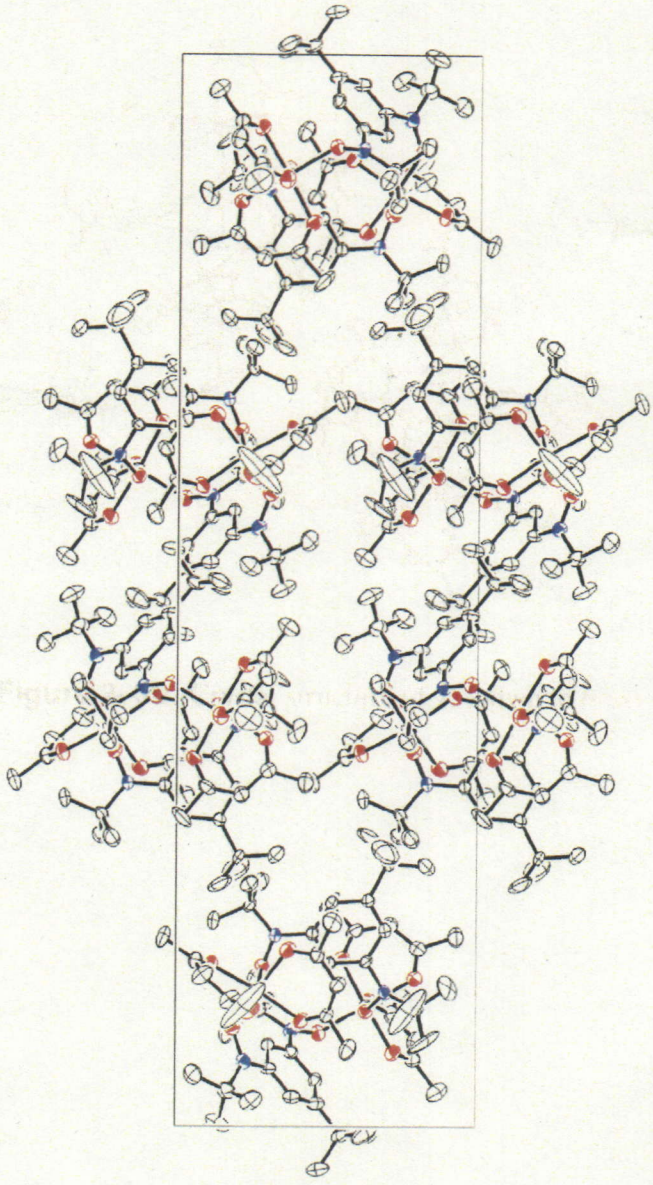

Figure 2–3a. Crystal structure of **1**. Down to *a*-axis.

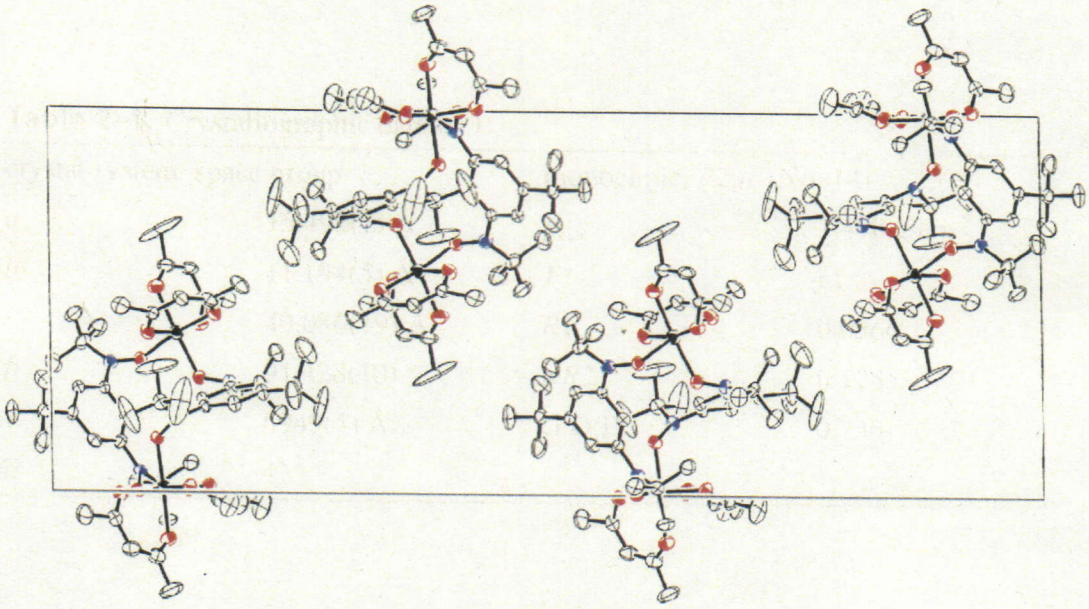

Figure 2–3b. Crystal structure of **1**. Down to *b*-axis.

Table 2–1. Crystallographic data of **1**.

crystal system, space group		monoclinic, $P2_1/c$ (No. 14)	
a	15.492(7) Å	ρ_{calc}	1.490 g cm^{-3}
b	11.194(5) Å	T	r.t.
c	40.086(19) Å	$R1$	0.0566
β	91.428(10) °	$wR2$	0.1285
V	6949(5) Å^3	G.O.F.	0.746
Z	4		

Table 2–2. Selected bond lengths (Å), bond angles (°) and atom–atom distances (Å).

Co1–Co2	7.476	nearest Co–Co$_{inter}$	9.492
Co1–O1	2.064(4)	Co2–O2	2.023(4)
Co1–O3	2.054(4)	Co2–O4	2.055(4)
Co1–O5	2.075(4)	Co2–O9	2.038(4)
Co1–O6	2.056(4)	Co2–O10	2.084(4)
Co1–O7	2.031(4)	Co2–O11	2.085(4)
Co1–O8	2.048(4)	Co2–O12	2.036(4)
O1–Co1–O5	175.57(17)	O2–Co2–O10	177.45(17)
O3–Co1–O8	170.57(16)	O4–Co2–O11	176.87(16)
O6–Co1–O7	167.15(16)	O9–Co2–O12	172.84(17)

2.5. Magnetic Properties

All magnetic measurements are carried out by polycrystalline samples. In the case of non-substituent BNO^H radical, its intramolecular ferromagnetic interaction (J_1 / k_B) estimated from ESR data was 430 K.[10] And in $[M(hfac)_2]_n$•$radical_m$ (M = Mn, Cu and Co) complexes, metal ions and coordinated radicals (J_2) are interacted antiferromagnetically. For example, in Mn complex which has similar structure with **1**, the magnetic interactions are reported as $J_1 > 0$ and $J_2 < 0$ and resulting this, its spin value is $S = 3$ ((5/2 – 1) × 2). In Figure 2–4, $1/\chi_m$ vs T and $\chi_m T$ vs T plots measured in applied field of 1 T are shown. The $\chi_m T$ curves have almost constant values in the temperature region from 300 to 50 K (2.194 ~ 2.140). Estimated Curie constant C from the fitting of $1/\chi_m$ vs T plot, was 2.162 emu K / Oe mol and $g_{eff} = 2.854$ using the equation 2. 1.

$$C = \frac{N_A (g_{eff})^2 (\mu_B)^2 S(S+1)}{3k_B} \quad (2.\ 1)$$

Here, $N_A = 6.022 \times 10^{23}$, $\mu_B = 9.274 \times 10^{-24}$, $S = 1$ and $k_B = 1.387 \times 10^{-23}$, considered from its centro-symmetrical molecular structure and C value, possible spin state is only $S = 1$. This value of 2.162 emu K / Oe mol can be assigned to the case of $S = 1$ with large magnetic anisotropy (theoretical value with $S = 1$ and $g = 2.00$ is 1.002 emu K / Oe mol). This result indicates that intramolecular magnetic interaction between Co ion and nitroxide radical is antiferromagnetic ($J_2 < 0$) and this molecule has large magnetic anisotropy. The magnetization value at high temperature limit, which is estimated by the extrapolation method from the $\chi_m T$ value at around 350 K, is ca. $5\mu_B$ (Figure 2–5). This value is further less than theoretical spin only value (approximately half value of $10\mu_B$ of $S = 5$ (= (1 + 3/2) × 2). This result is indicative of $J_{total} < 0$ at 350 K ($J_{total} = J_1 + J_2$). Below 50 K, the $\chi_m T$ values decreased and it reached to 0.380 emu K / Oe mol at 2 K. The origin of this decrease seems by the influence of intermolecular antiferromagnetic interactions in the low temperature region.

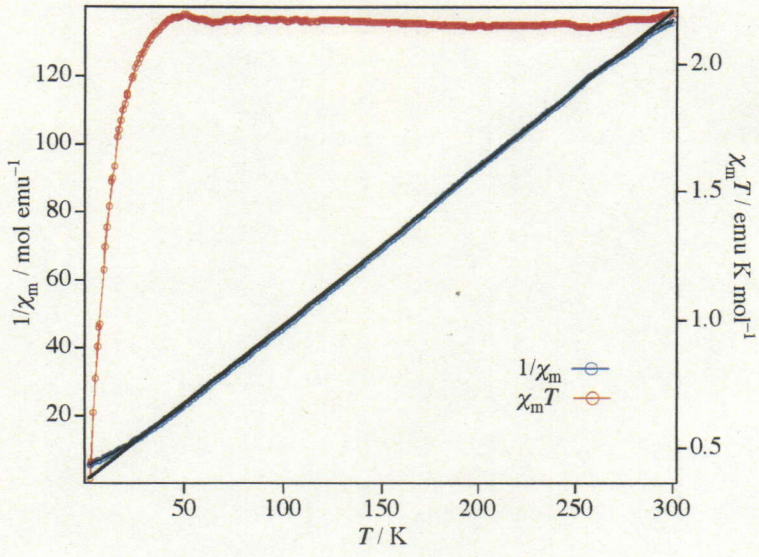

Figure 2–4. $1/\chi_m$ vs T (blue) and $\chi_m T$ vs T (red) plots. Black line is fitting of $1/\chi_m$ curve according to Curie-Weiss equation.

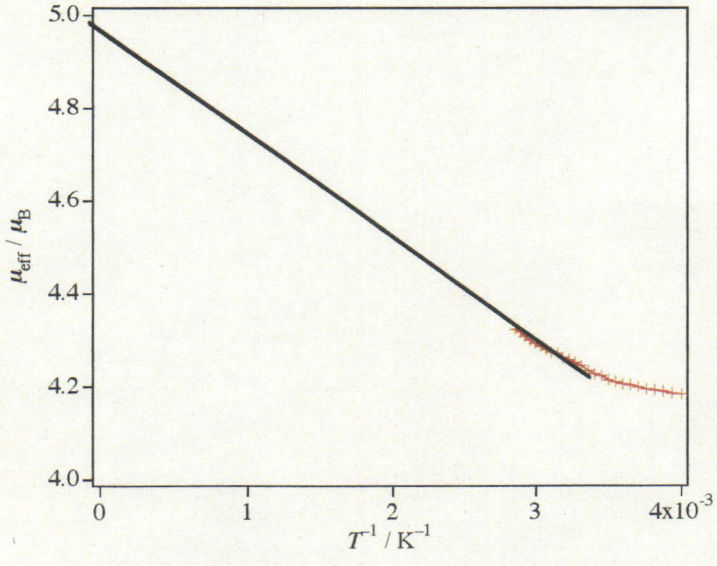

Figure 2–5. High temperature limit of μ_{eff}.

2.6. Conclusion

In summary, the author shows crystal structure and magnetic properties of cyclic dimer complex **1**. From crystal structure, its spin state is expected as $S = 1$. This molecule is paramagnetic and its estimated Curie constant is 2.162 emu K / Oe mol and $g_{eff} = 2.854$ using the Curie-Weiss equation (with $S = 1$). High temperature limit of effective magnetic moment estimated from $\chi_m T$ vs T plots at around 350 K, was ca. $5\mu_B$. This value is further few than theoretical spin only value $10\mu_B$. Though this cyclic dimer didn't have magnetic transition, they are revealed that Co radical system has strong intramolecular magnetic interactions between Co ion and BNO radical and large magnetic anisotropies from magnetic data.

2.7. References

1 (a) J. S. Miller, J. Calabrese, R. S. McLean, A. J. Epstein, *Adv. Mater.* **1992**, *4*, 498. (b) J. S. Miller, C. Vazquez, N. L. Jones, R. S. McLean, A. J. Epstein, *J. Mater. Chem.* **1995**, *5*, 707. (c) C. M. Wynn, M. A. Gîrţu, K. Sugiura, E. J. Brandon, J. L. Manson, J. S. Miller, A. J. Epstein, *Synth. Met.* **1997**, *85*, 1695. (d) C. M. Wynn, M. A. Gîrţu, J. S. Miller, A. J. Epstein, *Phys. Rev. B* **1997**, *56*, 14050. (e) L. N. Dawe, J. Miglioi, L. Turnbow, M. L. Taliafferro, W. W. Shum, J. D. Bagnato, L. N. Zakharov, A. L. Rheingold, A. M. Arif, M. Fourmigué, J. S. Miller, *Inorg. Chem.* **2005**, *44*, 7530.

2 (a) A. Caneschi, D. Gatteschi, R. Sessoli, A. L. Barra, L. C. Brunel, M. Guillot, *J. Am. Chem. Soc.* **1991**, *113*, 5873. (b) D. Gatteschi, R. Sessoli, *Angew. Chem. Int. Ed.* **2003**, *42*, 268. (c) N. Ishikawa, M. Sugita, W. Wernsdorfer, *J. Am. Chem. Soc.* **2005**, *127*. 3650. (d) D. Gatteschi, R. Sessoli, J. Villain, *Molecular Nanomagnets*, OXFORD UNIVERSITY PRESS, New York, **2006**.

3 (a) A. Caneschi, D. Gatteschi, N. Lalioti, R. Sessoli, G. Venturi, A. Vindigni, A. Rettori, M. G. Pini, M. A. Novak, *Angew. Chem. Int. Ed.* **2001**, *40,* 1760. (b) H. Miyasaka, R. Clérac, K. Mizushima, K. Sugiura, M. Yamashita, W. Wernsdofer, C. Coulon, *Inorg. Chem.* **2003**, *42*, 8203. (c) H. Miyasaka, R. Clérac, *Bull. Chem. Soc. Jpn.* **2005**, *78*, 1725. (d) T. Kajiwara, M. Nakano, Y. Kaneko, S. Takaishi, T. Ito, M. Yamashita, A. Igashira-Kamiyama, H. Nojiri, Y. Ono, N. Kojima, *J. Am. Chem. Soc.* **2005**, *127*, 10150. (e) N. Ishii, T. Ishida, T. Nogami, *Inorg Chem.* **2006**, *45*, 3837. (f) K. Bernot, L. Bogani, A. Caneschi, D. Gatteschi, R. Sessoli, *J. Am. Chem. Soc.* **2006**, *128*, 7947.

4 (a) A. Caneschi, D. Gatteschi, N. Lalioti, R. Sessoli, G. Venturi, A. Vindigni, A. Rettori, M. G. Pini, M. A. Novak, *Angew. Chem. Int. Ed.* **2001**, *40,* 1760. (b) H. Miyasaka, R. Clérac, K. Mizushima, K. Sugiura, M. Yamashita, W. Wernsdofer, C. Coulon, *Inorg. Chem.* **2003**, *42*, 8203. (c) H. Miyasaka, R. Clérac, *Bull. Chem. Soc. Jpn.* **2005**, *78*, 1725. (d) T. Kajiwara, M. Nakano, Y. Kaneko, S. Takaishi, T. Ito, M. Yamashita, A. Igashira-Kamiyama, H. Nojiri, Y. Ono, N. Kojima, *J. Am. Chem. Soc.* **2005**, *127*, 10150. (e) N. Ishii, T. Ishida, T. Nogami, *Inorg Chem.*

2006, *45*, 3837. (f) K. Bernot, L. Bogani, A. Caneschi, D. Gatteschi, R. Sessoli, *J. Am. Chem. Soc.* **2006**, *128*, 7947.

5 (a) M. A. Petrukhina, C. Henck, B. Li, E. Block, J. Jin, S. Zhang, R. Clerac, *Inorg. Chem.* **2005**, *44*, 77. (b) R. I. Pecsok, W. D. Reynolds, J. P. Fackler Jr., I. Lin, J. Pradilla-Sorzano, *Inorg. Synth.* **1974**, *15*, 96.

6 (a) F. Kanno, K. Inoue, N. Koga, H. Iwamura, *J. Phys. Chem.* **1993**, *97*, 13267. (b) F. Kanno, Master Thesis, University of Tokyo, **1992**.

7 G. Görlitz, T. Hayamizu, T. Itoh, K. Matsuda, H. Iwamura, *Inorg. Chem.* **1998**, *37*, 2083.

8 A. Altmare, M. C. Burla, M. Camalli, G. L. Gascarano, C. Giacovazzo, A. Guaglirdi, G. G. Molitemi, G. Polidori, R. Spagna, SIR-97, *J. Appl. Cryst.* **1999**, *32*, 115.

9 G. M. Sheldrick, SHEXL-97, University of Göttingen, Germany. **1997**.

10 (a) A. Calder, A. R. Forrester, P. G. James, G. R. Luckhurst, *J. Am. Chem. Soc.* **1969**, *91*, 3724. (b) Y. Hosokoshi, K. Katoh, Y. Nakazawa, H. Nakano, K. Inoue, *J. Am. Chem. Soc.* **2001**, *123*, 7921.

Chapter 3.

Field-induced Ferrimagnetic State in a New Molecule-based Magnet Consisting of Co^{II} ion and Chiral π-conjugated Triplet Radical

3.1. Introduction

In Chapter 1, the author showed interesting points of low dimensional magnets and explained that D-M interaction is proprtional to Δg ($\Delta g = g_{eff} - 2.00$). In Chapter 2, it was revealed that [Co(hfac)$_2$]–BNO system, even if it was discrete paramagnetic compounds, has a large magnetic anisotropy based on single ion anisotropy of Co^{II}. In consideration of these results, the author employed chiral bisnitroxide radical, BNO* and [Co(hfac)$_2$] as building blocks to prepare chiral structural magnets, which has strong magnetic anisotropy. The reaction between BNO* and [Co(hfac)$_2$] gave novel metamagnetic compound [Co(hfac)$_2$]•BNO* (**2**) (Chart 3–1). This molecule forms 1-D alternate chain structure and has chiral space group, triclinic *P*1. In thiese 1-D chains, magnetic spins aligne ferrimagnetically. This compound showed two magnetic phase transitions at around 4 and 20 K. At first, antiferromagnetic transition exists at 20 K and spin flip transition occurrs in certain applied magnetic field in the temperature range of 4 ~ 20 K. Consequently, at around 4 K, second transition occurrs. Below 4 K, large coercivity can be observed and its value reaches ca. 2.5 T at 2 K. In this Chapter, the author describes preparation, crystal structure, dc and ac magnetic properties and magnetic phase diagram.

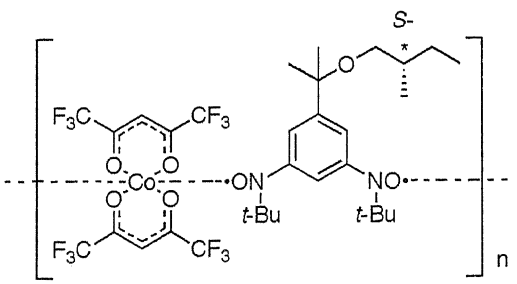

Chart 3–1.

3.2. Preparation

1,3,5-Tribromobenzene,[1] $[Co(hfac)_2(H_2O)_2]$[2] and BNOH*[3] were synthesized according to literature methods. *p*-Toluenesulfonylchloride, (*S*)-3-methyl-1-butanol, Ag_2O are commercially available.

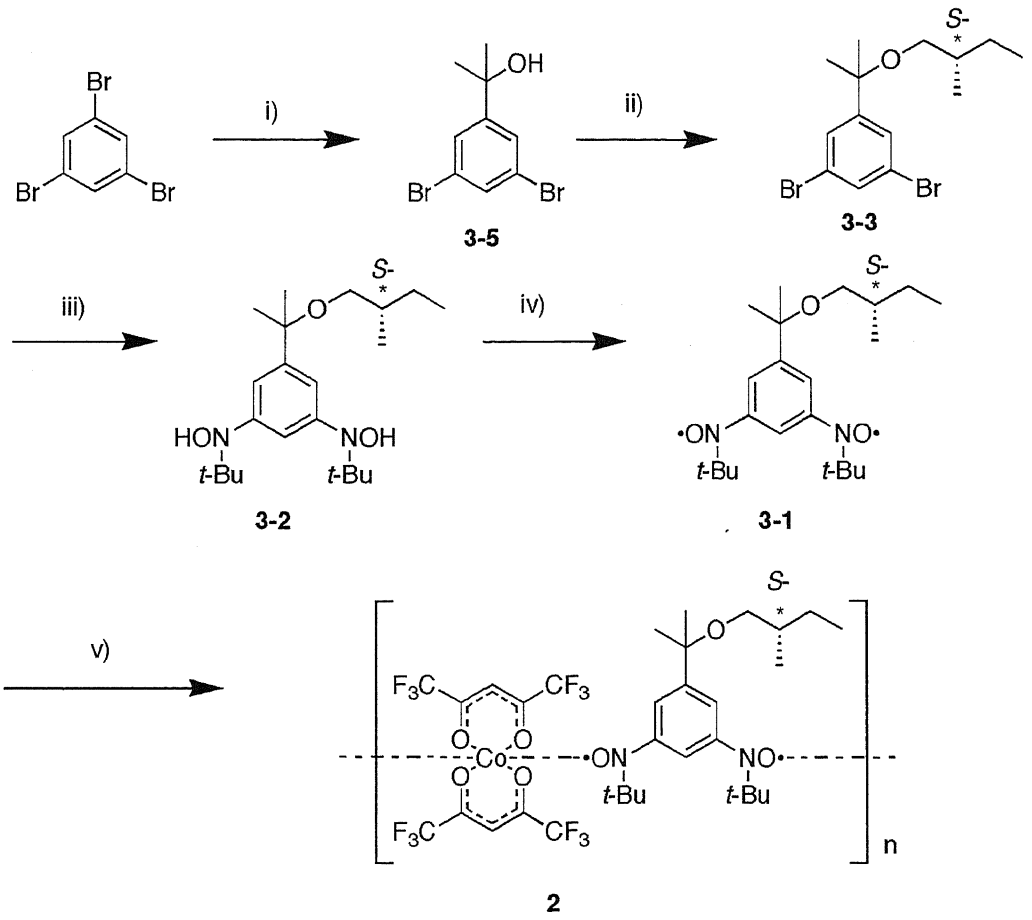

Scheme 3–1. Synthesis rout of **2**. i) *t*-BuLi, Et_2O, acetone, –78 °C, 2 steps, ii) KOH, TsO-(*S*)-*i*-amyl, diglyme, 110 °C, iii) *t*-BuLi, Et_2O, *t*-BuNO, –78 °C, 2steps, iv) Ag_2O, CH_2Cl_2, 0 °C, v) $[Co(hfac)_2]$, r.t.

Synthetic details

1,3-Dibromo-5-{(1'-hydroxy-1'-methyl)ethyl}benzene (3-5). To a solution of 1,3,5-tribromobenzene (2.00 g, 6.35 mmol) in 30 ml of distilled diethylether, 1.46 M *tert*-butyllithium (8.86 mL, 13.02 mmol) *n*-pentane solution was slowly added at –78 °C, and the mixture was warmed up to –30 °C and stirred for 2 h. Distilled acetone (0.5 mL, 6.67 mmol) was added to the solution and stirred for 4 h. After addition of aqueous solution of NH_4Cl and diethylether, organic layer was separated, washed with water and dried over anhydrous $MgSO_4$, concentrated under reduced pressure. The orange oil was chromatographed on silica gel and *n*-hexane as eluent at first, subsequently flashed with diethylether. The diethylether fraction was concentrated and distilled in reduced pressure (5 mmHg, 105 °C) to give 1.54 g (82.5 %) of **3-5** as colorless crystals. ^1H NMR (400 MHz, $CDCl_3$) δ 7.55 (d, 2H), δ 7.53 (d, 1H), δ 1.54 (s, 6H).

(*S*)-2-Methylbutyloxyltoluenesulfonyl (3-4). To a solution of *p*-toluenesulfonylchloride (8.87 g 46.5 mmol) in 20 mL of pyridine, (*S*)-3-methyl-1-butanol (5.0 ml, 46.5 mmol) was added and stirred at 0 °C for 1 day. To this suspension, water and *n*-hexane were added and separated. The organic layer was neutralized by dilute hydrochloric acid, and separated again. The organic layer was dried with $MgSO_4$ and $NaHCO_3$, filtrated and concentrated in reduced pressure to give 9.50 g (84.7 %) of **3-4** as colorless oil. ^1H NMR (400 MHz, $CDCl_3$) δ 7.78 (d, 2H), δ 7.34 (d, 2H), δ 3.84 (m, 2H), δ 2.45 (s, 3H), δ 1.71 (m, 1H), δ 1.39 (m, 1H), δ 1.14 (m, 1H), δ 0.87 (d, 3H), δ 0.82 (t, 3H).

1,3-Dibromo-5-(1'-methyl-1'-{2"-(*S*)-methylbutoxy}ethyl)benzene (3-3). To a solution of **3-4** (1.0 g, 3.40 mmol) in 20 mL of diethyleneglycoledimethyldiethylether (diglyme), ground KOH (85 %) powder (422 mg, 6.80 mmol) was added in small fractions and stirred for 2 h at room temperature. After color of the solution changed to red, then, it was warmed up to 110 °C. A solution of **3-5** (0.82 g, 3.40 mmol) in 20 mL of diglyme was slowly added to the mixture during 3 h, and stirred until color of the solution changed to cream yellow. To the mixture, 10 mL of water was added and separated, dried over with anhydrous $MgSO_4$, filtrated and concentrated in reduced

pressure to give 773 mg (62.4 %) of **3-3** as colorless oil. ^{1}H NMR (400 MHz, $CDCl_3$) δ 7.53 (d, 1H), δ 7.47 (d, 2H), δ 2.95 (m, 2H), δ 1.59 (m, 2H), δ 1.47 (m, 6H), δ 1.12 (m, 1H), δ 0.88 (q, 6H).

1,3-Bis(*N*-*tert*-butyl-*N*-hydroxyamino)-5-(1'-methyl-1'-{2"-(*S*)-methylbutoxy}-ethyl)benzene (3-2). A solution of (1.0 g, 2.75 mmol) in 20 mL of diethylether was cooled down to –78 °C, and 1.46 M *tert*-butyllithium (7.6 mL, 11.14 mmol) *n*-pentane solution was slowly added to the solution. The mixture was warmed gradually up to –30 °C and stirred for 2 h. A solution of 2-methyl-2-nitrosopropane dimer (0.49 g, 5.64 mmol) in 10 mL of diethylether was added in small fractions to the solution and stirred for 3 h at –30 °C. After addition of aqueous solution of NH_4Cl and diethylether, organic layer was separated, washed with water and dried over anhydrous $MgSO_4$, filtrated and concentrated in reduced pressure. To the mixture, a little amount of *n*-hexane was added and cooled for 1 day at –20 °C, 567 mg (54.2 %) of white powder of **3-2** was given. ^{1}H NMR (400 MHz, $CDCl_3$) δ 7.05 (s, 1H), δ 6.89 (s, 2H), δ 2.91 (m, 2H), δ 1.58 (m, 4H), δ 1.37 (m, 6H), δ 1.15 (m, 18H), δ 1.04 (q, 1H), δ 0.84 (m, 6H).

1,3-Bis(*N*-*tert*-butyl-*N*-oxylamino)-5-(1'-methyl-1'-{2"-(*S*)-methylbutoxy}ethyl)-ben zene (3-1). A solution of **3-2** (100 mg, 0.26 mmol) in 15 mL of dichloromethane was cooled by ice bath to 0 °C and to this solution, Ag_2O (500 mg, 2.16 mmol) was added, stirred for 2 h. The mixture was purified by silica gel column chromatography with dichloromethane as eluent to give 98 mg (98 %) of **3-1** as orange oil. It was consequently used for next step.

[Co(hfac)$_2$]•BNO* (2). [Co(hfac)$_2$(H_2O)$_2$] (132 mg, 0.26 mmol) was refluxed in *n*-hexane to remove water of hydration by azeotropic distillation. To this solution, a solution of BNO* (98 mg, 0.26mmol) in dichloromethane was added and stirred for 30 minutes at 80 °C. The mixture was cooled at –20 °C for 1 week to give 106 mg (47.8 %) of the dark red crystals of **2**. This crystal was suitable for X-ray measurement. Anal. calcd. for $C_{32}H_{40}CoF_{12}N_2O_7$ (**2**): C, 45.13; H, 4.73; N, 3.29. Found: C, 45.75; H, 4.05; N, 3.29. IR (KBr); ν = 1644, 1554, 1504, 1257, 1196, 1150, 795, 669, 587 cm^{-1}.

3.3. Experimental Section

Physical measurement.

Dc and ac magnetic susceptibilities were measured by Quantum Design MPMS-XL SQUID magnetometer. Temperature dependences of magnetic susceptibilities were corrected by Pascal's constants. IR spectrum was measured on KBr disk with a JASCO FT/IR-660 plus spectrometer.

Crystallography.

Single crystal of **2** using for X-ray crystallography was prepared by the described method in the preparation section. The single crystal was mounted on a glass fiber and its size was 0.50 × 0.25 × 0.18 mm^3. The X-ray data were collected at 100 K with a Bruker SMART-APEX diffract meter, equipped with CCD area detector (graphite monochromated $Mo_{K\alpha}$ radiation, λ = 0.71073 Å, ω-scan mode (0.3 ° step), semi-empirical absorption correction on Laue equivalents). The structure was solved by direct method and refined by full-matrix least squares against F^2 of all data, using SIR-97 and SHELXTL softwares.[4,5] All non-hydrogen atoms were refined anisotropically. All hydrogen atoms were placed in calculated positions, and not refined. The refinement converges with R1 = 7.14 % for 7856 data ($I > 4\sigma(I)$), wR2 = 19.60 % for 9717 unique data ($1.18 \geq \theta \geq 28.39$), Flack parameter = –0.03(2), max/min residual electron density 1.34 / –1.03 $e\text{Å}^3$.

3.4. Crystal Structure

X-ray structural analysis of **2** revealed the identity of the triclinic *P*1 (No. 1) space group and crystallographic data are presented in Table 3–1. In the unit cell, there are two crystallographically independent units of $[Co(hfac)_2]$•BNO*. $[Co(hfac)_2]$ and BNO* radical form a uniform one-dimensional *R*-type helical chain structure along the crystallographic *c*-axis. Figure 3–1 is a view of the 1-D chain structure. In the unit cell, there is only one helical chain which consistents of two different $[Co(hfac)_2]$•BNO* units. The aminoxyl groups of BNO* are rotated out of the phenylene ring plane. The chiral substitute of all BNO* molecules have the *R*- configuration. These alkyl groups are situated between the 1-D chains; therefore, the interchain distances are elongated (Figure 3–2). All Co ions, which exhibit octahedral coordination with the four oxygen atoms of two hfac ligands and the two oxygen atoms of the aminoxyl groups of two different molecules of BNO* in *trans*- configurations. The $Co\text{-}O_{hfac}$ bond lengths are ranging from 2.037(5) to 2.056(6) Å and $Co\text{-}O_{rad}$ are ranging from 2.075(6) to 2.096(6) Å. The bond angles made by two oxygen atoms located at the diagonal corners of coordination octahedra and central Co ion are almost 180 ° (The angles lie in the range 178.4(3)–179.5(3) °). The intrachain Co-Co distances of Co(1)-Co(2) and Co(2)-Co(1') are 8.722 Å and 8.696 Å, respectively; additionally, the shortest interchain Co-Co distance is 10.697 Å. Other selected Co–Co distances are predicted in Figure 3–3. Selected bond lengths, bond angles, torsion angles and intrachain Co–Co distances are given in Table 3–2.

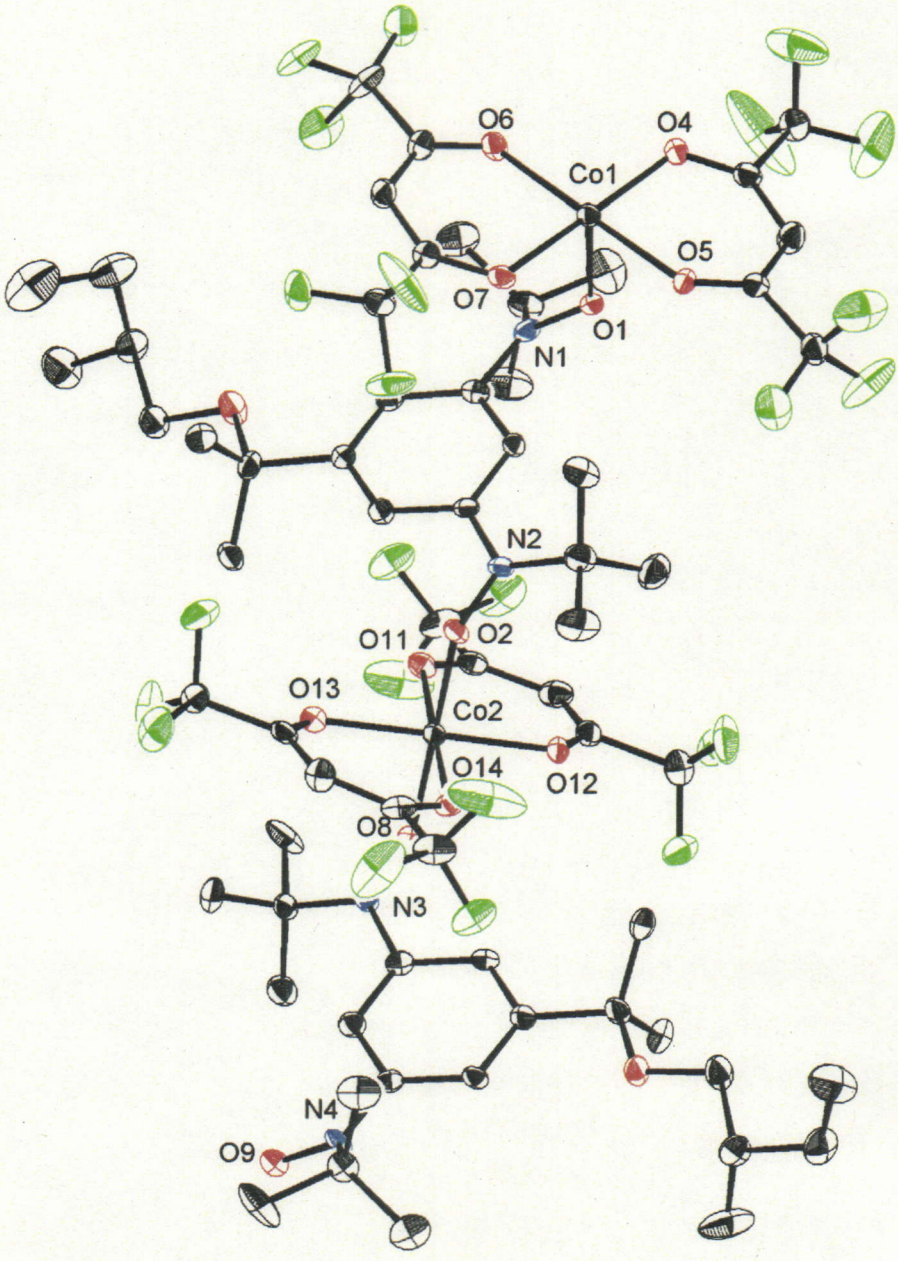

Figure 3–1. ORTEP drawing of **2**. Thermal ellipsoids are at the 40 % level. Hydrogen atoms are omitted for clarify. Co are labeled black, red: oxygen, blue, nitrogen, green: fluorine and black: carbon.

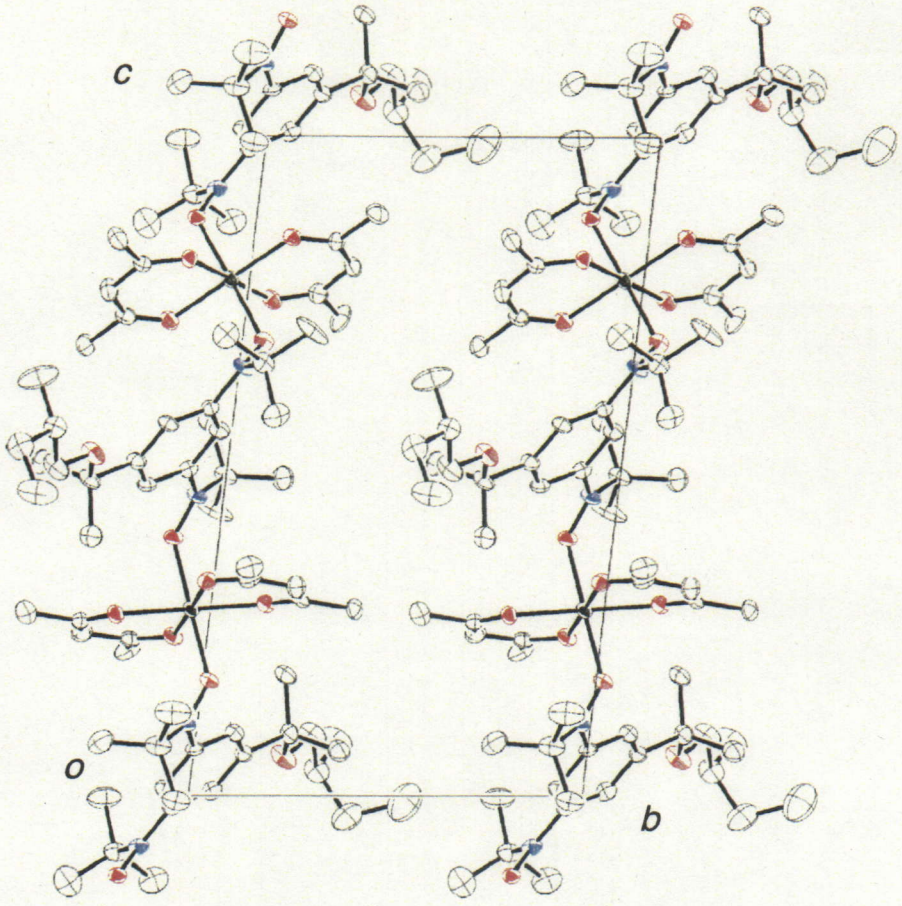

Figure 3–2a. Projections of crystal structures of **2** down to *a*-axis.

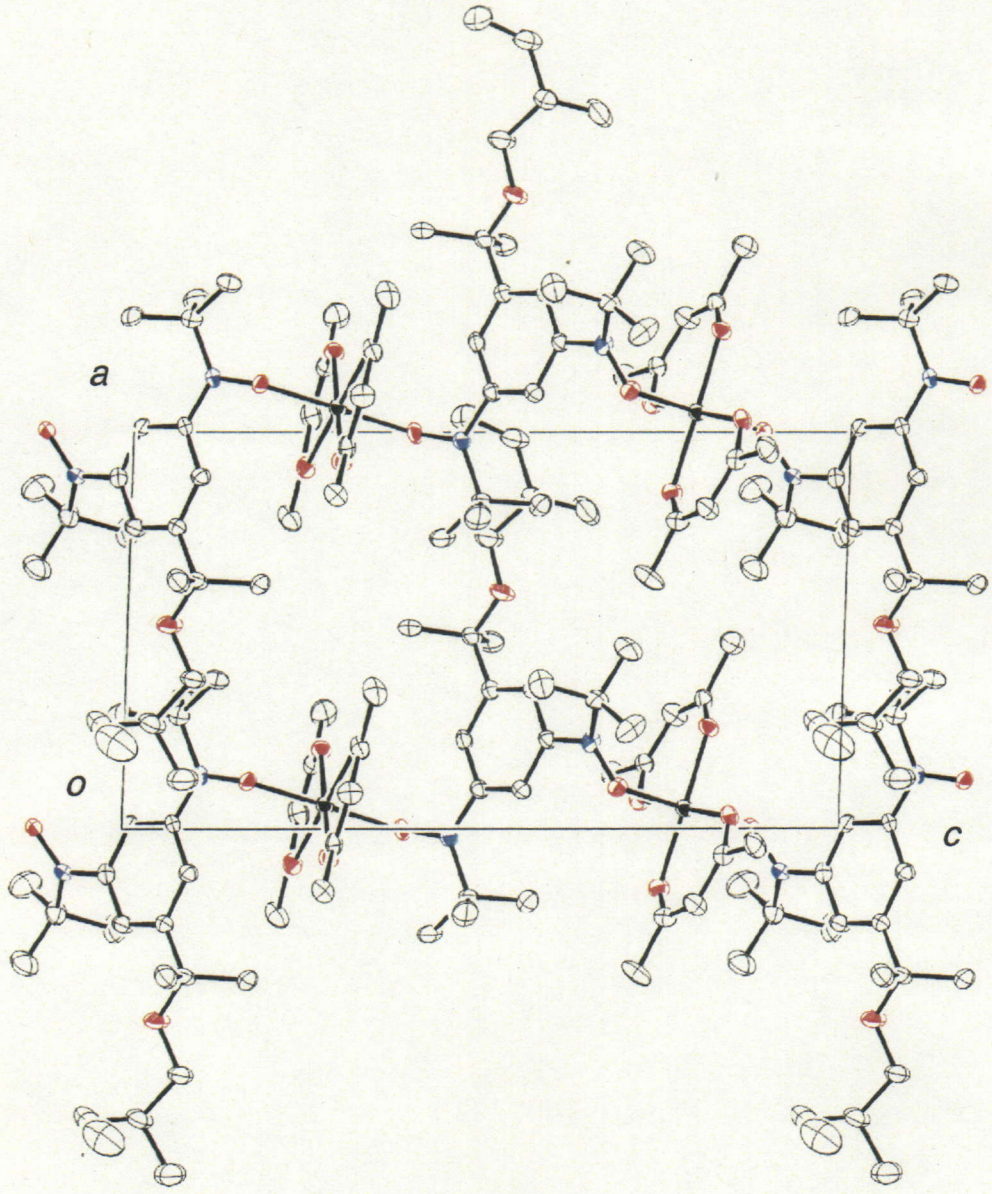

Figure 3–2b. Projections of crystal structures of **2** down to *b*-axis,

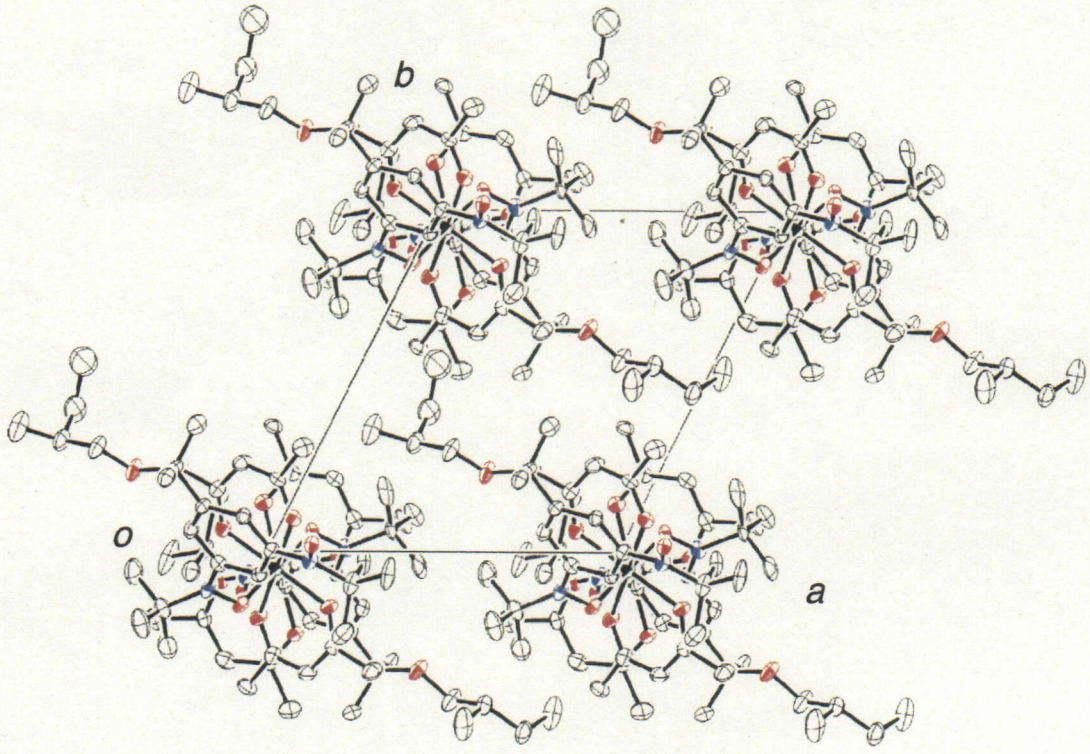

Figure 3–2c. Projections of crystal structures of **2** down to *c*-axis.

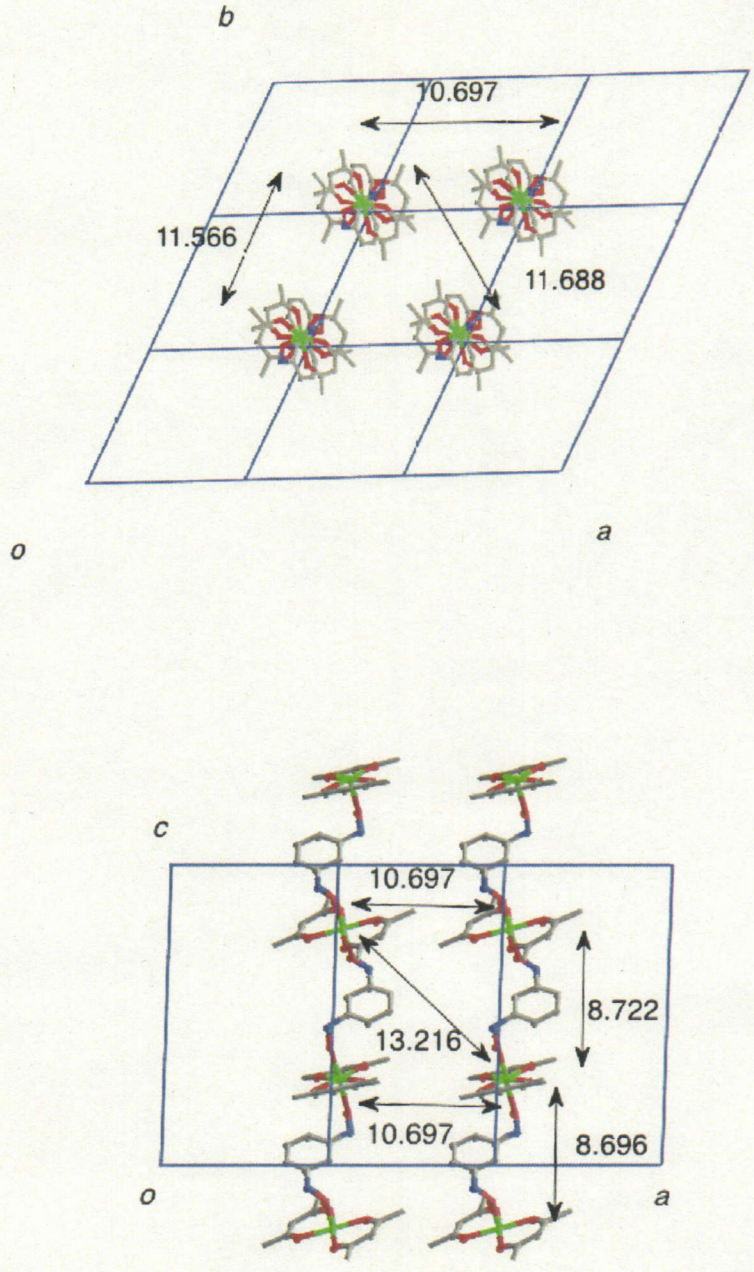

Figure 3–3. Intra- and Interchain Co–Co distances (Å) of **2**.

Table 3–1. Crystallographic data of **2**.

formula	$C_{32}H_{40}CoF_{12}N_2O_7$
mol. wt.	851.59
crystal system	triclinic
space group	*P*1 (No. 1)
a, Å	10.704(4)
b, Å	11.573(5)
c, Å	17.429(7)
α, °	81.647(7)
β, °	84.643(7)
γ, °	63.195(6)
V, Å^3	1905.6(14)
Z	2
no. of ref., unique	9717
no. of ref., used	7856
G. O. F.	1.000
*R*1 (*wR*2)	0.0714 (0.1960)
flack factor	–0.03(2)

Table 3–2. Selected bond lengths, bond angles, torsion angles and intrachain Co-Co distances.

Co1		Co2	
Co1–O1 2.075(6)		Co2–O2 2.093(5)	
Co1–O9' 2.081(5)	N1–O1 1.303(9)	Co2–O8 2.096(6)	N3–O8 1.283(9)
Co1–O4 2.054(6)	N2–O2 1.296(9)	Co2–O11 2.037(5)	N4–O9 1.286(9)
Co1–O5 2.048(5)	Co1–Co2 8.722	Co2–O12 2.046(5)	Co2–Co1' 8.696
Co1–O6 2.056(6)		Co2–O13 2.040(6)	
Co1–O7 2.049(6)		Co2–O14 2.056(6)	
O1–Co1–O9' 179.1(3)		O11–Co2–O14 179.0(3)	O8–Co2–O14 95.1(2)
O4–Co1–O7 179.5(3)	O5–Co1–O7 92.2(2)	O12–Co2–O13 178.4(3)	O11–Co2–O12 88.5(2)
O5–Co1–O6 179.3(3)	O5–Co1–O9 93.4(2)	O2–Co1–O8 179.3(3)	O11–Co2–O13 93.1(2)
O1–Co1–O4 86.1(2)	O6–Co1–O7 88.5(2)	O2–Co2–O11 95.9(2)	O12–Co2–O14 90.7(2)
O1–Co1–O5 85.7(2)	O6–Co1–O9 86.3(2)	O2–Co2–O12 94.4(2)	O13–Co2–O14 87.7(2)
O1–Co1–O6 94.6(2)	O7–Co1–O9 86.4(2)	O2–Co2–O13 85.2(2)	O8–N3–C33–C38 −15.4(10)
O1–Co1–O7 93.8(2)	O1–N1–C1–C6 150.2(7)	O2–Co2–O14 84.8(2)	O9–N4–C35–C36 −150.5(7)
O4–Co1–O5 88.3(2)	O2–N2–C3–C4 16.0(10)	O8–Co2–O11 84.2(2)	
O4–Co1–O6 91.0(2)		O8–Co2–O12 86.5(2)	
O4–Co1–O9 93.7(2)		O8–Co2–O13 94.0(2)	

3.5. Magnetic Properties

The *m*-phenylene-bisnitroxide radicals have the triplet ground state; moreover its intramolecular ferromagnetic interaction, J_1/k_B is large as 430 K for non-chiral BNO^H (BNO^H = 1,3-bis(*N*-*tert*-butyl-*N*-oxylamino)benzene) (Figure 3–4).[6]

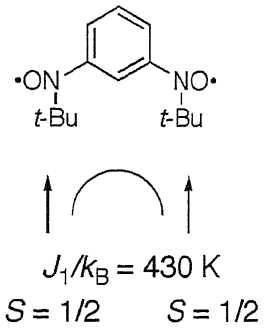

Figure 3–4. Intramolecular magnetic interaction of BNO^H.

The magnetic interaction between nitroxide radical and Co^{II} ion (J_2) appears to be antiferromagnetic owing to the overlapping magnetic orbital of the nitroxide radical and Co^{II}. This value is not available in the literature; however it is observed as $J_2 \ll 0$ (There are strong antiferromagnetic interactions).[7] All magnetic measurements were performed for the polycrystalline sample. The $\chi_m T$ and $1/\chi_m$ vs T plots are presented in Figure 3–5. The $\chi_m T$ values have a minimum at 220 K, which suggests the presence of the ferrimagnetic interaction within chains in **2**. Considering the molecular structure of **2**, this ferrimagnetic spin arrangement is assigned to –NO•···Co···•ON– (S = –1/2, 3/2, –1/2) (Figure 3–6). Weiss temperature, θ, which was estimated from the $1/\chi_m$ vs T plot as –89.9 K in the temperature range of 220 – 300 K, indicates $J_2 \ll 0$.

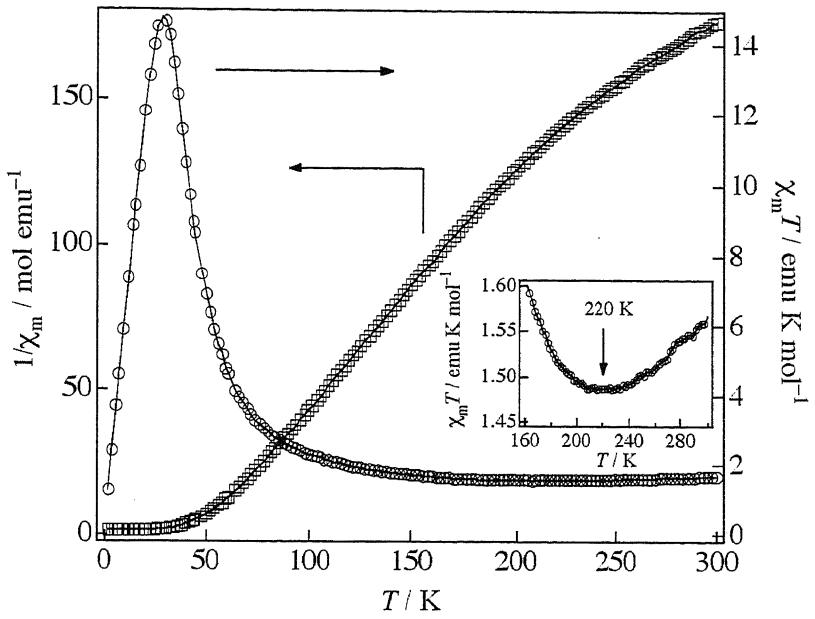

Figure 3–5. $1/\chi_m$ vs T (circle) and $\chi_m T$ vs T (square) plots measured in 1 T. Inset: magnification of the $\chi_m T$ curve at around minimum point.

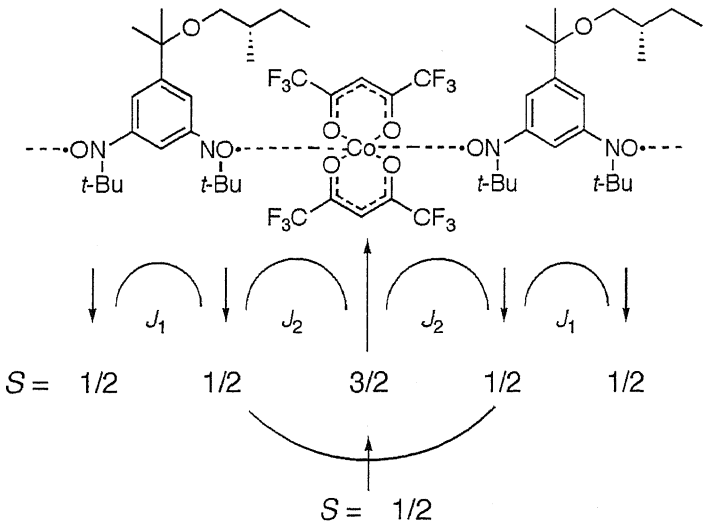

Figure 3–6. Magnetic interactions in 1-D chain structure of **2**.

The peak temperatures in M–T curves are around 20 K and shift to lower temperatures by increasing dc field (Figure 3–7) which is indicative of the appearance of an antiferromagnetic (AF) long-range order below $T_N \approx 20$ K.

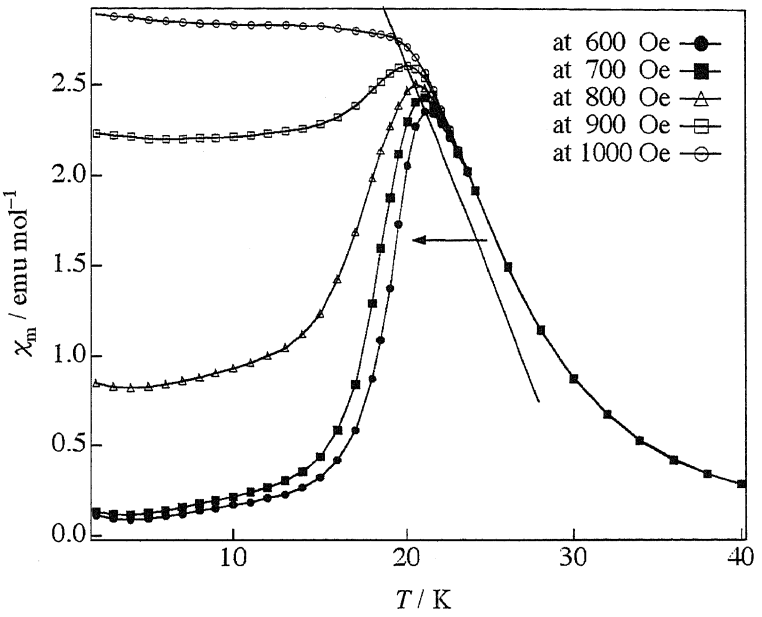

Figure 3–7. Magnetic field dependent peak top shift.

The magnetic susceptibility for zero field-cooled (χ_{ZFC}) sample and field-cooled sample (χ_{FC}) were measured at 500 Oe and 5000 Oe (Figure 3–8). At 500 Oe, the χ_{ZFC} and χ_{FC} exhibit similar values in the temperature region of 4 – 100 K. At temperatures $4 < T < 16$ K, a shoulder is evident for both of χ_{ZFC} and χ_{FC}. This shoulder indicates that another phase transition occurs at around this temperature range. At 4 K, the χ_{ZFC} value increases abruptly; subsequently, it saturates and decreases gradually with further increasing temperature. Below 4 K, $\chi_{ZFC}(T)$ and $\chi_{FC}(T)$ are split and demonstrate constant values below 3.2 K. At 5000 Oe, the χ_{ZFC} value is also a constant in the temperature range of 2 – 3.2 K.

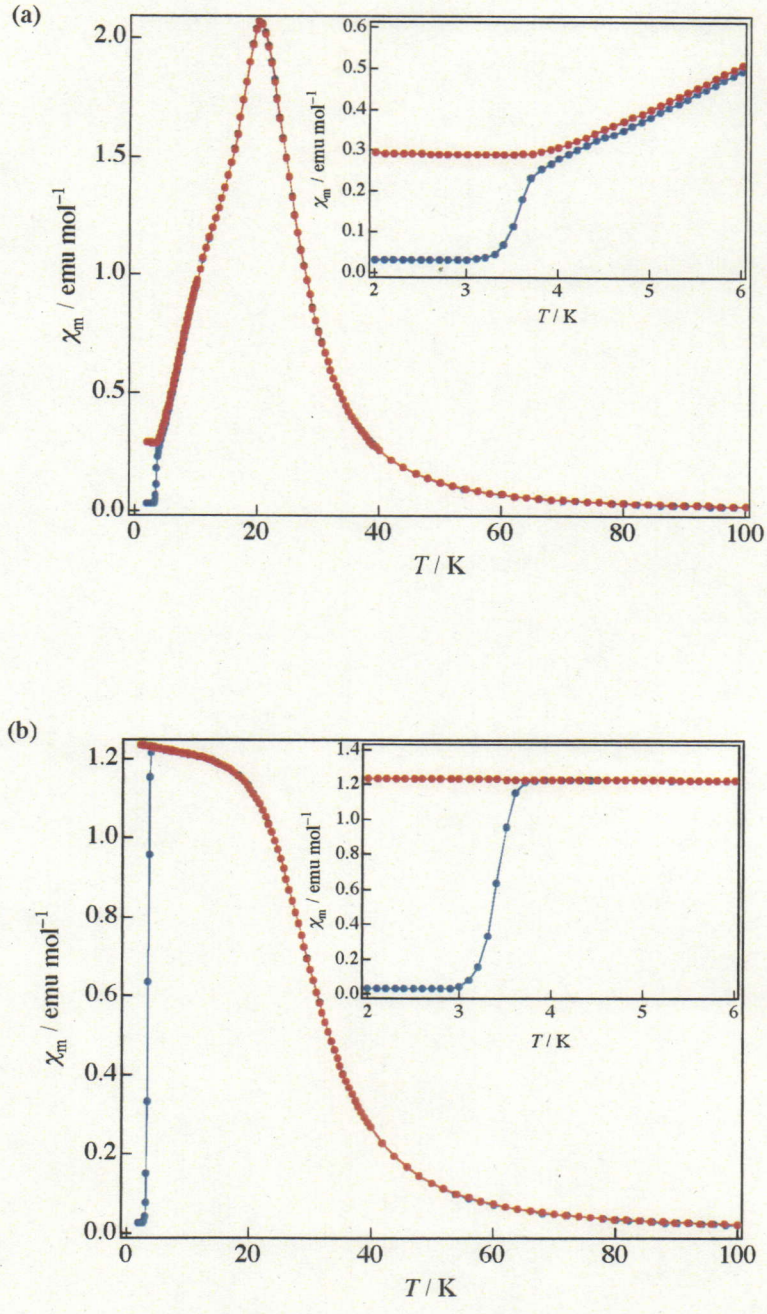

Figure 3–8. ZFC (blue) and FC (red) magnetization curves measured at (a) 500 Oe and (b) 5000 Oe.

The different types of half cycle of hysteresis loops were observed from 1.8 to 30 K. In the temperature interval 4 – 18 K, the $M(H)$ dependences (shown in Figure 3–9) seem to be typical for antiferromagnets revealing a metamagnetic transition under application of an external field. This field-induced phase transition occurs when an applied field reaches a critical value of order of the interchain antiferromagnetic interaction.

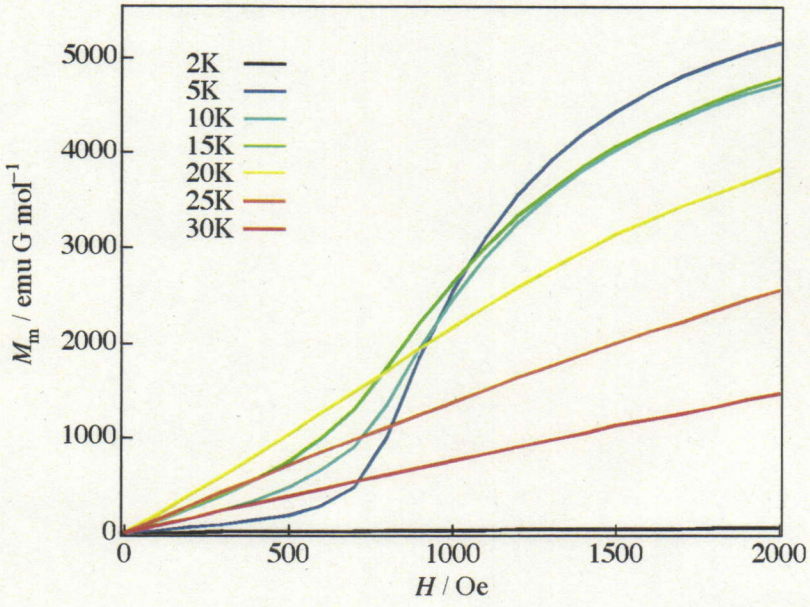

Figure 3–9. Initial magnetization curves of **2**.

In Figure 3–10, full cycle hysteresis loop of **2** measured at 2 K is shown. The saturated magnetization value (M_S) of **2** is approximately 1.16μ_B per formula unit. This value is slightly higher than that expected (1μ_B) for a simple ferrimagnetic model that is consistent with the unit of high spin Co^{II} (S = 3/2) and BNO* (S = 1) which are coupled antiferromagnetically. This discrepancy may be due to the presence of a nonzero orbital moment of Co^{II}. (theoretical effective magnetic moment of single ion of Co^{II} is 3.873μ_B)

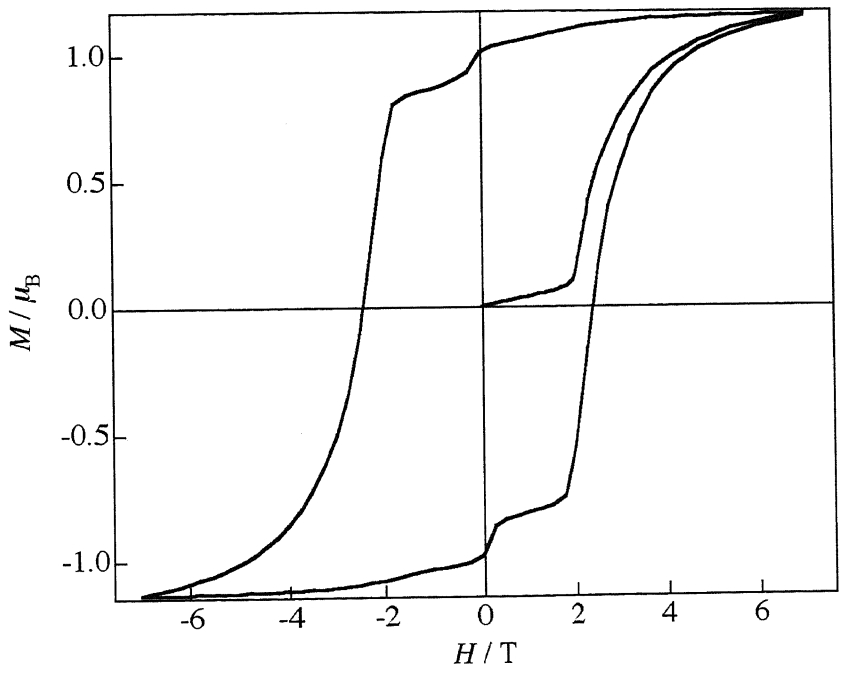

Figure 3–10. Full cycle hysteresis loop of **2** measured at 2 K.

As it follows from Figure 3–11, the phase transition from the AF state to the forced ferrimagnetic (FoFi) state around 850 Oe is accompanied by the hysteresis, however the hysteresis value, ΔH_c, does not exceeds the critical field and the remnant magnetization is zero above 4 K.

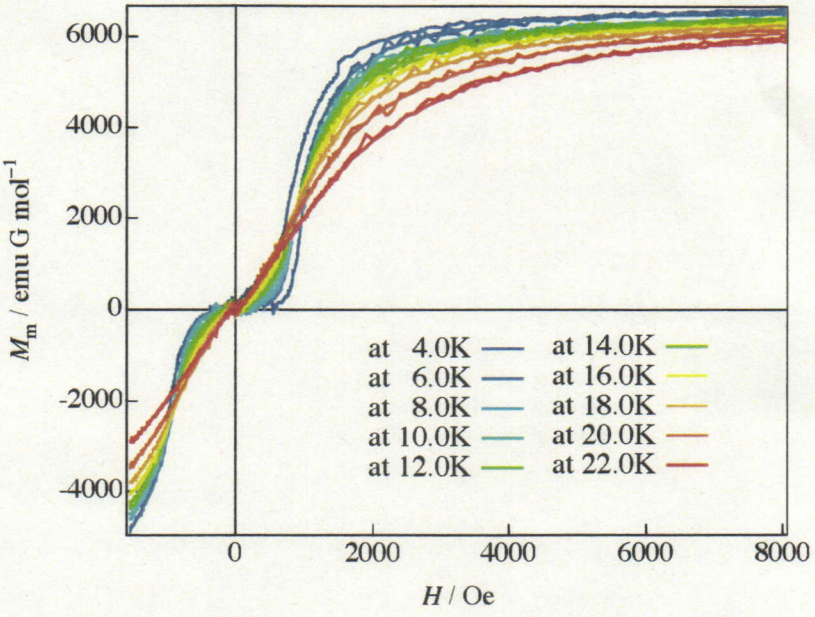

Figure 3–11. Hysteresis loops of 2 measured at selected temperatures (4 ~22 K).

However, when the temperature decreases below 4 K the hysteresis value increases abruptly leading to the constricted shape of the loop at temperatures 3.6 K < T < 4 K (see Figure 3–12) and to the "magnet-type" hysteresis loop with further lowering temperature. The coercive field reaches a value about 25 kOe below 2.6 K. It is considered that the change of the shape of $M(H)$ dependences and large increase of the hysteresis with increasing temperature below 4 K originates in freezing of domain wall displacement due to the crossover from a Heisenberg type antiferromagnet to an Ising type antiferromagnet based on single ion anisotropy of Co^{II} ion.[8,9]

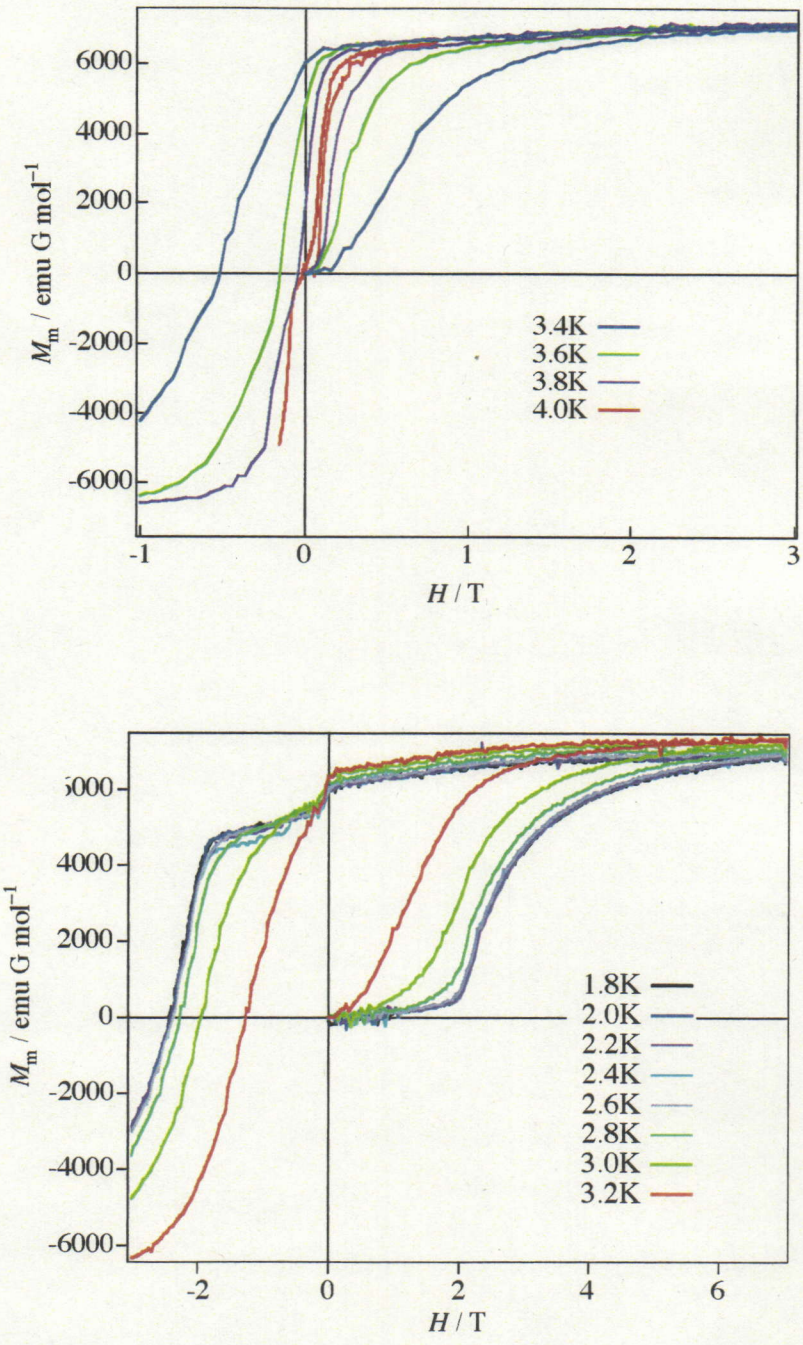

Figure 3–12. Magnetization cycles measured at different temperatures. (above) T = 3.4 ~ 4 K, and (below) T = 1.8 ~ 3.2 K.

In the temperature dependences of ac magnetic susceptibility measurements in zero magnetic field, the χ_{ac}' values show frequency dependence in the temperature range of 4 – 8 K. Because ordered antiferromagnet doesn't show frequency dependence, this data support the crossover from Heisenberg type to Ising type occurred in this temperature range.[8,9] The temperatures of peak at around 20 K were frequency independent (Figure 3–13a,b). The χ_{ac}" values have a peak at around 4 – 6 K and the peak has frequency dependence (1 ~ 1500 Hz) (Figure 3–13a). In the ac magnetic susceptibility measurements in the magnetic field of 500 Oe, the χ_{ac}' and χ_{ac}" curves show resemble behavior with χ_{ac}' and χ_{ac}" curves of 0 Oe (Figure 3–13b). The frequency dependent region of χ_{ac}' curves is increased by increasing the strength of dc magnetic field below 500 Oe. The χ_{ac}" peaks correspond to the phase transition from AF to field-induced ferrimagnetic (FiFi) phase (vide infra). The behaviors of χ_{ac}' and χ_{ac}" are completely different in dc 5000 Oe. The χ_{ac}' values show a sharp rise at around 5 K and a frequency independent peak at around 30 K (Figure 3–13c). The peaks at 30 K correspond to the phase transition from paramagnetic state to forced ferrimagnetic (FoFi) state.

(a)

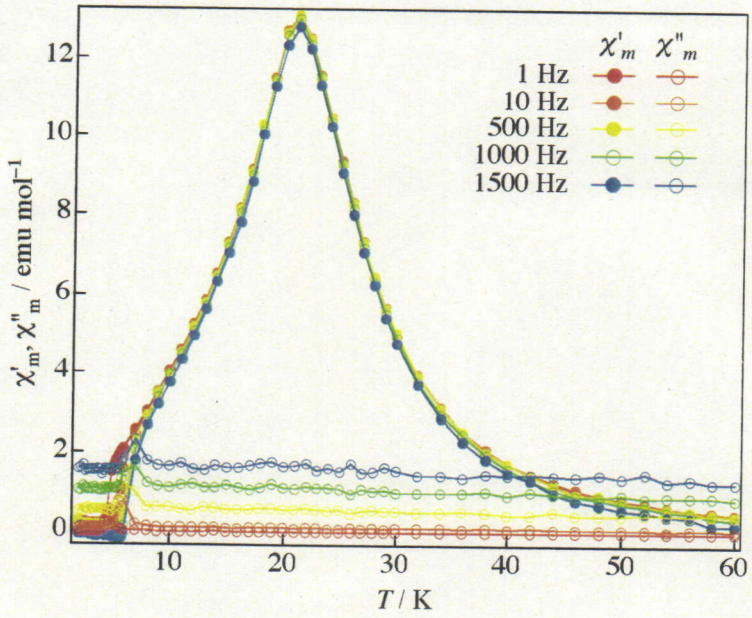

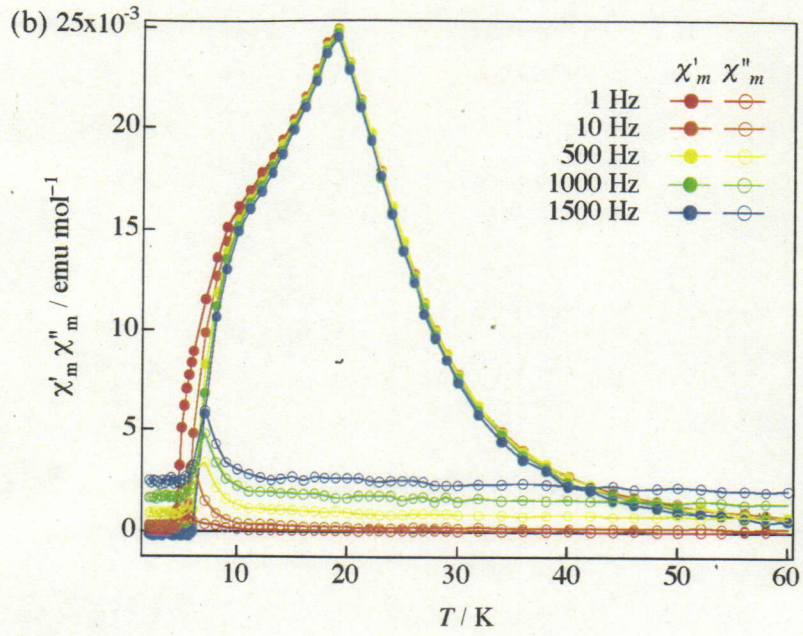

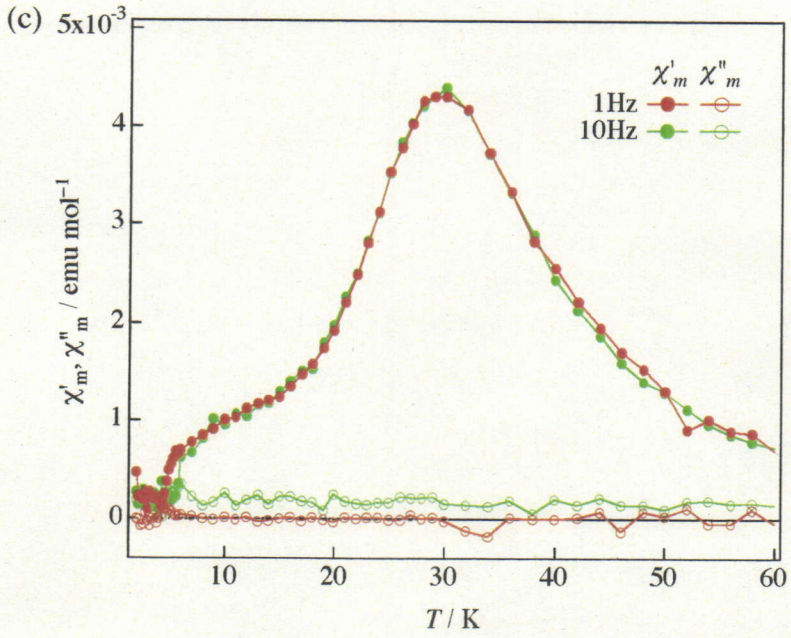

Figure 3–13. Ac χ_m' and χ_m" vs T plots measured at different dc magnetic field (ac amplitude was 5 Oe). (a) dc 0 Oe, (b) dc 500 Oe and (c) dc 5000 Oe.

The magnetization change with magnetic field is found to reveal different dynamics below and above this crossover temperature. It is clearly seen from dc field dependences of the ac susceptibility presented in Figure 3–14 at selected temperatures. At 20 K, it starts to behave as antiferromagnet (Figure 3–14g). There is no frequency dependence of the χ_{ac}' and χ_{ac}" values within the frequency range used (1-1000 Hz). At 7.5K, i.e. above the crossover temperature, the $\chi_{ac}'(H_{dc})$ dependence shows frequency dependent peaks at around 850 Oe, and χ_{ac}" also shows a field dependent peak (Figure 3–14d). This peak indicates the spin-flip transition, which is associated with the nucleation of the FoFi state within AF phase and displacement of the domain walls separating AF phase and FoFi state. However, the author could not observe any peak of the χ_{ac}' and χ_{ac}" in the vicinity of the field-induced AF-FiFi transition in *M–H* measurements below 4 K (Figure 3–14a and 3–14b). These data are indicative of very slow spin movement or the domain wall freezing below the crossover temperature. χ_{ac}–*H* plots at 12, 10 and 5 K are presented in Figure 3–14f, 3–14e and 3–14c. To understand its magnetic properties more clearly, the magnetic phase diagram was constructed.

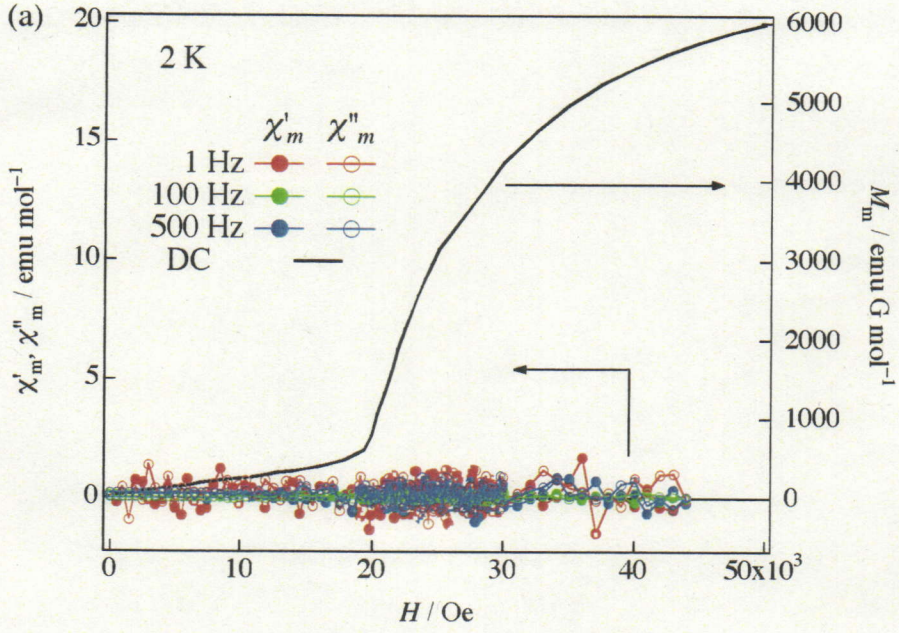

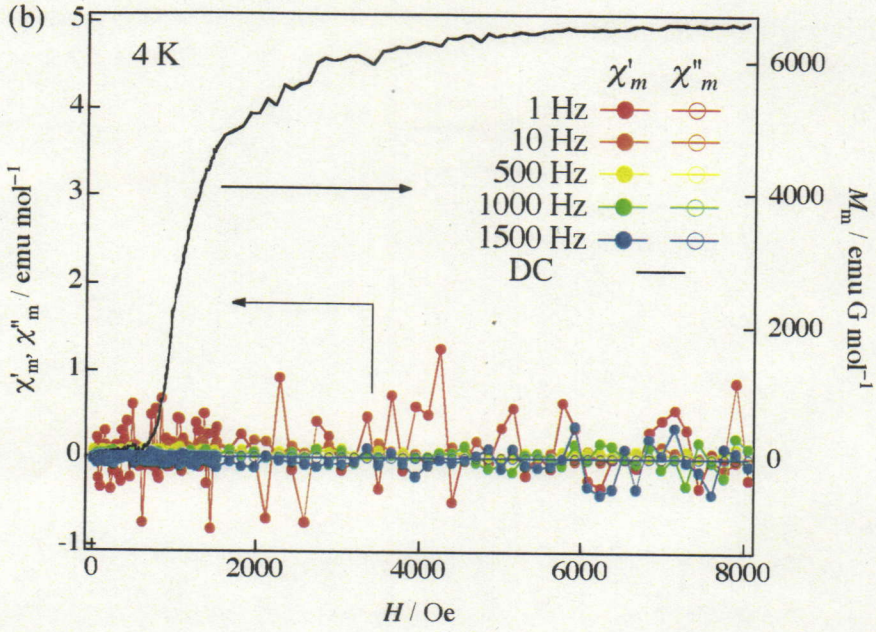
(b)
4 K
χ'm χ"m
1 Hz
10 Hz
500 Hz
1000 Hz
1500 Hz
DC
χ'm, χ"m / emu mol−1
Mm / emu G mol−1
H / Oe

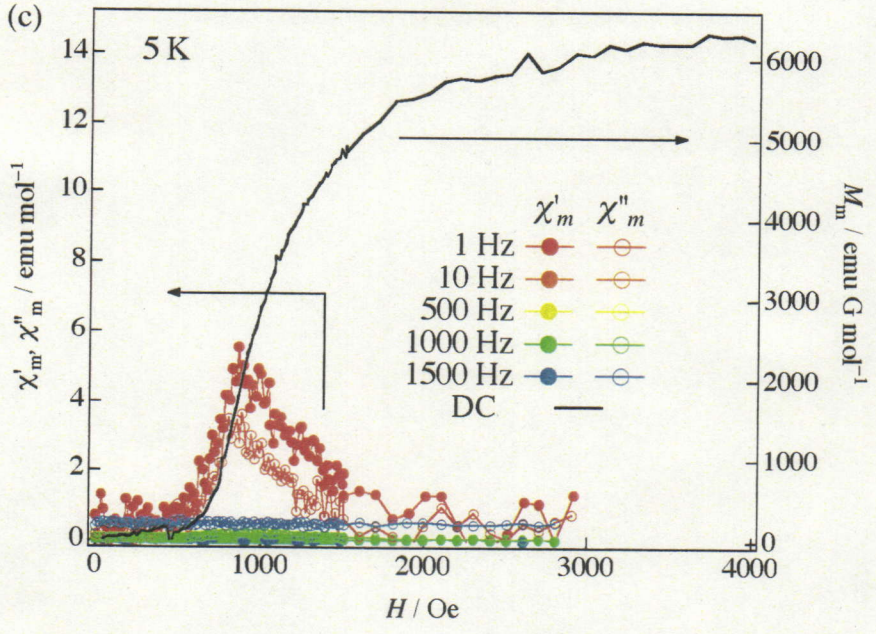
(c)
5 K
χ'm χ"m
1 Hz
10 Hz
500 Hz
1000 Hz
1500 Hz
DC
χ'm, χ"m / emu mol−1
Mm / emu G mol−1
H / Oe

(d)

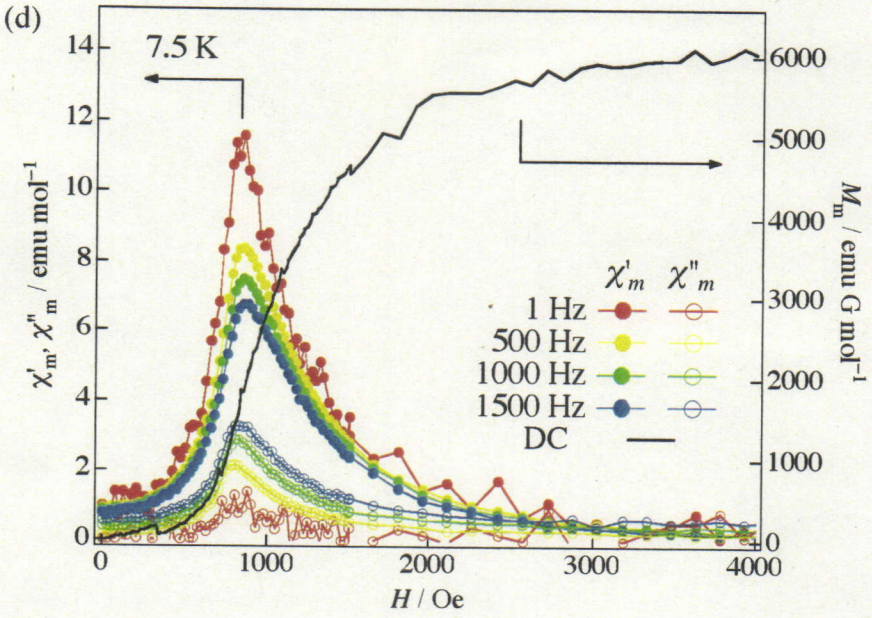
7.5 K
χ'_m χ''_m
1 Hz
500 Hz
1000 Hz
1500 Hz
DC
χ'_m, χ''_m / emu mol^{-1}
M_m / emu G mol^{-1}
H / Oe

(e)

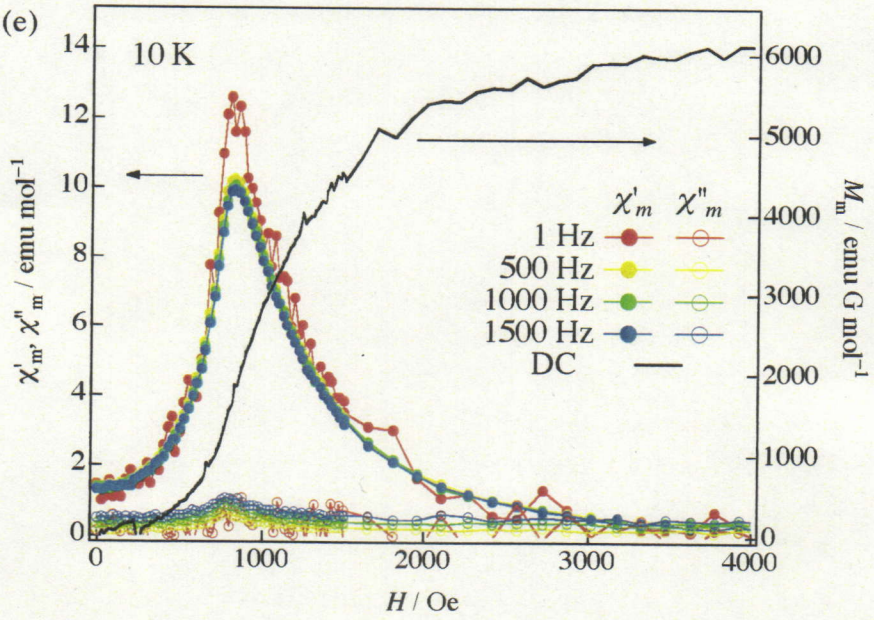
10 K
χ'_m χ''_m
1 Hz
500 Hz
1000 Hz
1500 Hz
DC
χ'_m, χ''_m / emu mol^{-1}
M_m / emu G mol^{-1}
H / Oe

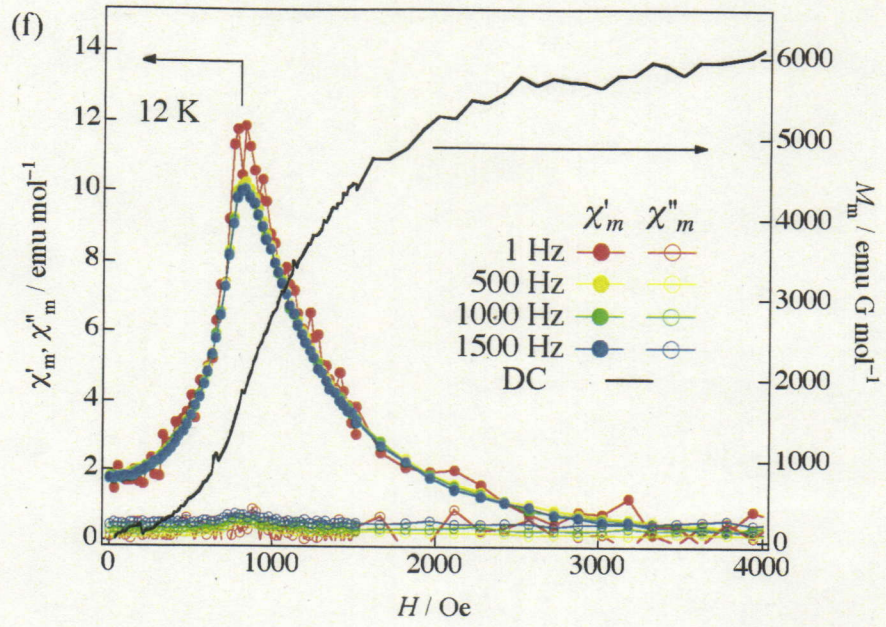

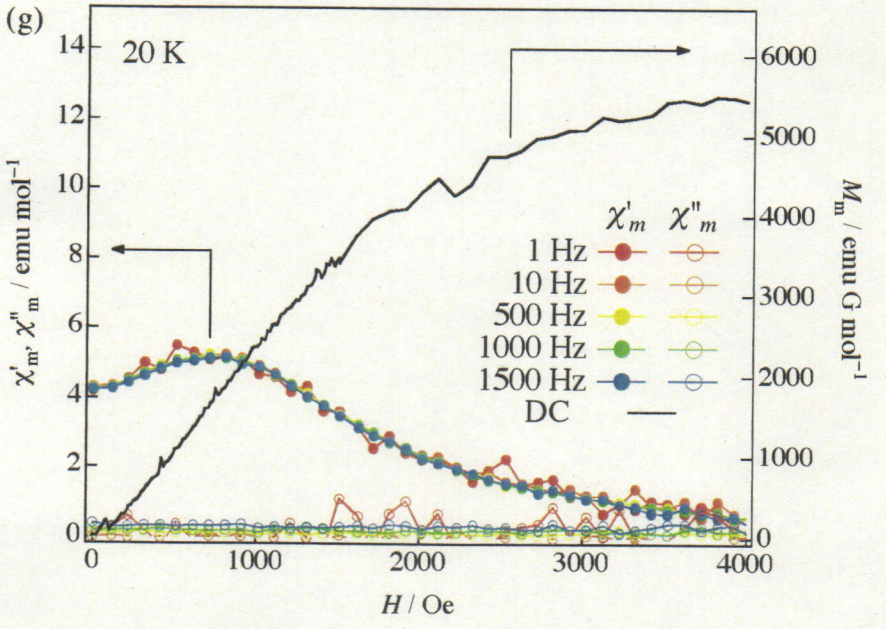

Figure 3–14. Ac χ_m' and χ_m" vs H measured at selected temperatures At (a) 2 K, (b) 4 K, (c) 5 K, (d) 7.5 K, (e) 10 K, (f) 12 K and (g) 20 K, respectively. Ac magnetic field amplitude was 2 Oe.

3.6. Magnetic Phase Diagram

The magnetic phase diagram in the low temperature region is displayed in Figure 3–15. Three lines in the phase diagram, H_C^{up} (critical field of initial magnetization process), H_C^{down} (critical field of demagnetization process) and ΔH_C (difference between H_C^{up} and H_C^{down}) represent the boundary of the field-induced ferrimagnetic (FiFi) state (antiferro- and ferrimagnetic ordered state),[8,9,10] the forced-ferrimagnetic (FoFi) phase and the antiferromagnetic (AF) phase, respectively. The H_C^{up} value corresponds to the spin-flip field. This diagram exhibits five magnetic phases and state. The paramagnetic phase exists above 20 K. In the temperature region 4 – 20 K, this molecule behaves as a metamagnet. The value of the critical field of the AF-FoFi transition corresponds to the interchain exchange interaction. An upturn of ΔH_C with decreasing temperature below 4 K is associated with freezing of the domain wall motion in the Ising type magnetic structure. Below 3.2 K, the compound displays a large coercive field (ca. 25000 Oe at 2 K) and hysteresis loop seems to be typical for hard magnetic materials. After application of a strong magnetic field in this temperature range, further variation of an external field does not lead to the reappearance of the initial AF state in the compound. Thus, this FiFi state is metastable state. The hysteresis value in the Ising state is controlled by the exchange interaction within chains and thermal activation of the domain displacement. However, the increase of the hysteresis value with decreasing temperature is stopped below ~ 2.8 K, which can be ascribed to the change in the mechanism of the domain wall displacement from the thermal activation to macroscopic quantum tunneling.[11]

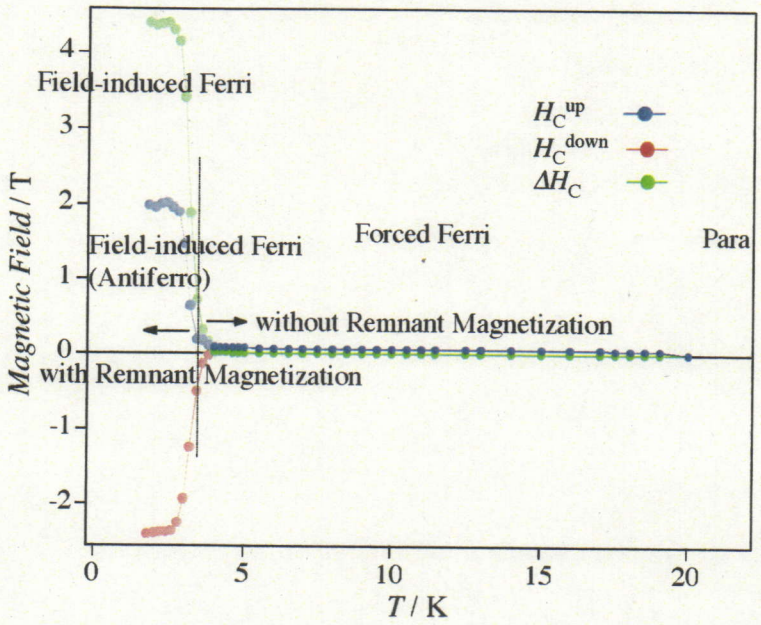

Figure 3–15a. Magnetic phase diagram of **2**.

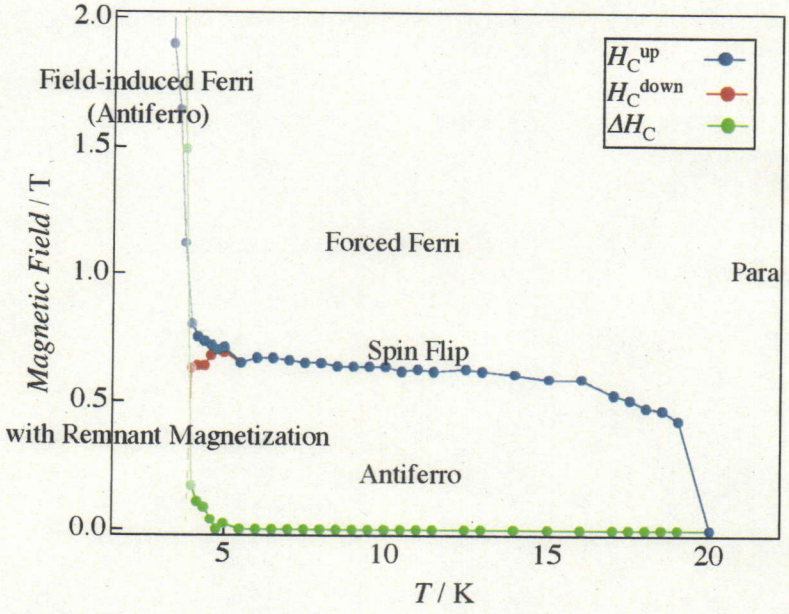

Figure 3–15b. Phase diagram (Magnify).

3.7. Conclusion

The author successfully synthesized a novel organic-inorganic hybrid type chiral structural antiferromagnet, which was comprised of [Co(hfac)$_2$] and chiral bisnitroxide radical. This magnet possesses 1-D helical chain structure; additionally, the structure is characterized by *R*- type helicity. Initially, in the high temperature region above 20 K, this molecule displays behavior as a paramagnetic state. Below 20 K, antiferromagnetic interaction dominates among 1-D ferrimagnetic chains, and the ground state of this compound is 3-D antiferromagnetic. In the temperature range of 3.2 – 20 K, this compound behaves as a metamagnet and its M_S is ~ 1.16μ_B. However, below ~ 4 K the thermal activated motion of the domain wall between the AF and FoFi phases is frozen owing to the high single ion anisotropy of Co ions. It is considered that this behavior is caused by crossover from a Heisenberg type antiferromagnet to an Ising type antiferromagnet. As a result, a sample undergoing magnetization by application of a high magnetic field remains in the field-induced ferrimagnetic FiFi state after zeroing field. Moreover, further variation of the field does not return the sample to the initial AF state. The initial AF alignment of the magnetic moments of the chains may be re-instated upon heating the sample above 5 K, followed by cooling at zero field. In the FiFi state, the sample demonstrates hard magnetic properties characterized by coercive field value of approximately 25 kOe below 3 K and with M_S ~ 1.16μ_B. With decreasing temperature below ~ 2.5 K, the width of the hysteresis loop becomes temperature-independent (Figure 3–12 bottom). Above 2.5 K, the widths of the hysteresis loops show remarkable temperature dependence. These results are indicative of crossover of the thermal activated domain wall motion with quantum tunneling behavior in Ising type magnets.

3.8. References

1 G. H. Coleman, W. F. Talbot, *Org. Synth.* **1943**, *2*, 592.

2 (a) M. A. Petrukhina, C. Henck, B. Li, E. Block, J. Jin, S. Zhang, R. Clerac, *Inorg. Chem.* **2005**, *44*, 77. (b) R. I. Pecsok, W. D. Reynolds, J. P. Fackler Jr., I. Lin, J. Pradilla-Sorzano, *Inorg. Synth.* **1974**, *15*, 96.

3 H. Kumagai, K. Inoue, *Angew. Chem. Int. Ed.* **1999**, *38*, 1601.

4 A. Altmare, M. C. Burla, M. Camalli, G. L. Gascarano, C. Giacovazzo, A. Guaglirdi, G. G. Molitemi, G. Polidori, R. Spagna, SIR-97, *J. Appl. Cryst.* **1999**, *32*, 115.

5 G. M. Sheldrick, SHEXL-97, University of Göttingen, Germany. **1997**.

6 (a) A. Calder, A. R. Forrester, P. G. James, G. R. Luckhurst, *J. Am. Chem. Soc.* **1969**, *91*, 3724. (b) Y. Hosokoshi, K. Katoh, Y. Nakazawa, H. Nakano, K. Inoue, *J. Am. Chem. Soc.* **2001**, *123*, 7921.

7 L. M. Field, M. C. Morón, P. M. Lahti, F. Palacio, A. Paduan-Filho, N. F. Oliveira, *Inorg. Chem.* **2006**, *45*, 2562.

8 (a) M. Kurmoo, H. Kumagai, M. A. Green, B. W. Lovett, S. J. Blundell, A. Ardavan, J. Singleton, *J. Sol. State Chem.* **2001**, *159*, 343. (b) B. W. Lovett, S. J. Blundell, H. Kumagai, M. Kurmoo, *Synth. Met.* **2001**, *121*, 1814. (3) M. Kurmoo, H. Kumagai, S. M. Hughes, C. J. Kepert, *Inorg. Chem.* **2003**, *42*, 6709.

9 (a) J. S. Miller, J. Calabrese, R. S. McLean, A. J. Epstein, *Adv. Mater.* **1992**, *4*, 498. (b) J. S. Miller, C. Vazquez, N. L. Jones, R. S. McLean, A. J. Epstein, *J. Mater. Chem.* **1995**, *5*, 707. (c) C. M. Wynn, M. A. Gîrţu, K. Sugiura, E. J. Brandon, J. L. Manson, J. S. Miller, A. J. Epstein, *Synth. Met.* **1997**, *85*, 1695. (d) C. M. Wynn, M. A. Gîrţu, J. S. Miller, A. J. Epstein, *Phys. Rev. B* **1997**, *56*, 14050. (e) L. N. Dawe, J. Miglioi, L. Turnbow, M. L. Taliafferro, W. W. Shum, J. D. Bagnato, L. N. Zakharov, A. L. Rheingold, A. M. Arif, M. Fourmigué, J. S. Miller, *Inorg. Chem.* **2005**, *44*, 7530.

10 (a) N. V. Baranov, A. N. Pirogov, A. E. Teplykh, *J. Alloys Comp.* **1995**, *226*, 70. (b) N. V. Baranov, N. V. Mushnikov, T. Goto, Y. Hosokoshi, K. Inoue, *J. Phys. Condens. Matter.* **2003**, *15*, 8881.

11 (a) E. Lhotel, E. N. Khatsko, C. Paulsen, *Phys. Rev. B* **2006**, *74*, 020402. (b) A. Maignan, V. Hardy, S. Hébert, M. Drillon, M. R. Lees, O. Petrenko, D. M. K. Paul, D. Khomskii, *J. Mater. Chem.* **2004**, *14*, 1231. (c) S. Yuan, H. D. Raedt, S. Miyashita, *J. Phys. Soc. Jpn.* **2006**, *75*, 084073.

Chapter 4. Studies for Direction Dependences of Magnetizations and Magnetic Structure of Chiral Molecule-based Magnet, $[Mn(hfac)_2]$•BNO*

(*Chem. Lett.* **2007**, *36*, 534)

Chapter 4.

Studies for Direction Dependences of Magnetizations and Magnetic Structure of Chiral Molecule-Based Magnet, $[Mn(hfac)_2]$•BNO*

4.1. Introduction and Known Informations of $[Mn(hfac)_2]$•BNO*

In Chapter 1.3, the author introduced first chiral structural molecule-based magnets, $[Mn(hfac)_2]$•BNO*, which chirality is induced by chiral substituent (Chart 4–1). In such structurally chiral magnets, asymmetric electronic dipole moments survive. The asymmetric dipole fields stabilize ferroic Dzyaloshinsky-Moriya (DM) vectors.[1] From these situations, the chiral magnetic structures are expected. Recently, many chiral structural magnets are prepared by that strategy (vide supra), and investigating their magnetic, optical and other physical properties.[2,3]

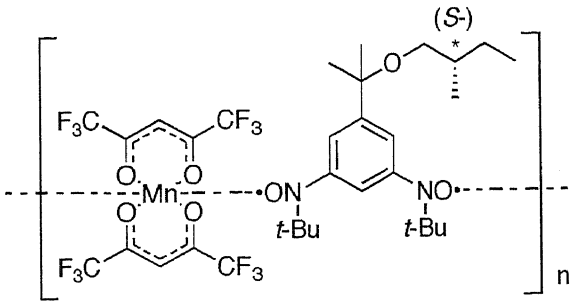

Chart 4–1.

By the way, magnetic easy and hard axes exist in all magnets, which come from single ion magnetic anisotropies and dipole magnetic interactions. For the simple antiferromagnets, total magnetic moments of materials are canceled in long range below Néel temperature (T_N). And below T_N, magnetization curves show spin flop at a magnetic field which magnetic energy corresponds to the energy of antiferromagnetic interactions between nearest neighbor spins. On the other hand, low dimensional ferro- or ferrimagnetic systems frequently show metamagnetic behaviors. The spin structures of

metamagnets are understood as the antiferromagnetic orderings of ferro- or ferrimagnetic one-dimensional chains or two-dimensional sheets. In Figure 4–1a,b, spin flip models of simplified case is shown, ferrimagnetic 1-D chains interact antiferromagnetically.

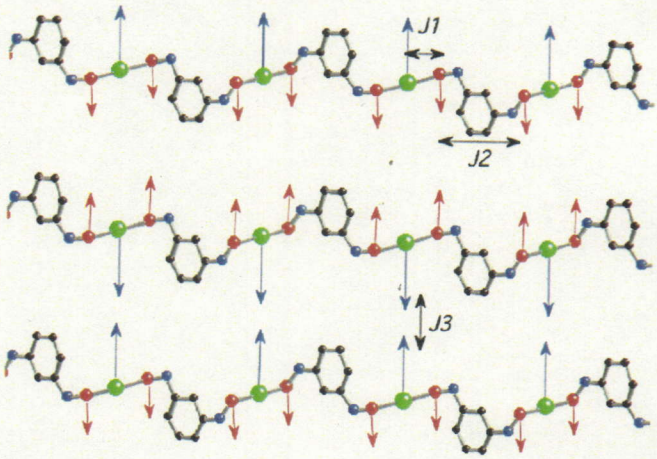

Figure 4–1a. Antiferromagnetic spin alignment of ferrimagnetic chain below T_N. Allows mean amount and direction of the spins. In the case of J_1, $J_3 < 0$, $J_2 > 0$ and applied magnetic field, $H < J_3$.

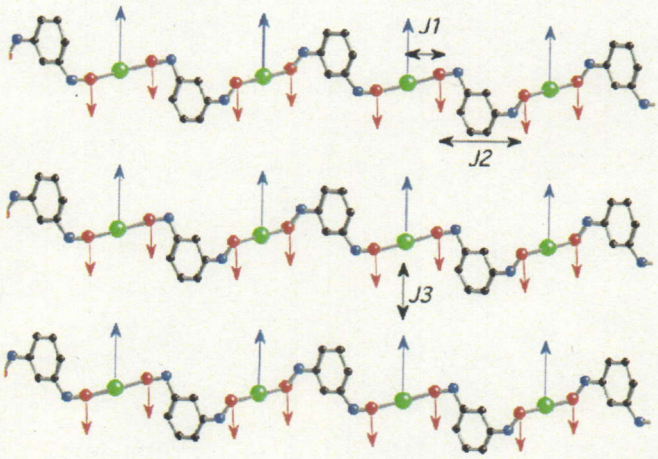

Figure 4–1b. After spin flip transition in metamagnet. In the case of J_1, $J_3 < 0$, $J_2 > 0$ and $H > J_3$.

In such case, these materials show spin flip transition at a critical magnetic field. In the single crystal of metamagnets and antiferromagnets, the magnetization curves show the angular dependent behaviors. These behaviors depend on the directions of applying magnetic field and spin direction. If magnetic field and spin direction are parallel ($H_{//}$), spin flip transition is observed in certain magnetic field (easy axis) and in the case that magnetic field and spin direction are perpendicular ($H_{\perp}$), magnetization values increase gradually and saturate (hard axis) below T_N in the field dependences of magnetization. In Figure 4–2, the models of *M–H* plots of metamagnets in the case of $H_{//}$ and $H_{\perp}$ and in Figure 4–3, and *M–T* plots of antiferro- (meta-) magnets in the case of $H_{//}$ and $H_{\perp}$ (*H* is weaker than antiferromagnetic interactions) are shown.[4] However, the chiral structural molecule-based metamagnet, [Mn(hfac)$_2$]•BNO* (Figure 4–2) shows the spin flip transitions for all crystallographic axes. The author shows magnetic properties of single crystals of **3** and calculated possible magnetic structure in this Chapter.

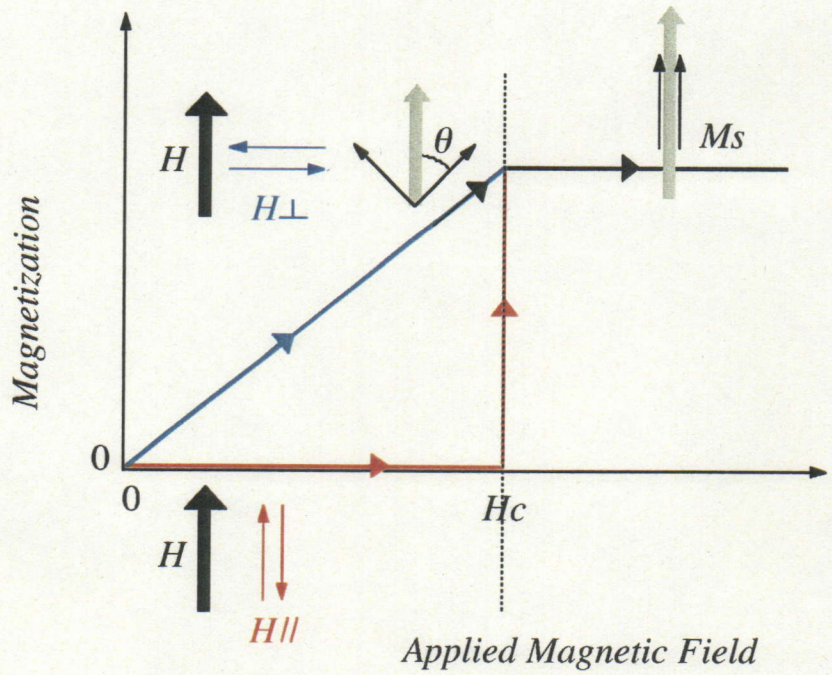

Figure 4–2. Spin flip mechanism in the single crystal of metamagnets.

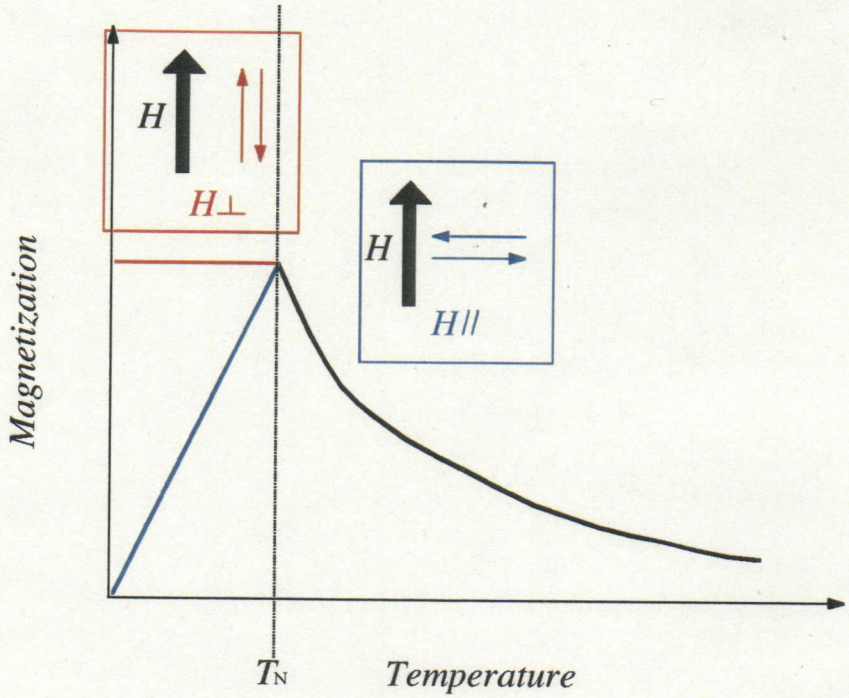

Figure 4–3. Direction dependent behavior of *M–T* plots in the single crystal of antiferro-(meta-) magnets in weak magnetic field.

Crystal structure and magnetic properties of polycrystalline sample of **3** are already reported (Figure 4–4).[5] This compound is constructed by [Mn(hfac)$_2$] and chiral bisnitroxide radical molecules and alternate one-dimensional chain with *R*-helicity lies along to crystallographic *c*-axis. Space group of this compound is chiral triclinic *P*1 (No. 1). Interchain Mn–Mn distances are more than 10 Å and intrachain Mn–Mn distances are shorter than 8.9 Å. This magnet undergoes antiferromagnetic phase at T_N = 5.4 K. Below 5.4 K, spin-flip transition is observed. The observed saturated magnetization value corresponds to expected value in the case of Mn^{II} (S = 5/2) and two aminoxyl groups (S = 1) are interacted antiferromagnetically (Figure 4–5).

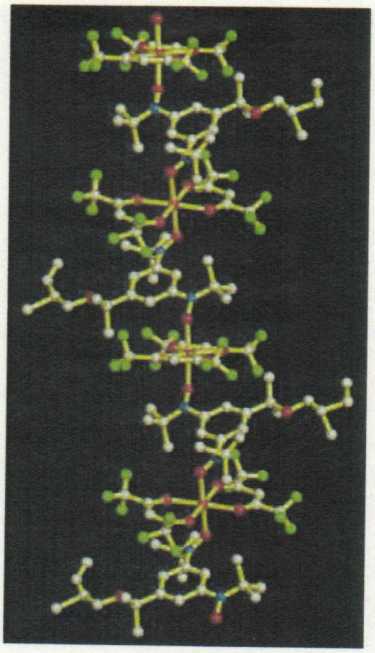

Figure 4–4. 1-D chain structure of **3**.[5]

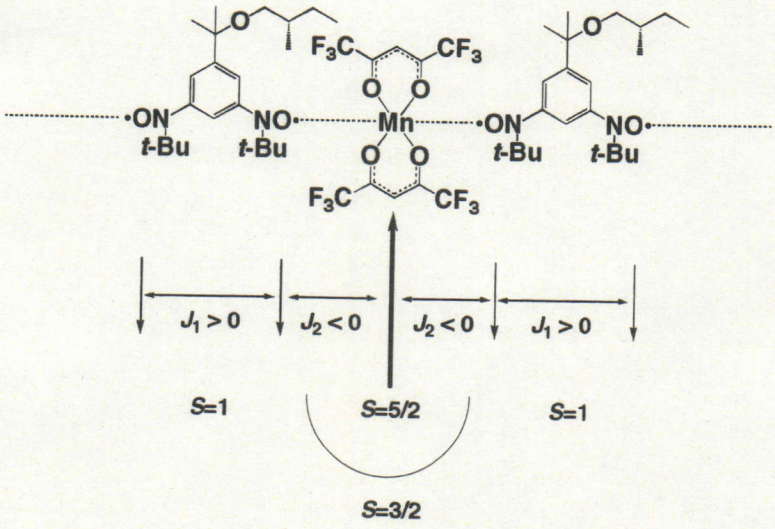

Figure 4–5. Ferrimagnetic 1-D magnetic chain of **3**.

4.2. Preparation

Single crystal of **3** was grown according to literature method (Scheme 4–1).[5] In Chapter 3, more accurately description is presented in Co case, and Mn complex can be prepared using $[Mn(hfac)_2(H_2O)_2]$ in stead of $[Co(hfac)_2(H_2O)_2]$ by similar method.

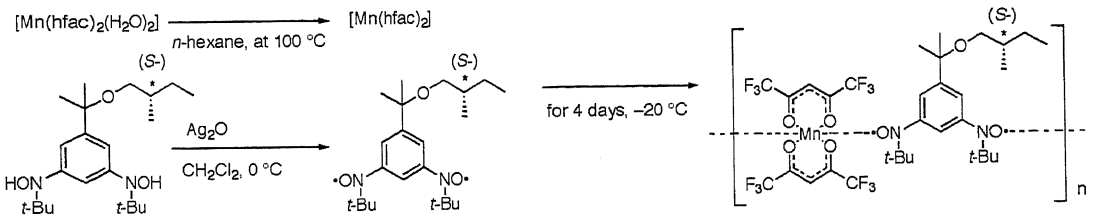

Scheme 4–1.

4.3. Sample Setting for Physical Measurements

Magnetic measurements were carried out using Quantum Design MPMS-5S SQUID magnetometer and all data were corrected by Pascal's constants. The single crystal of **3** was mounted by Apiezon-M grease in the straw. Crystal dimension of these measurements was 750 × 600 × 450 mm^3 and weight was 0.2346 mg. Face indices were decided by X-ray measurement using Bruker SMART-APEX software. Schematic drawing is shown in Figure 4–6.

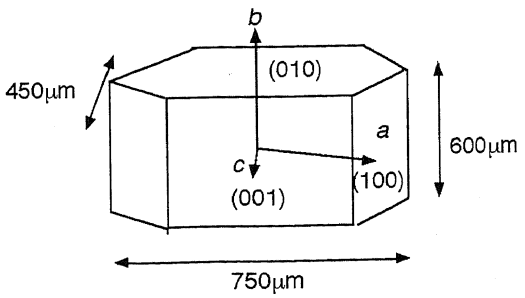

Figure 4–6. Schematic drawing of the single crystal using for the experiments.

4.4. Magnetic Properties of Single Crystal

Figure 4–7 shows the temperature dependences of magnetization values in different crystallographic axes measured at 100 Oe (field cooled). All magnetization curves show sharp peak at 5.4 K and decrease by further cooling. It seems every *a*-, *b*- and *c*-axis behave as antiferromagnetic easy axis (see Figure 4–3, magnetic behaviors of *M-T* plot in the case of magnetic easy and hard axis are presented). At 2 K, magnetization values are 53 (*H* // *a*), 148 (*H* // *b*) and 223 (*H* // *c*) emu mol^{-1} in 100 Oe.

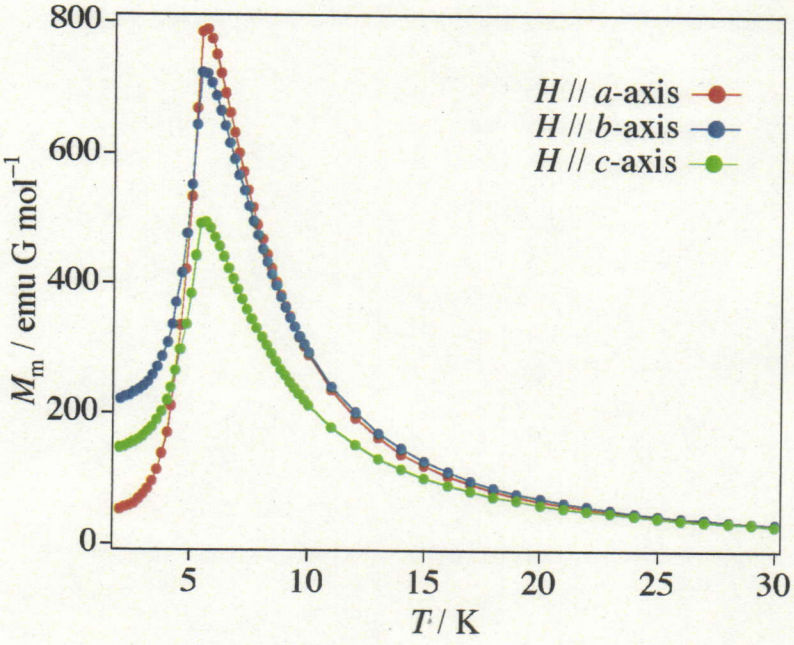

Figure 4–7. Direction dependences of field cooled magnetizations vs *T* plots measured in 100 Oe.

Figure 4–8 shows the direction dependent *M–H* plots measured at 2 K and spin flip transitions were observed in all axes at 640 Oe (*H* // *a*), 1000 Oe (*H* // *b*) and 1250 Oe (*H* // *c*), respectively. The magnetization values in all axes rise sharply at different critical field (Figure 4–5 inset). These results suggest that absence of metamagnetic hard axis in measured directions. To reveal its spin structure, the author tried to calculate the angles between crystallographic axis and antiparallel spin couples.

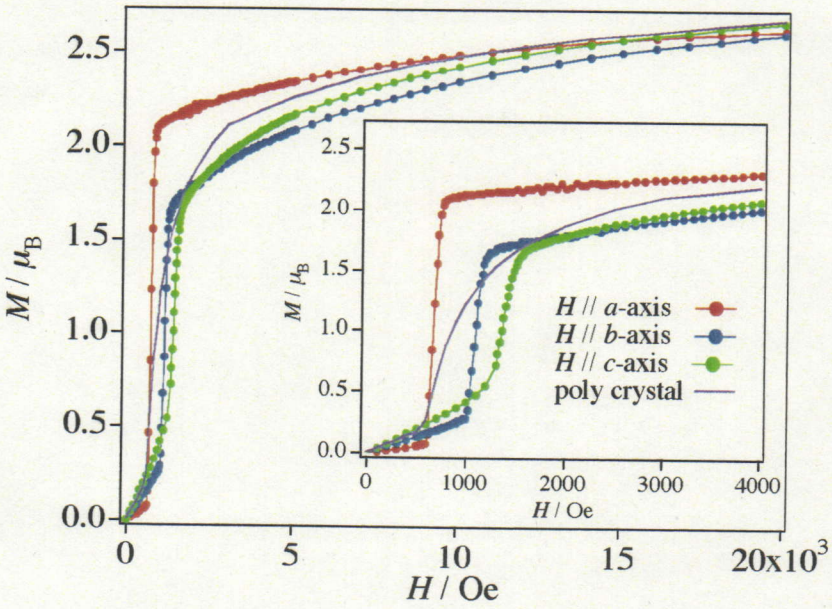

Figure 4–8. *M–H* plots of **3** measured at 2 K. Inset: the magnification in magnetic field range from 0 to 4000 Oe.

4.5. Magnetic Structure

The author calculated the angles between antiferromagnetic spin couples and each crystallographic axes using with magnetic data (see Figure 4–2 and 4–8). The ΔM values, which corresponds to the difference between the magnetization values before and after spin flip transition (Figure 4–8). Calculated angles between spins and *a*-axis is 50.53 °, *b*-axis is 67.15 ° and *c*-axis is 73.60 °, respectively. These angles correspond to the projection angles of spin components in each plane and spin orientations can be calculated from these angles. The author draws possible magnetic structure of **3** and its projections (in the unit cell) and 4–10 (in the plane) in Figure 4–11. This magnetic structure is synthesized one: all spins in antiferromagnetic sublattice are packed into one unit cell and resulting that its magnetization values are normalized per formula unit.

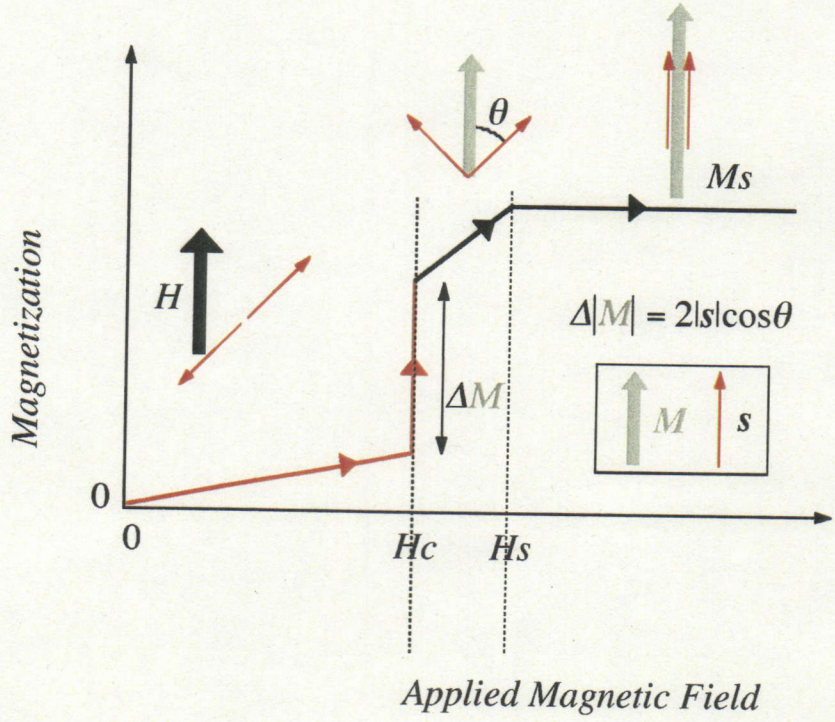

Figure 4–9. Spin flip mechanism and angles between applied field and antiparallel spin couples.

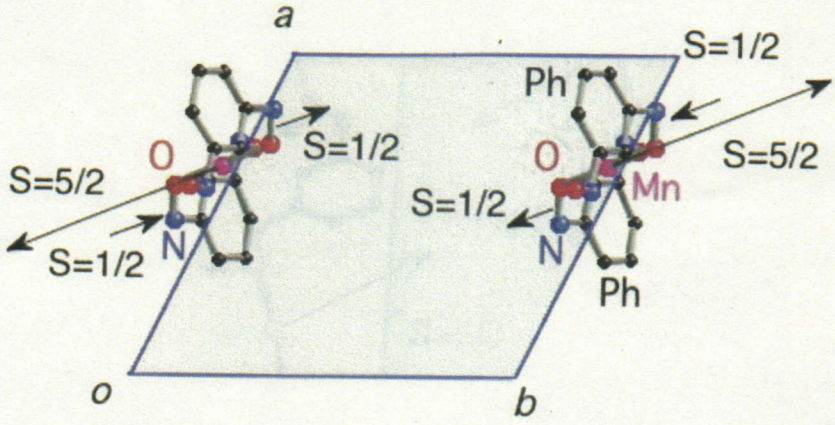

Figure 4–10a. Projections of spin components in *ab* plane. Only selected atoms are presented for clarify. Allow directions and lengths mean directions and amounts of every spin components.

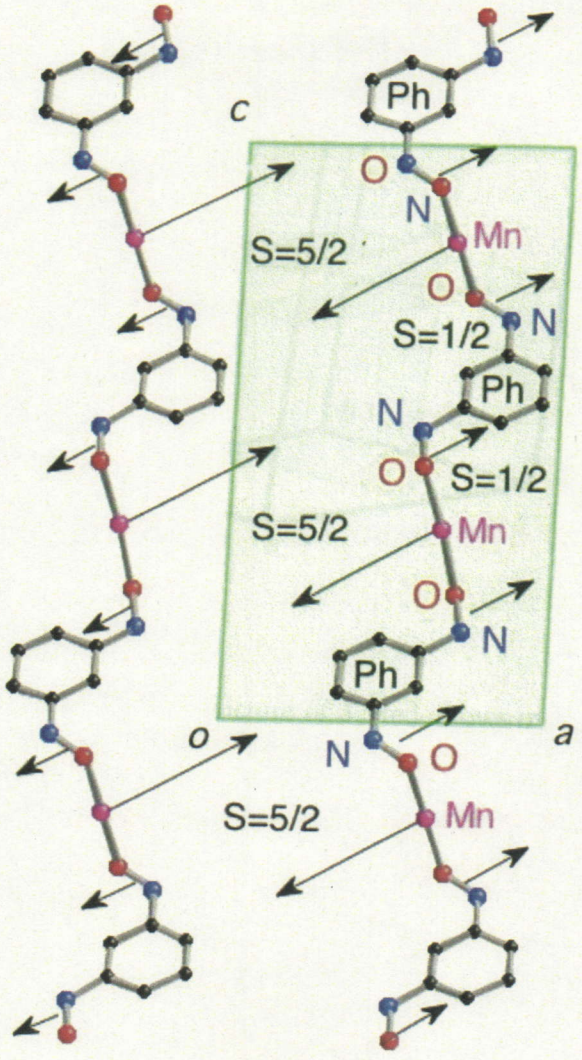

Figure 4–10b. Projections of spin components in *ac* plane. Only selected atoms are presented for clarify. Allow directions and lengths mean directions and amounts of every spin components.

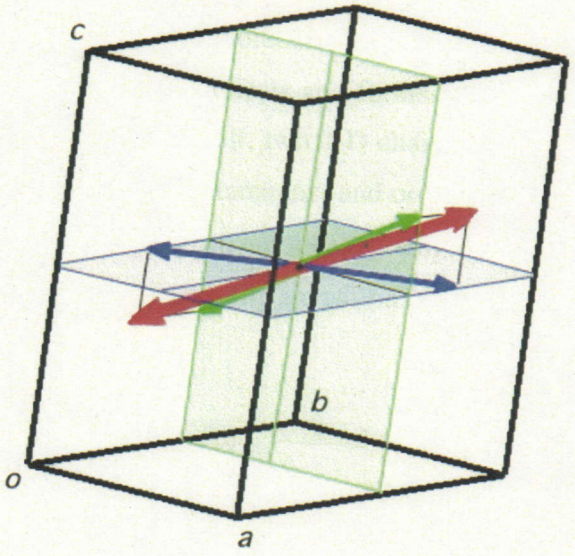

Figure 4–11. Possible magnetic structure of **3**. Red allows mean total spin component of **3** (S = 3/2 + (–3/2)). Blue plane and allows mean projection of spin component in *ab* plane and green ones are in *ac* plane. They are related with Figure 4–10.

Normally, it is expected that magnetic spins, which are interacted antiferromagnetically, orient each other without extraordinary anisotropy or frustration. However, all projected spin components in every plane, are deviated from Mn–Mn line in this crystal. DM interaction is mentioned that possible reason to cause spin canting in such chiral crystals. Therefore, to reveal the influence of chirality, magnetic properties of resemble, but achiral compound, $[Mn(hfac)_2]$•BNO^H is considered and compared with **3**.

To compare with **3**, the magnetic behaviors of single crystal of $[Mn(hfac)_2]$•BNO^H (Chart 4–2) are shown in Figure 4–11.[6] This compound crystallized in achiral space group, monoclinic $P2_1/n$. Two hfac molecules coordinate to Mn ion as *cis*- manor and $[Mn(hfac)_2]$ are bridged by BNO^H radicals and forms zigzag 1-D chain structure along crystallographic *b*-axis. In the unit cell, two 1-D chains exist and each chain has Δ- or Λ-chirality. This molecule is also metamagnet and orders at 5.5 K antiferomagnetically. The field dependences of magnetizations of single crystal measured in three crystallographic axes, they show spin flip transitions in *b*- and *c*-axis and *a*-axis is hard axis (Figure 4–11).

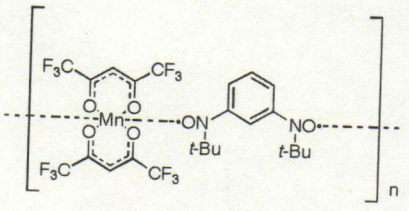

Chart 4–2.

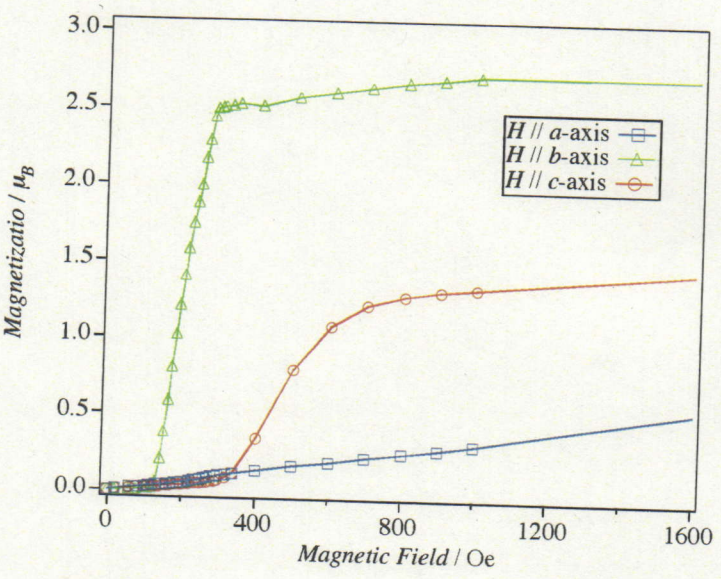

Figure 4–11. Direction Dependent *M-H* plots of single crystal of $[Mn(hfac)_2]$•BNO^H measured at 1,8 K.

From these data, spin arrangement is also considerable. Antiparallel spin couples are perpendicular to crystallographic *a*-axis (Figure 4–12) and antiparallel spins direct each other over the inversion center in achiral crystal. Taking account of these results, it is expected that DM interaction is the origin of spin canting of **3**.

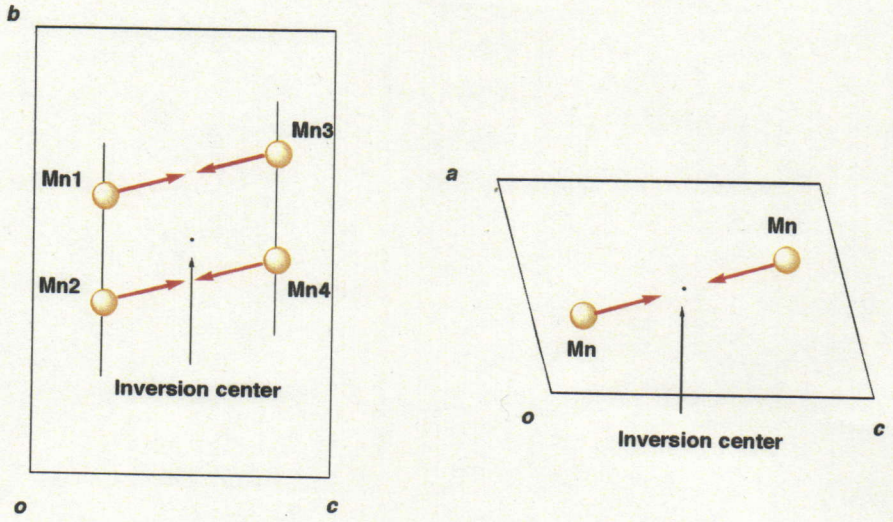

Figure 4–12. Spin arrangement in *ac*- and *bc*-plane of $[Mn(hfac)_2]$•BNO^H.

To consider the relationship of spin canting and DM interaction, Figure 4–13 shows the magnetic structural models that DM interactions affect to 1-D chains of **3** in different manors. In these cases, only intrachain DM interactions are considered. In the case of Figure 4–13d, it is possible to construct calculated spin arrangement by the synthesis of spin components.

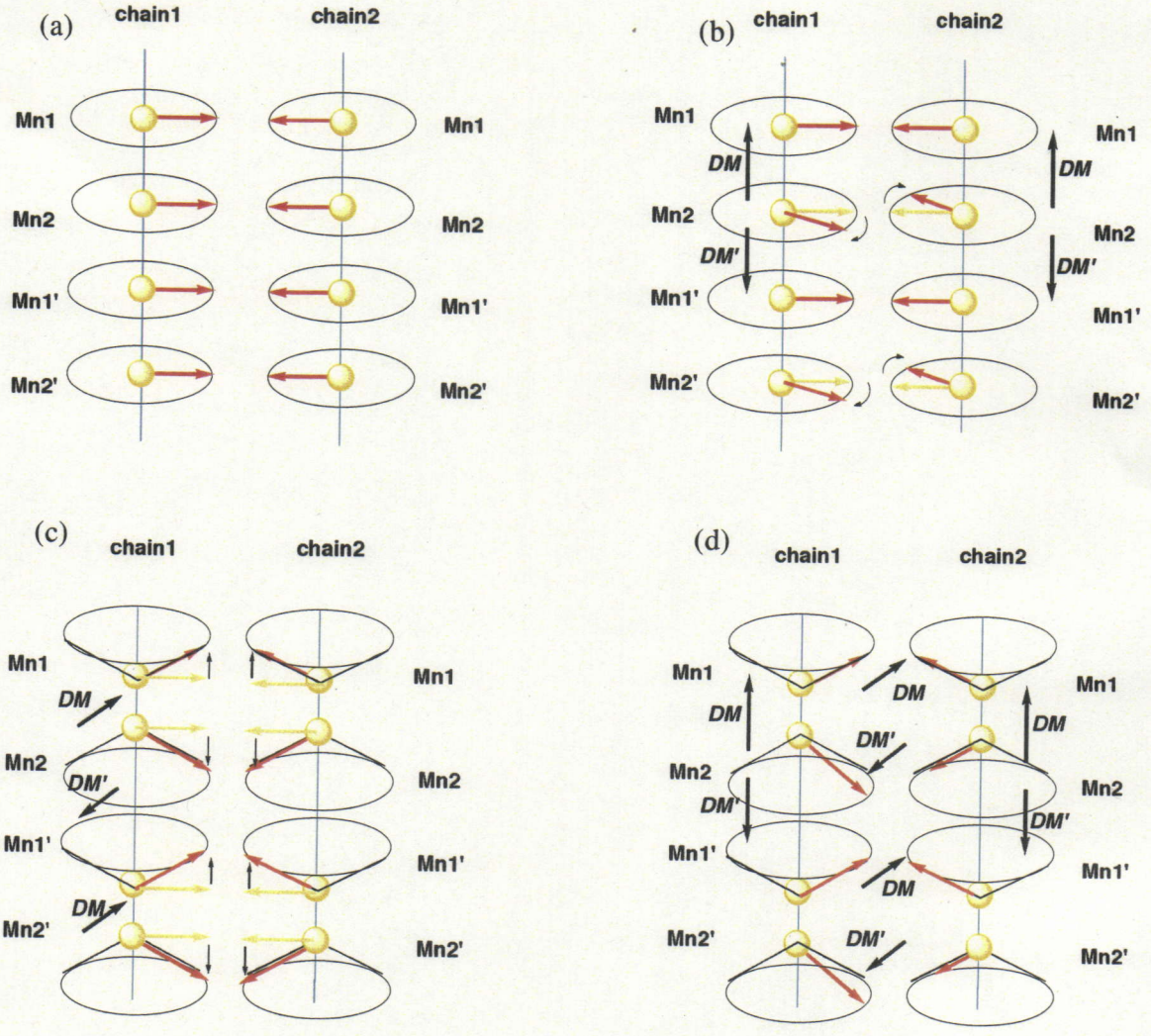

Figure 4–13. Spin arrangements in the case of $J_{intra} > 0$ and $J_{inter} < 0$ with *DM*. (a) *DM* = 0, (b) *DM* // 1-D chains, (c) *DM* ⊥ 1-D chains and (d) *DM* // and ⊥ 1-D chains.

4.6. Conclusion

The author observed metamagnetic spin flip phenomena in all crystallographic axes in chiral molecule-based magnet **3**. The crystal direction dependences of critical field were measured in its single crystal. This novel magnetic behavior indicates that the existence of tilted spin arrangement from all crystallographic axes in the crystal of **3**. This magnetc structure is considered that magnetic spins are canted by ferroic DM interaction, which is stabilized in asymmetric electronic dipole field. The author calculated the angles between spins and crystallographic axes, and possible magnetic structure. Calculated spin orientation seems like it has no relation with crystal structure. Calculated spin arrangement was compared with the spin arrangement of resemble structural achiral compounds. Resulting this, existence of the influence of chirality is suggested. Finally, the author showed it is possible to construct calculated spin arrangement by synthesis of canted spin components.

4.7. Reference

1 (a) I. Dzyaloshinsky, *J. Phys. Chem. Soc.* **1958**, *4*, 241. (b) T. Moriya, *Phys. Rev.* **1960**, *120*, 91.

2 (a) A. Hoshikawa, T. Kamiyama, A. Purwanto, K. Ohishi, W. Higemoto, T. Ishigaki, H. Imai, K. Inoue, *J. Phys. Soc. Jpn.* **2004**, *73*, 2597. (b) J. Kishine, K. Inoue, Y. Yoshida, *Prog. Theor. Phys. Suppi.* **2005**, *159*, 82.

3 Solid state NMR, ESR, XMCD, X-ray magnetic diffraction, neutron diffraction and other physical measurements of [Mn(*R* or *S*-pnH)(H_2O)][$Cr(CN)_6$]•H_2O are in progress.

4 (a) J. H. Van Vleck, *J. Chem. Phys.* **1941**, *9*, 85. (b) L. Néel, *Ann. Phys.* **1948**, *3*, 137. (c) L. Néel, *Ann. Physic.* **1949**, *4*, 249. (d) J. Becquerel, J. van den Handel, *J. Phys. radium* **1939**, *10*, 10. (e) I. S. Jacobs, *J. Appl. Phys.* **1961**, *32*, 61S.

5 H. Kumagai, K. Inoue, *Angew. Chem. Int. Ed.* **1999**, *38*, 1601.

6 (a) Inoue, K.; Iwamura, H. *J. Chem. Soc., Chem. Commun.* **1994**, 2273. (b) K. Inoue, H. Iwahori, A. S. Markosyan, H. Iwamura, unpublished data.

Chapter 5. Concluding Remarks

Chapter 5.

Concluding Remarks

The author prepared three molecule-based magnets, which are consisting of metal-organic radical. In Chapter 2, the author synthesized discrete cyclic $(Co–BNO)_2$ system. From the magnetic data of this molecule, large magnetic anisotropy was estimated. 1-D chiral Co–BNO alternate chain shows remarkable magnetic properties. Two times temperature dependent magnetic phases and state (Para-, Heisenberg type antiferro- and Ising type antiferromagnetic state) and two different field-induced magnetic phase transitions (Meta- and Field induced ferrimagnetic states), respectively. These transitions reflect low dimensional molecular structure and Ising type magnetic interactions (Chapter 3). Mn–BNO* system shows charasteristic spin flip transition in single crystal. It is considerable that this magnetic property is based on its chiral structure. The author calculated magnetic structure and predicted. Its magnetic structure forms canted antiferromagnetic structure as the author expected (Chapter 4).

Acknowledgment

まず始めに金銭面や精神面などから支えて下さった両親に心の底からお礼申し上げます．両親からのサポートが無ければ絶対に学位を取得する事はできなかった事でしょう．また，研究テーマ，研究環境，様々な研究に関するアドバイスを与えて下さった指導教官の井上克也教授に深い感謝の念を表したいと思います．広島大学，速水真也準教授，秋田素子助教には研究に取り組む姿勢から，細かい合成に関するアドバイスまで様々な助力を頂きました．そのおかげで何とか３年という期間内で論文を纏める事ができました．また，広島大学，有機典型元素化学講座，山本陽介教授，河内敦準教授には NMR を貸して頂きました．有機化合物の同定に非常に役立ちました．分子科学研究所，田中晃二教授には籍を分子研に残したまま広島大学に行く事になった私の分子研での受け入れ教授になって頂きました．当時の広島大学固体物性学講座メンバーの現日本大学，山田康治教授，信州大学，大木寛準教授，また，学生の皆様には新しく移ってきて何も分からない私にいろいろな事を教えて下さり非常に助かりました． Université Louis Pasteur の Dr. Mohamedally Kurmoo にはフランスに訪れた際に研究面でのサポートだけでなく日常面においてもフランスでのルールなど何も分からない私に親切に世話をして頂きました． Ural State University の Prof. Nicolai Baranov にはこの論文のメインワークである Co 錯体の磁性研究に関して非常に役に立つアドバイスを頂きました．後輩の中では，吉田祐輔くん，東川大志くんら，広大井上研初期メンバーの皆様には様々な手助けだけでなく一緒に遊んだりする事により精神的な面からも非常にフォローして頂きました．また，その後グループに入ってきた学生の皆さんにも実験，私生活共に様々な手助けをして頂きました．また，広島大学化学科事務及び分子科学研究所大学院担当係の皆様，分子研小林グループ太田明代秘書には事務的な面から支えて頂きました．数々のご迷惑をおかけしてしまいましたが皆様のおかげで何とか乗り切る事ができました．皆様のお力添えがなければ絶対にこの学位論文の完成は無かったと改めて実感しています．最後にもう一度皆様へ感謝の意を表し，締めとさせて頂きます．今後ともお世話になった方々への感謝を忘れず謙虚にしかし貪欲に研究に励んでいきます．